Review

Straight to Low-Sinuosity Drainage Systems in a Variscan-Type Orogen—Constraints from Tectonics, Lithology and Climate

Harald G. Dill [1,*], Andrei Buzatu [2] and Sorin-Ionut Balaban [3]

1 Department of Mineralogy, Gottfried Wilhelm Leibniz University, Welfengarten 1, D-30167 Hannover, Germany
2 Department of Geology, Faculty of Geography and Geology, Alexandru Ioan Cuza University, Carol I Boulevard, RO-700505 Iaşi, Romania; buzatu_andrei@yahoo.com
3 Department of Earth and Planetary Sciences Birkbeck, University of London Malet Street, Bloomsbury, London WC1E 7HX, UK; balaban_sorin_ionut@yahoo.com
* Correspondence: h.geo.dill@gmx.de

Abstract: A holistic-modular approach has been taken to study the evolution of three straight to low-sinuosity drainage systems (=SSS) in an uplifted basement block of the Central European Variscides. The development of the SSS is described by means of a quadripartite model. (1) The geological framework of the SSS: Forming the lithological and structural features in the bedrock as a result of different temperature, pressure and dynamic-metamorphic processes. (2) Prestage of SSS: Forming the paleo-landscape with a stable fluvial regime as a starting point for the SSS. (3) Proto-SSS: Transition into the metastable fluvial regime of the SSS. (4) Modern SSS: Operation of the metastable fluvial regime Tectonics plays a dual role. Late Paleozoic fold tectonic creates the basis for the studied SSS and has a guiding effect on the development of morphotectonic units during the Neogene and Quaternary. Late Cenozoic fault tectonics triggered the SSS to incise into the Paleozoic basement. The change in the bedrock lithology has an impact on the fluvial and colluvial sediments as well as their landforms. The latter reflects a conspicuous modification: straight drainage system ⇒ higher sinuosity and paired terraces ⇒ hillwash plains. Climate change has an indirect effect controlling via the bedrock the intensity of mechanical and chemical weathering. The impact on the development of the SSS can be assessed as follows: Tectonics >> climate ≅ bedrock lithology. The three parameters cause a facies zonation: (1) wide-and-shallow valley (Miocene), (2) wide-angle V-shaped valley (Plio-Pleistocene), (3) acute-angle V-shaped valley (Pleistocene), (4) V-shaped to U-shaped valleys (Pleistocene-Holocene). Numerical data relevant for the hydrographic studies of the SSS are determined in each reference area: (1) Quantification of fluvial and colluvial deposits along the drainage system, (2) slope angles, (3) degree of sinuosity as a function of river facies, (4) grain size distribution, (5) grain morphological categorization, (6) grain orientation ("situmetry"), (7) channel density, (8) channel/floodplain ratios. Thermodynamic computations (Eh, pH, concentration of solubles) are made to constrain the paleoclimatic regime during formation of the SSS. The current model of the SSS is restricted in its application to the basement of the Variscan-Type orogens, to an intermediate crustal maturity state.

Keywords: straight to low-sinuosity drainage systems (SSS); fold- and fault tectonic; metamorphic and granitic bedrocks; Neogene-Quaternary transition; SE German variscan basement

1. Introduction

Fluvial drainage systems have been in the focus of geomorphologists from different backgrounds, such as geology, geography and others. Their studies cover a wide range of different targets, from morphological studies of the fluvial drainage patterns to the degree of sinuosity and the measurements of the fluvial discharge [1–10] Studies of the straight and low-sinuosity channel systems (=SSS) are often eclipsed by more prominent braided, anastomosing, and meandering drainage systems. This lack of emphasis is also true for

the studies on the control of endogenous parameters which have always been sidelined in favor of exogenous ones, such as climate change [11]. Structural analyses, particularly in neotectonics, are not anything out of the ordinary in geomorphology but frequently related to issues of civil engineering and sister drainage systems of the SSS [12–25]. A broader view has been taken on the evolution of fluvial drainage system as a function of tectonics in some comprehensive studies [17,26–34]. Similar comprehensive studies dealing with the mineralogy and petrography of straight to low-sinuosity drainage systems cannot be quoted for the Variscan basement in Central Europe. Therefore, in the current terrain analysis emphasis is placed on a combination of geomorphology with tectonic, petrographic and climatic issues. The study area selected has one basement region with similar tectonic history and lithologies where the geological and geomorphological influences on the evolution of the 3 SSS can be investigated. Such an ideal study area is offered by the NE-Bavarian Basement, at the NW edge of the Bohemian Massif (Figure 1a,b).

One can find there three geodynamic units, which are drained by rivers heading towards the W and tributary to a common trunk river system, the Rhein-Main fluvial network. The hydrographic setting enables them to take a catena-like approach from the source (watershed) to the depocenter in the adjacent foreland of the drainage system. The three reference sites, albeit situated side-by-side with each other in the basement, are markedly different from each other with regard to their histories of the P (pressure) and the T (temperature) regimes both of which are decisive for the way composition and deformation of fluvial bedrocks can impact on the SSS. The changing physical parameters during the Paleozoic orogeny provoked a change of the bedrock lithology and the type of structural geology that influenced the formation of the landscape during the Cenozoic (see Sections 5.2 and 5.3). Consequently, these physical parameters form a good basis for a tripartite subdivision: (1) Frankenwald (very-low grade, VLG-type), (2) Münchberg Gneiss Complex with marginal facies (low- to high-grade, LHG-type), (3) Fichtelgebirge (low-grade with granitic intrusions LGG-type) [35] (Figure 1b,c, Table 1).

The uplifted basement block is part of the Central European Variscides framed by two sets of planes. It is bounded towards the Mesozoic foreland by a deep-seated sub-vertical lineamentary fault zone called the "Franconian Line Fault Zone" which herein is abbreviated to FLFZ and a concealed NW-SE structure forming the divide between the Rhein-Main and Elbe/Labe drainage basins and, hence, demarcating the study area to the NE. In vertical the crustal section is truncated by subhorizontal paleosurfaces arranged in a staircase-like way that play a major role in the fluvial evolution [38,39] (Figure 1b). The "stairs" demarcate the lithological outcrops within and the height of "stairs" control the gradient and longitudinal profile of the fluvial drainage systems (Section 5.2.1).
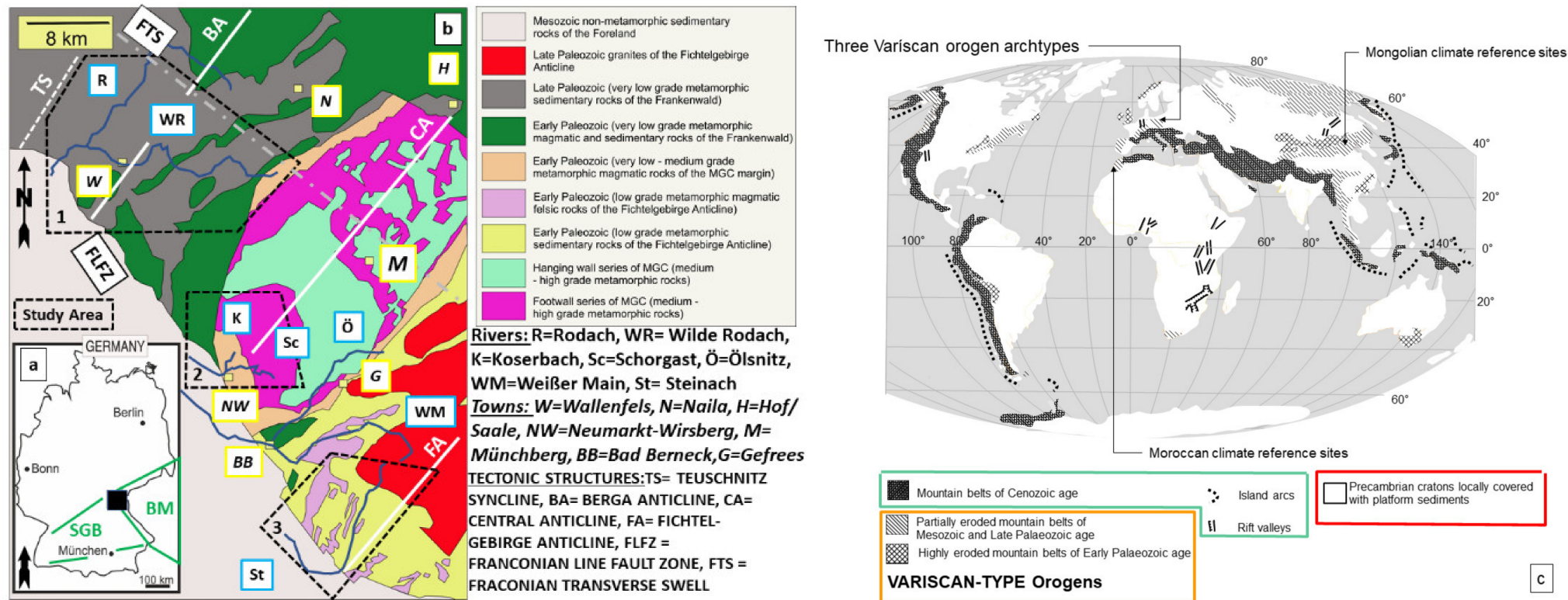
Figure 1. Position and the geological setting of the study area in SE Germany with three type localities framed by stippled line: 1. VLG-type area, 2. LHG-type area, 3. LGG-type area. For features of each reference site see Table 1. (**a**) Position of the study area in the Central European Variscides in SE Germany at the NW edge of the uplifted basement of the Bohemian Massif (BM) and at the NE margin of the South German Block (SGB) representative of the Mesozoic and Cenozoic foreland basin. Rivers, towns and tectonic structures as well as geology are shown on the right-hand side, (**b**) The geological setting of the three type localities at the NW edge of the Bohemian Massif. Geological basis [35] (**c**) The position of the study areas referred to in the text in relation to the geomorphological-geodynamic setting and the distribution of Variscan-type orogens Maturity of crustal section: green: pre-mature, orange: mature, red: super-mature [36].

Table 1. Synoptical overview of the three straight to low-sinuosity reference drainage types as a function of the metamorphic grade and presence of intrusive rocks in the bedrock lithology. The three type were categorized according to the bedrock lithology the minerals of which decrease from left to right and the tectonic structures get obliterated in the same direction. both of which are besides climate the key elements of the origin of the SSS and form the framework stage. The rows describe the dual approach taken in the current study (see Figure 2). Blue: Geoscientific anamnesis and visual examination. Yellow: Geoscientific measurements, analysis, and computations. The "Basement region" denotes the three areas at the western edge of the Bohemian Massif (Figure 1). The "Basement and foreland lithologies" provide an overview of the lithologies shown on the geological maps 1:25,000, a compilation of which is given in Figure 1. The landform series are described according to the proposals of Easterbrook (1999) and Bridge (2003) [8,37]. Approx. 300 samples/station points have been analyzed lithologically and mineralogically. Degree of sinuosity has been calculated according to the equation referred to in the text for each river section in the maps following the recommendations of Charlton (2014) [10] and using the ArcGis software 10.2.2. The sediment petrography of gravel is based on 2442 samples.

1st Order Classification		VLG-Type	LGG-Type	LHG-Type
2nd Order Classification				
Basement **Saxothuringian realm of the Central European Variscides**	Basement type	Very-Low Grade metamorphic basement	Low-Grade metamorphic basement intruded by Granites	Low/medium- to High-Grade metamorphic basement
	Basement region	Franconian Slate Mts. "Frankenwald" (FW)	Fichtelgebirge Mts. "Fichtelgebirge" (FG)	Münchberg Gneiss Complex plus marginal facies "Münchberg Gneismasse" (MGC)
	Basement lithology	Slate, black slate ("alum shale"), greywacke, sandstone, quartzite, conglomerate, bright/black chert (proximal see DA), metabasalt (diabase), keratophyre, limestone, lamprophyre	Syeno-/monzogranite, meta-rhyolites ("epi-gneiss"), quartz (+hematite) dike rocks, dolerites, band and massive metaquartzites, phyllites	Biotite-muscovite gneiss, amphibolite, hornblende, calcsilicates, gneiss, serpentinite, eclogite, metagranodiorites/-granite-hornfels (orthogneiss), phyllite, prasinite, talc schists
Foreland	Foreland lithology (detrital matter proximal—see DA)	Black chert ("lydite"), diabase, quartzite, greywacke, slates, siliceous conglomerate	Phyllite, banded meta quartzite, quartz dike rocks, massive and porphyritic epi-gneiss, porphyritic volcanites, syeno-/monzogranite, Early Triassic sandstone and carnelian	Black chert ("lydite"), diabase, prasinite, amphibolite, muscovite gneiss, orthogneiss, Late Triassic sandstone
Topography	Uppermost paleosurface (meter a.m.s.l.)	760 (max. height Döbraberg 795—chert)	940 (max. height Schneeberg 1052—monzogranite)	620 (max. height Weißenstein 668—eclogite, eclogite amphibolite, pegmatoid)
	Lower most floodplain (meter a.m.s.l.)	340	400	355

Table 1. *Cont.*

| 1st Order Classification | | VLG-Type | LGG-Type | LHG-Type |
2nd Order Classification				
Landform Series according to Summerfield (1991) [36]	Fluvial processes	CA: Relic large-and-shallow valleys/peneplain, straight to low sinuosity stream, single channels, non-alluvial to alluvial TA: Straight to high-sinuosity streams, flood plains. V-shaped in the upper reaches, U-shaped in the lower reaches, intermediate sediment trap Pools, riffles, steps DA: Low-sinuosity to strongly meandering stream with wide floodplain and stacked pattern of terraces within the basement and foreland, alluvial fans	CA: Straight to low-sinuosity streams, multiple channels, alluvial > (non-alluvial), dentritic pattern cascades, step-pool TA: Straight to low-sinuosity streams, intermediate sediment traps, pools, riffles, steps DA: High-sinuosity to moderately meandering stream with wide floodplains	CA: Relic large-and-shallow valleys/peneplain, low- to high sinuosity streams, single channels, alluvial drainage systems TA: Straight to low sinuosity muddy streams, Pools, riffles, steps DA: Low- to high-sinuosity streams within the foreland, hill wash plain, pediments (fluvial part/confined flow)
	Mass wasting processes	CA: Forested mountains with rounded tops, rare exposure of bare rocks of chert, quartzite, greywacke, sandstone talus and soil creep, TA: Solifluction, talus and soil creep DA: Solifluction	CA: Forested mountains with tors and boulder strewn tops and slopes with block streams TA: Solifluction, talus and soil creep, debris flow DA: Solifluction, talus and soil creep, debris flow	CA: Forested hills and mountains with palisades and boulder strewn tops and slopes (blockfield, block streams), monadnocks rare (metabasic to metaultrabasic rocks) TA: Solifluction, talus and soil creep, debris flow DA: pediments (colluvial part/unconfined flow)
	Cryogenic processes	DA: Ice wedge-cryoturbation	CA: cryoturbation, nivation cirques DA: Dragged and distorted pocket fills underneath terraces-cryoturbation	CA: cryoturbation
Quantification of fluvial and colluvial deposits	Fluvial deposits (%)	CA: 8.81 TA: 6.93 to13.61 DA:16.70 to 25.71	CA: 0.0 to 1.32 TA: 1.34 to 3.41 DA: 2.76–11.41	CA: 5.39 TA: 1.89 DA: 7.33–21.51
	Mass wasting deposits (%)	CA: 3.80 TA: 0.70 to 0.76 DA: 0.0 to 1.36	CA: 13.54 to 21.93 TA: 3.80 to 22.32 DA: 9.06 to 11.56	CA: 10.43 TA: 11.63 DA: 9.73 to 17.97

Table 1. *Cont.*

1st Order Classification		VLG-Type	LGG-Type	LHG-Type
2nd Order Classification				
Mineralogy of supergene alteration	Argillitization zone	CA: Regolith: illite, illite-chlorite-vermiculite mixed-layer, vermiculite, kaolinite, chlorite	CA: Regolith: kaolinite (common), smectite, vermiculite, nontronite, illite, chlorite (mainly on granite),	CA: Regolith: kaolinite (common), illite, chlorite, talc, serpentine, vermiculite (only on metabasic and ultrabasic bedrocks)
	Duricrusts/ore-cretes	CA: Fe-Mn orecretes: cryptomelane, psilomelane, todorokite, lithiophorite, rare gibbsite, goethite, "manganomelane" Silcretes: silica Phoscretes: apatite, Al-Fe phosphate	CA: U orecretes Silcretes (uraniferous) Phoscretes (uraniferous) DA: ferricretes	CA: ± ferricretes ("limonite")
Hydrography	Degree of sinuosity as a function of river facies	CA: 1.0748 TA: 1.1251 to 1.5802 DA: 1.1668 to 2.6938 (basement + foreland)	CA: 1.1157 TA: 1.0229 to 1.2118 DA: 1.5069 (foreland)	CA: 1.2754 to 1.4066 TA: 1.1029 to 1.2351 DA: 1.1789 to 1.3143 (foreland)
	Slope angle as a function of river facies	CA: 5–22° TA: 17–37° CA: 5–36° (basement + foreland)	CA: 12–19° TA: 10–35° DA: 5–10°	CA: 5–15° TA: 16–35° DA: 5–13°
	Orientation relative to bedrock structures + fluvial pattern and channel morphology	Single-channel to antler-shaped See Table 2	Dentric to parallel See Table 2	Dentric to antler-shaped See Table 2
Sediment Petrography	Grain size distribution (%)	Clay + silt: 12.2 Sand: 14.9 Pebble:38.9 Cobble + boulder: 34.0	Clay + silt: 11.4 Sand: 6.2 Pebble: 2.8 Cobble + boulder: 79.6	Clay + silt: 56.6 Sand: 12.3 Pebble: 15.2 Cobble + boulder: 15.9
	Grain morphology	See Table 3b	See Table 3a	See Table 3a
	Grain orientation ("situmetry")	See Table 3b	See Table 3a	See Table 3a

The study deals with a drainage system characterized by SSS and it is aimed to provide answers to the following questions:

- What is the impact of the different types of structural geology on the fluvial systems?
- What is the impact of the varied bedrock lithologies on the hydrography and the hydrodynamic evolution?
- What is the impact of Neogene-Quaternary climate on the drainage systems?
- To what extent can the GMS gravel (granulometry-morphology-situmetry) analysis contribute to the hydrodynamics of coarse-grained fluvial deposits?
- Is the elaborated genetic model of the fluvial drainage system applicable to all landform systems in orogenic realms or geodynamically restricted to a special state of crustal maturity?

The current study is designed to account for the genesis of the SSS in a basement terrain and to provide a manual for a holistic-modular geomorphological approach. The modular workflow chart of Figure 2 forms the platform for the investigation and interlocks methods, results, and discussion.
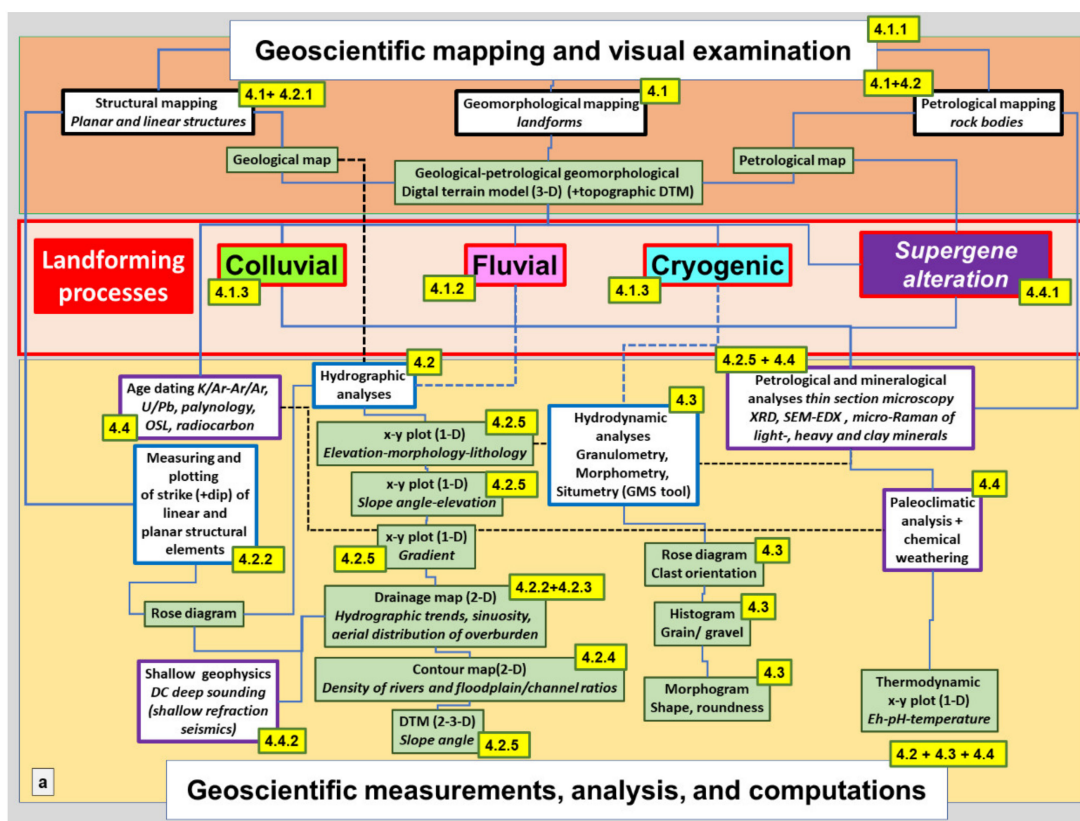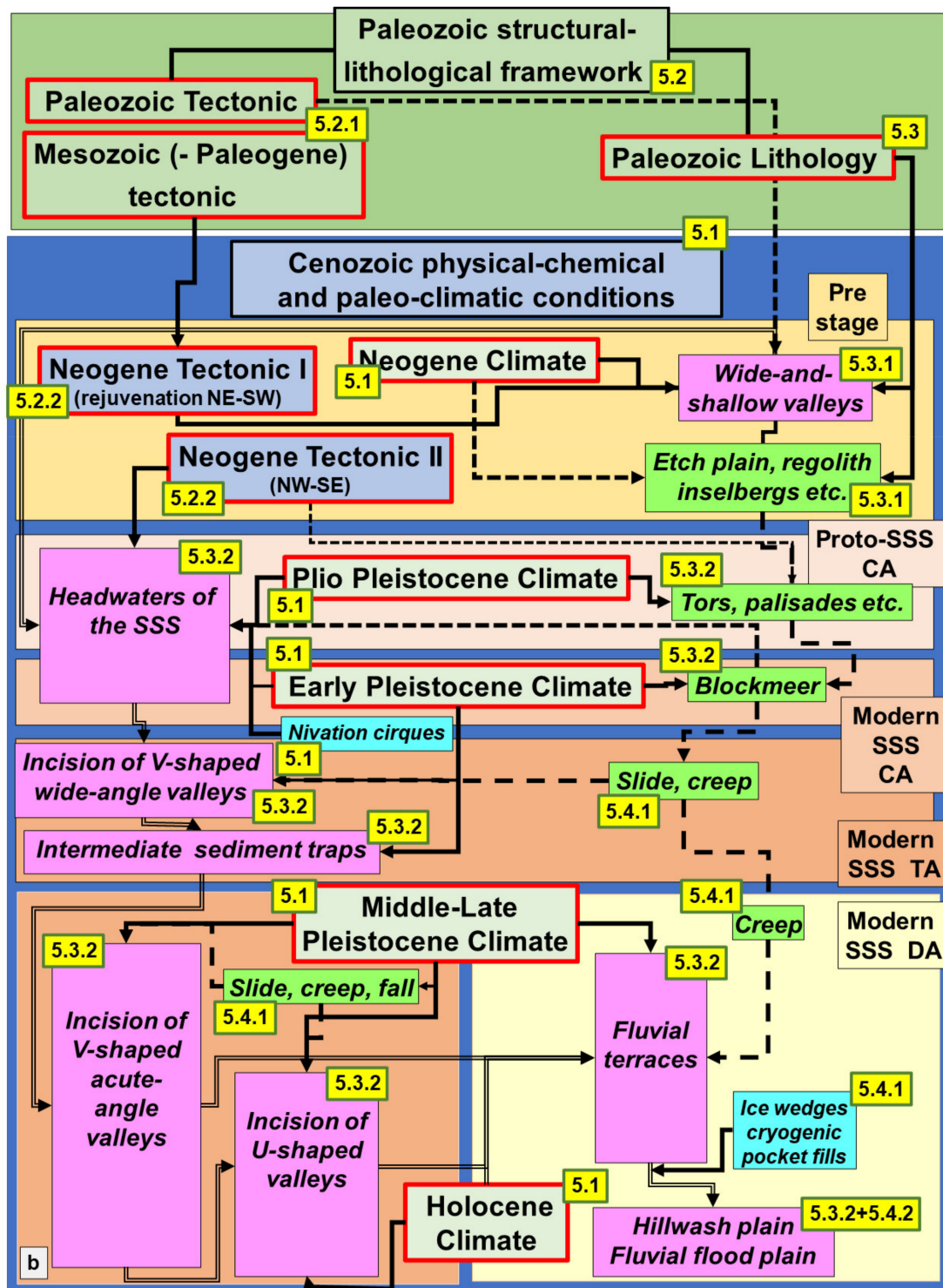

Figure 2. *Cont.*

Figure 2. Flow charts of the holistic-modular approach taken to study the SSS in a basement landscape. It is a dual-use approach flow chart placing emphasis on the methodology (**a**) and the origin of the SSS (**b**) with the land-forming processes linked by color codes. (**a**) The flow chart to link methods (descriptive diagnosis -upper part, processes center part, numerical methods lower part): Multicolored boxes: processes relevant for the SSS (see also color code in (**b**)); White boxes: Methods; Green boxes: Tools and products; Yellow boxes/framed in dark green with Arabic numerals reference to "Results". (**b**) The genetic flow chart to link genetic parameters as a function of evolutionary stages (framework, prestage, proto-SSS/CA, modern SSS/CA, modern SSS/TA, modern SSS/DA): Multicolored boxes: processes relevant for the SSS (see also color code in (**a**)); Blue boxes framed in red: Tectonic drivers and their age of operation; Beige boxes framed in red: Climatic drivers and the age of operation; Yellow boxes/ framed in dark green with Arabic numerals reference to "Discussion".

2. Methodology—A Holistic-Modular Approach to Study the Straight to Low Sinuosity Drainage Systems (SSS)

### 2.1. Strategy of the Flow Chart

The current paper takes a multidisciplinary approach, encompassing methods from geomorphology, sedimentology, structural geology, mineralogy, geophysics and radiometric age dating (Figure 2a). They are focused on landforms that are defined as physical recognizable forms or features, e.g., plains, valleys, slope, and hills of the Earth's surface, having a characteristic shape and produced by natural causes [40] (Figures 3–5).
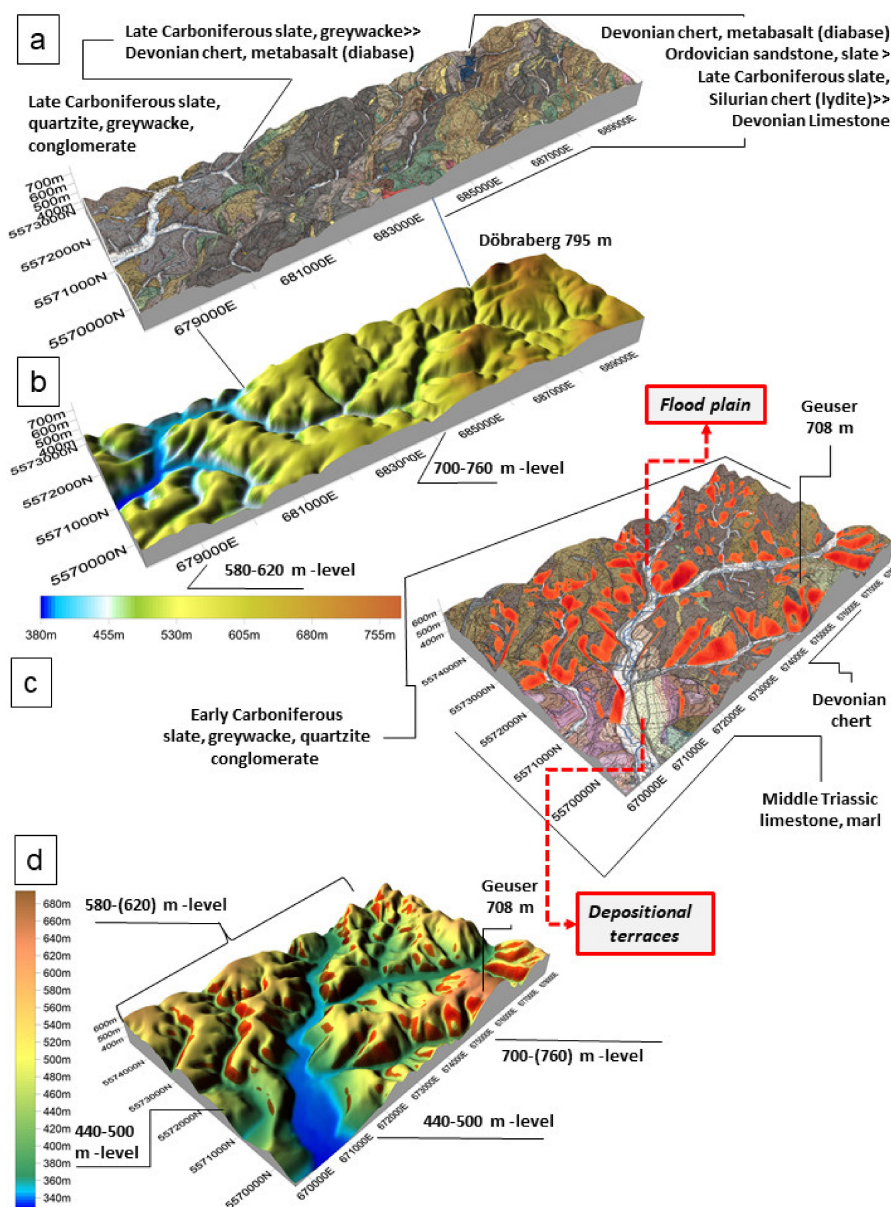
Figure 3. The drainage system in the Frankenwald (FW) (Table 1-VLG-type) in digital terrain models (DTM) The V-shaped valleys are highlighted by the slope angle shaded in red (see angle bar = midslope). Rectangles framed in red denote landforms of fluvial relevance. (**a**) Geology and the geomorphological setting in the upper reaches (headwaters = (CA)) transitional into the proximal transport area (TA)); (**b**) Excerpt of the topography and the level of paleosurfaces of (**a**); (**c**) Geology and the geomorphological setting in the lower reaches (distal TA transitional into the depositional area (DA) within the basement and proximal foreland); (**d**) Excerpt of the topography and the level of paleosurfaces of (**c**).
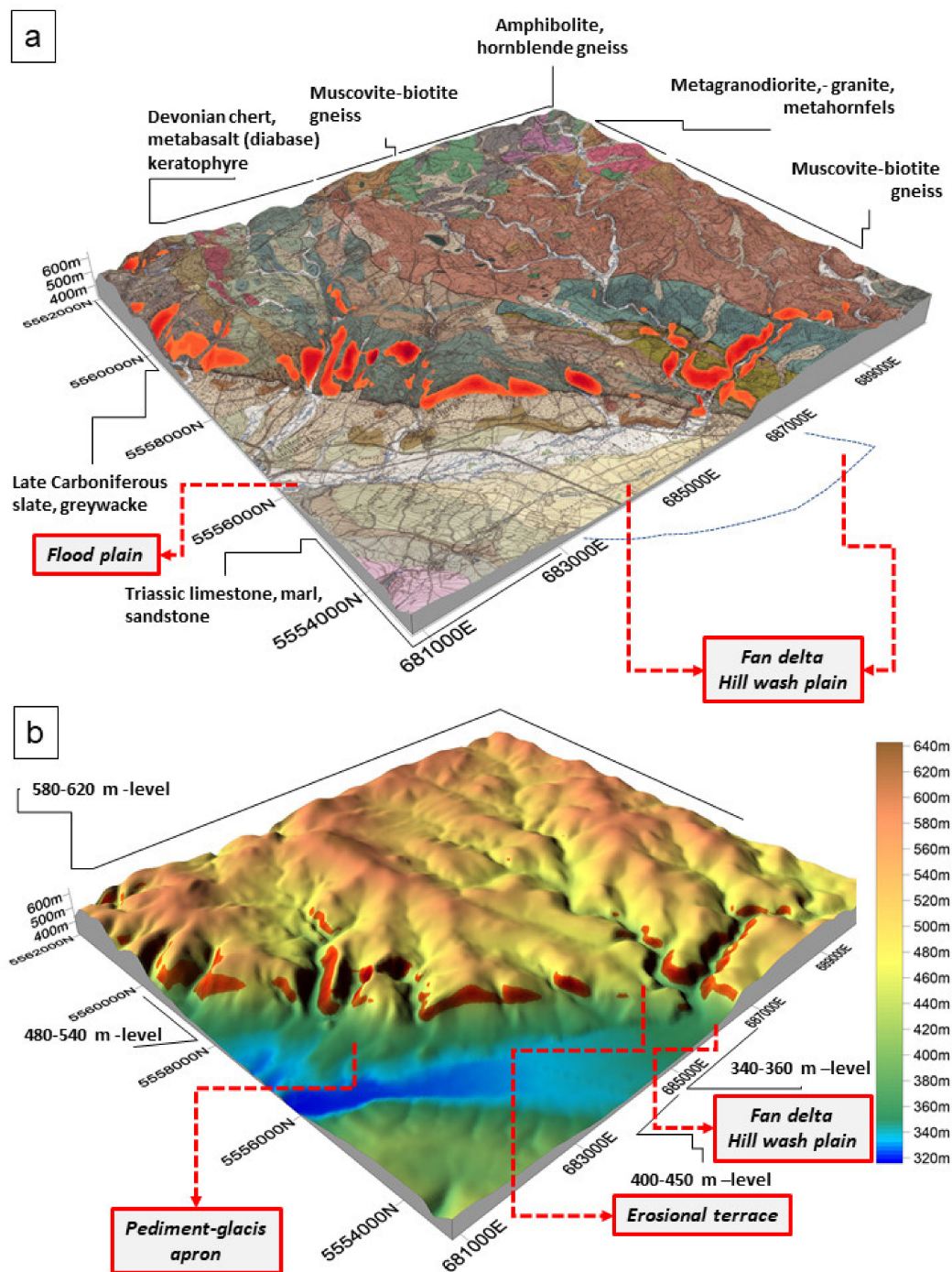
Figure 4. The drainage system of the Münchberg Gneiss Complex (MGC) (Table 1-LHG-type). For legend see Figure 3; (**a**) Geology and the geomorphological setting. Blue stippled line marks the fan onto the hillwash plain; (**b**) Excerpt of the topography and the level of paleosurfaces of (**a**).
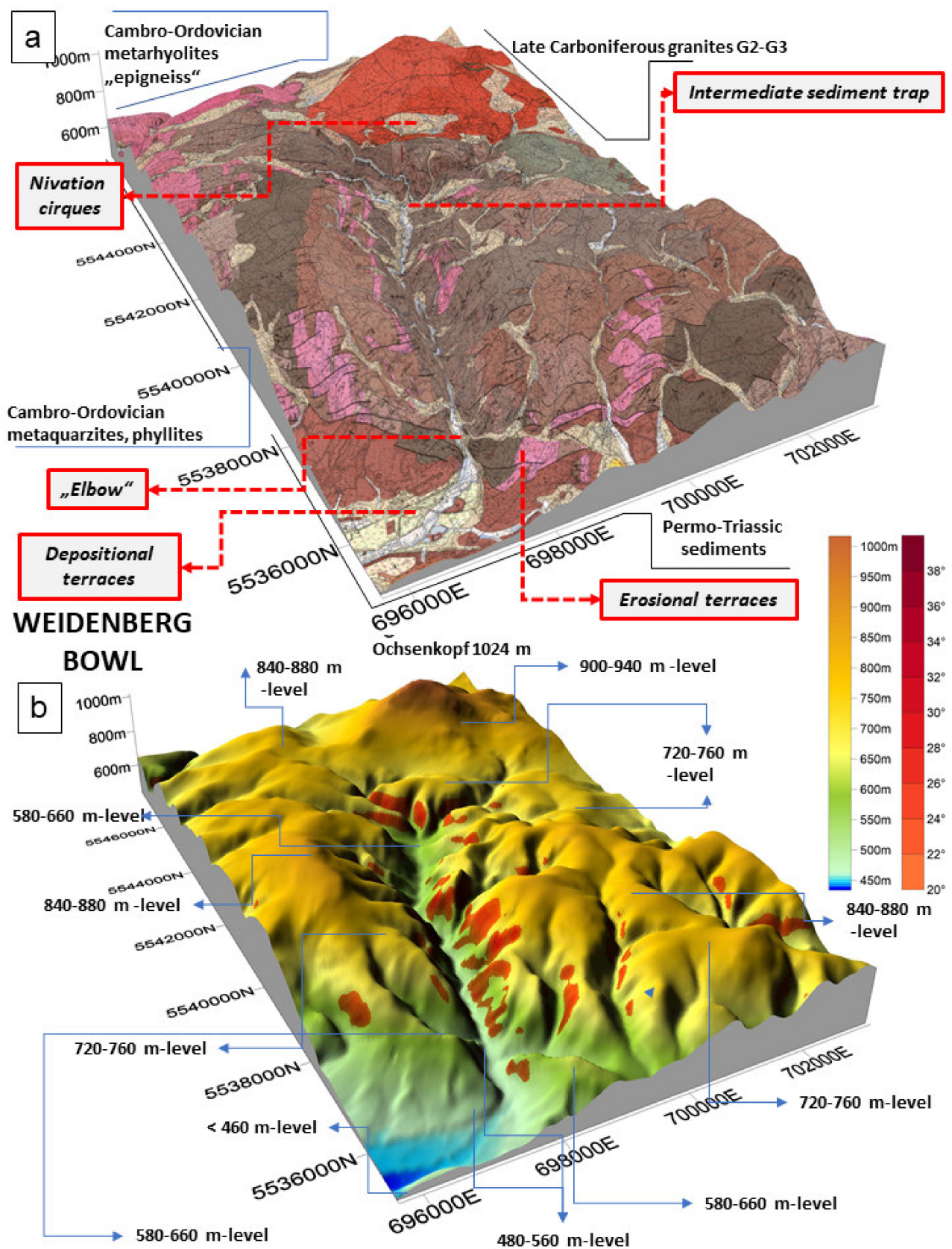
Figure 5. The drainage system of the Fichtelgebirge Anticline (Table 1-LGG-type): (**a**) Geology and the geomorphological setting; (**b**) Excerpt of the topography and the level of paleosurfaces of (**a**).

The classical geomorphology places a strong emphasis on the description of the Earth´s surface [3], whereas more recently emphasis has also been placed on measurements using digital terrain models (DTM) and different types of maps and x-y plots to achieve solutions for issues of shaping the landscape [41]. Both approaches are likewise important in providing solutions to geomorphological issues but they should not cast in the role of stand-alone-procedures. That is the reason why a holistic approach has been taken in the current study to fill in the gap between descriptive and numerical methods relevant for landform evolution. It is a sort of a "semi-automated" technique used by the senior author in applied geomorphology and economic geology in central E Africa [42].

A holistic-multidisciplinary study cannot be performed in a simple way and presented as a unidirectional workflow. The various parameters, disciplines, and methods as well as processes and landforms are closely interlocked with each other so that the links between them have to be illustrated at the beginning in a special diagram. The qualitative-quantitative approach taken in the current study is illustrated in a binary flow chart with multiple links on display and the same codes numbering the (sub)sections in the text are used in both flow charts, too (Figure 2a,b). Figure 2a is linking methods and results and Figure 2b the genetic model with the discussion. The genetic flow chart is to link genetic parameters with landforms of fluvial, mass wasting and cryogenic processes and arranged stage-wise in chronological order.

2.2. Geoscientific Mapping and Visual Examination

To create a geological and petrological mapping platform on the scale 1:25,000 is a prerequisite of any field study and of further investigations. In combination with a topographic map a composite digital terrain model (DTM) is created for each of the three study areas at the same scale (Figures 3–5). The XYZ data were obtained from "Geoportal Bayern", at a 50 m resolution, for the whole of Bavaria, in a GeoTIFF format. The GeoTIFF data were then cropped to fit the area of interest using QGIS and subsequently processed in Golden Software's Surfer to obtain a virtual 3 DTM by using the kriging method of gridding and data interpolation.

It can be used for all further geological-petrological-geomorphological terrain analyses throughout the entire study and assists in visual examination of geomorphological landforms in the field, their mapping (e.g., depositional terraces, floodplains) and the establishment of different relief generations (Figures 3–7). Furthermore, this DTM and the pertinent geological and petrological maps aid in delineating the supergene alteration zone and subdividing the regolith zone into duricrusts and argillitization (Figure 2). The first principal part named "Geoscientific anamnesis and visual examination" results in the subdivision of the three reference landform series colluvial, cryogenic and fluvial. The latter landform series is categorized into master rivers (1st order) and tributary rivers (2nd order). The 1st order rivers, Rodach (VLG-Type), Steinach (LGG-Type), Schorgast-Coserbach drainage systems (LHG-Type) are in the focus of the current investigations and used in the presentation of the results and the discussion unless stated otherwise.
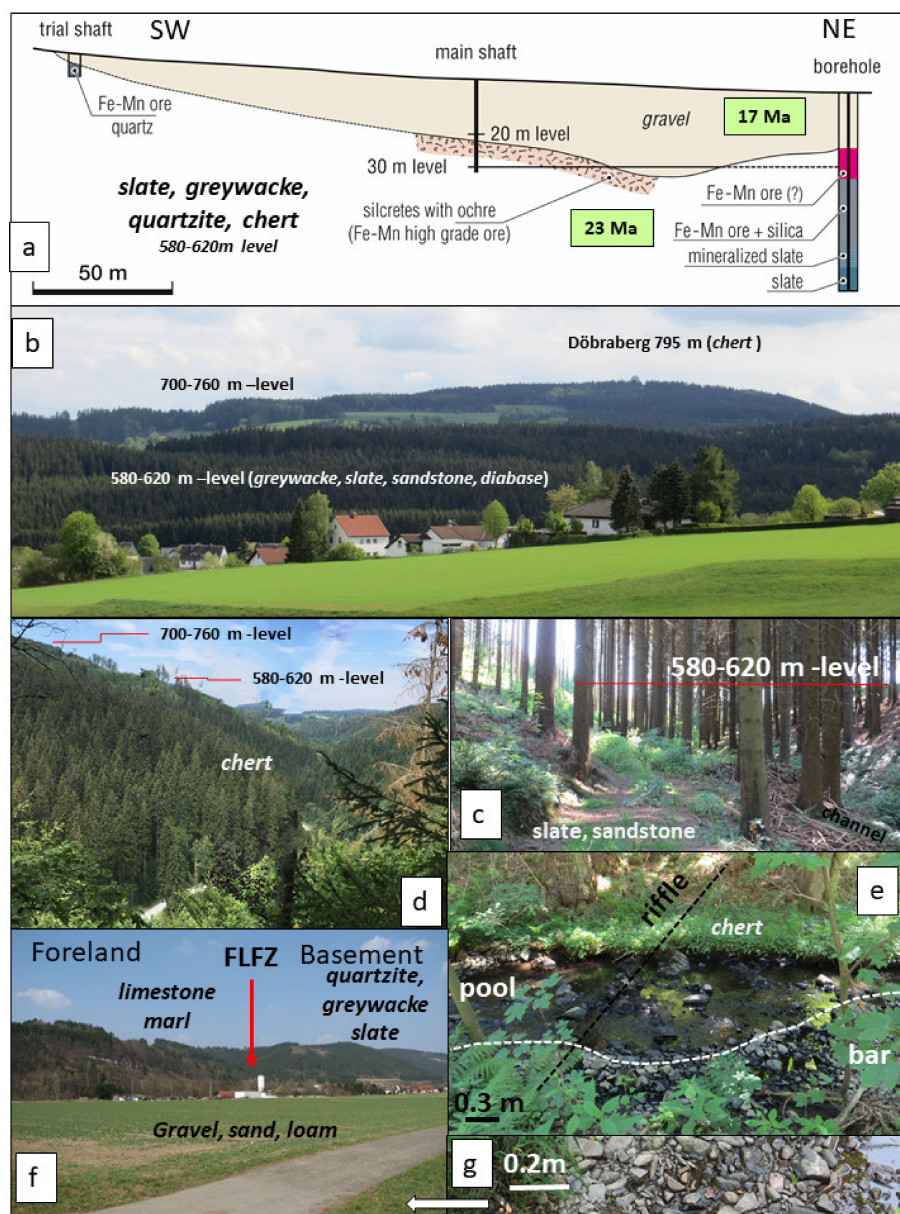
Figure 6. Fluvial landforms from the CA, TA and DA of the VLG-type (Table 1). For peneplains, erosional and depositional terraces, and floodplains see Figure 3. (**a**) Wide-and-shallow valley of the proto-drainage system (peneplain in the CA) filled with coarse-grained alluvial-fluvial deposits and Fe-Mn ore. The age of formation of the cryptomelane at the bedrock-valley floor and as cement are given in green boxes. (**b**) The monadnock of the Döbraberg representative of a relic peneplain in the CA. A wide-and-shallow valley in the foreground (see also (**a**)). (**c**) Wide-angle single-channel alluvial V-shaped valley evolved in loamy regolith near the watershed (slope angle $15° \Rightarrow 20°$, talweg angle $3.3° \Rightarrow 1.2°$). (**d**) Incision of the acute-angle single-channel non-alluvial V-shaped valley of the Wilde Rodach into the Neogene peneplains (slope angle $30° \Rightarrow 35°$, talweg angle $2.7° \Rightarrow 0.7°$) (photograph by courtesy of H. Schmalfuss). (**e**) Close-up view of the channel of (**d**) with steps and pools in Devonian chert (stippled white line = strike of bedding) and the onset of wandering channels to evolve. (**f**) Transition from the TA into the DA while crossing the Franconian Lineamentary Fault Zone (FLFZ) between the uplifted basement and the foreland at the 440–500 m level (modern floodplain = 340 m). A U-shaped valley with steep slopes and wide flood plain evolved between paired terraces (slope angle/ basement $30° \Rightarrow 35°$, talweg angle $0.3° \Rightarrow 0.2°$), in places > 35°; slope angle/ foreland $25° \Rightarrow 30°$, talweg angle $0.2° \Rightarrow 0.3°$). (**g**) Close-up view of the flood plain deposits (mainly greywacke, quartzite) of (**f**).
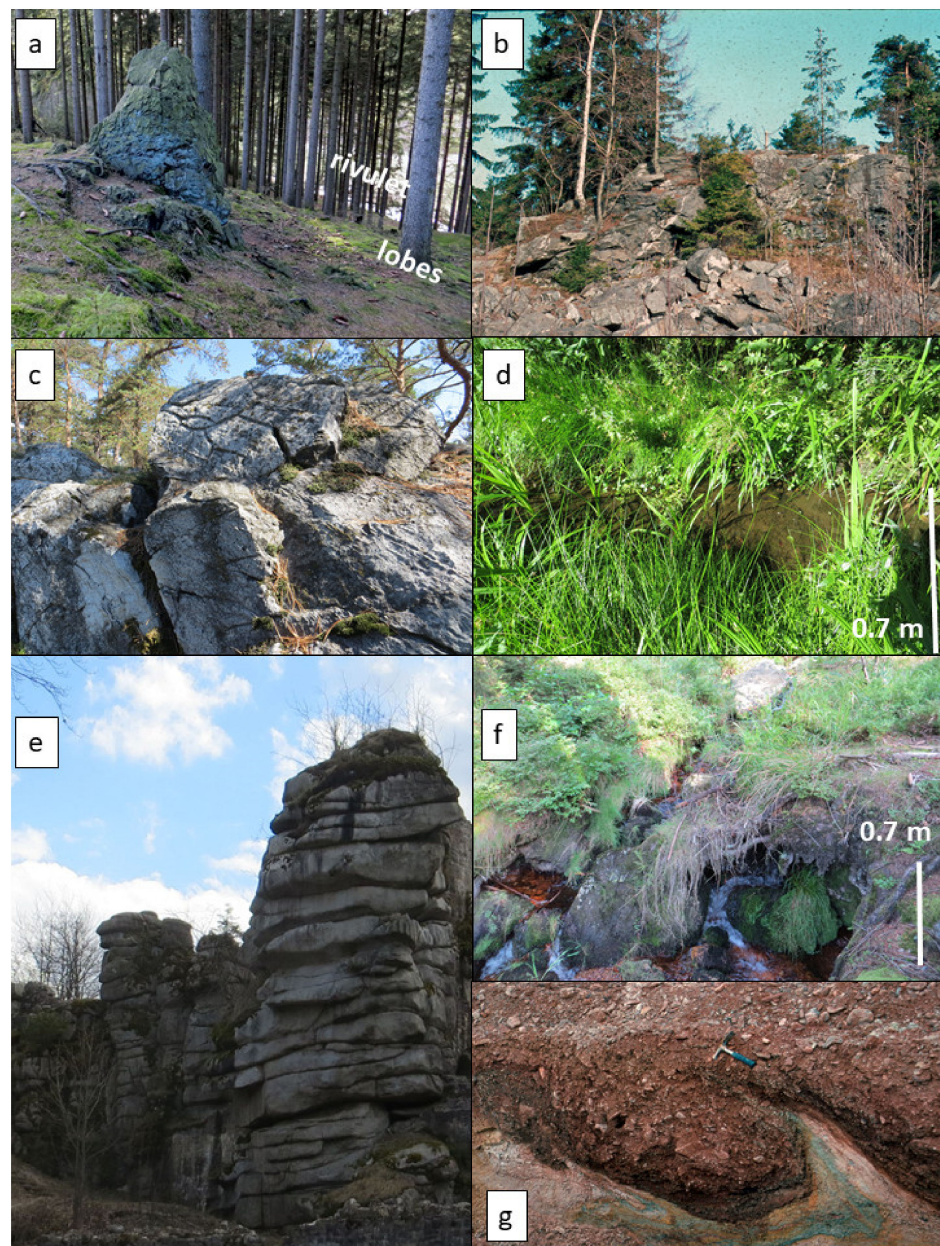
Figure 7. Landforms created by mass wasting and cryogenic processes associated in the SSS. (**a**) Pinnacle of Ordovician very angular quartzite and siliceous slates (VGL-type) on a hilltop of the 580–620 m level upslope of a straight channel (rivulet) with lobes of confined soil and talus creep, inactive on account of being densely forested by softwood trees (slope angle 25° ⇒ 30°). (**b**) Monadnock at outcrop as angular to subangular palisades (LHG-type) of eclogite-amphibolite intruded by white veinlets of zoisite pegmatoid on top of the 580–620 m level (668 m) passing from blockfields into boulder strewn gently dipping slopes (slope angle 10° ⇒ 15°). (**c**) Monadnock with subrounded exposures of bronzite-serpentinite (LHG-type) displaying typical features of "silica karst" on top of the 580–620 m level (589 m) (slope angle 15° ⇒ 20°). (**d**) The bronzite-serpentinite is surrounded by an apron of solifluction lobes deprived of any gravelly rock fragments, with waterlogged meadows. They are cut by a network of alluvial channels filled down to a depth of 0.5 m with muddy hillwash (slope angle 10° ⇒ 15°). (**e**) Rounded boulders piled up as tors on top of the Central Granite G1 (LGG-type) (slope angle 10° ⇒ 15°). (**f**) Subrounded blocks of the Core Granite G3 embedded into grus and dislodged into one of the channels of the Steinach River in the CA (LGG-type) (slope angle 5° ⇒ 15°). (**g**) Pocket in the bedrock of the Steinach River filled with cryoturbated gravel. It is overlain by fluvial gravel in the DA (LGG-type).

2.3. Geoscientific Analysis, Measurements, and Computations

The second part of the workflow chart denominated as "Geoscientific measurements, analysis, and computations" is split into two subsections, one dealing with indoor-only (laboratory) methods and another one working at the passage from field to laboratory.

2.3.1. Laboratory Methods

Dependent on the practical experience and knowledge a great deal of geoscientific identification and classification work in the field can be performed with the unarmed eye. For fine-grained, earthy and complex mineral aggregates, however, supplementary laboratory work is necessary (Table 1).

Petrographic microscopy: Routine thin section analysis was carried out in combination with optical microscopy of heavy and light minerals with 200 to 300 grains counted per sample. Heavy mineral separation was carried out for each sample to the grain size fractions richest in heavy minerals (the 3–4 ø fraction) using sodium polytungstate of a density of 2.9 g/cm^3 [43]. Approximately 70 samples were subjected to this mineralogical analysis.

X-ray analysis: X-ray diffraction (XRD) patterns are a supplement to the afore-mentioned method and were recorded using a diffractometer (Cu-Kα radiation generated at 40 kV and 40 mA), equipped with a 1° divergence slit, a secondary monochromator, a point detector and a sample changer (sample diameter 28 mm). The samples were investigated from 2° to 80° 2Θ with a step size of 0.02° 2Θ and a measuring time of 3 s per step. For specimen preparation the top loading technique was used.

Electron microscopy: Scanning-electron analyses (SEM-EDX) were carried out under low-vac-chamber conditions (1 to 10 mbar), no sputter coater was used prior to analysis. It is run in combination with the XRD analysis.

Raman spectroscopy: The micro-Raman spectra were acquired by using the Renishaw InVia Raman Microscope system, equipped with two laser sources with wavelengths of 532 nm and 785 nm and full power of 500 mW, with a CCD detector. The measurements were performed with the 532 nm wavelength laser with 1800 L/mm holographic grid, at a power of 10%, exposure time of 1–5 s, 10–20 acquisitions, using the zoom objective 50× from the Leica microscope attached to the spectrometer. The interpretation of the micro-Raman spectra was done using the LabSpec software by means of baseline correction and peak-fitting. It is the most advanced level and used for fine-tuning of the mineralogical results.

The mineralogical analyses are applied to the bedrock of the channel system during hydrographic analysis together with measurements of the elevation and morphology of the valley of the SSS (Figure 2a). The current data obtained are also of assistance during petrological fine-tuning of gravel-sized debris in the course of the hydrodynamic analyses as well as useful for thermodynamic computations of the Eh, pH and temperature, all of which are essential to constrain the paleoclimate regime operative during the Late Cenozoic when these SSS came into being [44]. The latter goal can only be achieved in context with precise age dating mentioned in the succeeding paragraph.

Age dating: For the chronological studies of geomorphological processes radiocarbon dating and the OSL dating is common practice [45,46]. Both methods do not cover the period of time from the late Pleistocene through the Neogene relevant for the current investigation. Therefore, only the classical U/Pb and K/Ar or Ar/Ar age dating methods appropriate for K-bearing manganese oxide-hydrate and uriniferous silicates and phosphates can successfully been used [47–50]. In a few places where syngenetic organic matter has been identified in Neogene sediments palynology may be useful [51].

2.3.2. Field and Desk(top) Methods

Structural analysis: To investigate the spatial relation between structural elements mapped in the bedrock and the orientation of the SSS, the strike of faults, joints, cleavage planes and fold axes is determined and statistically treated in rose diagrams in plain view. In the course of this study, the areas under consideration are subdivided into litho- and morphotectonic units, each of which is characterized by a full-circle mirror rose diagram

with 10° sectors displaying the frequency distribution by percentage values (Figures 8–10). By contrast, the overview diagram of the entire VLG-Type area is plotted as a semicircle rose diagram with 20° sectors, a technique which has been tested statistically to be sufficient for the different scales 1:25,000 and 1:200,000 (Figure 8e).
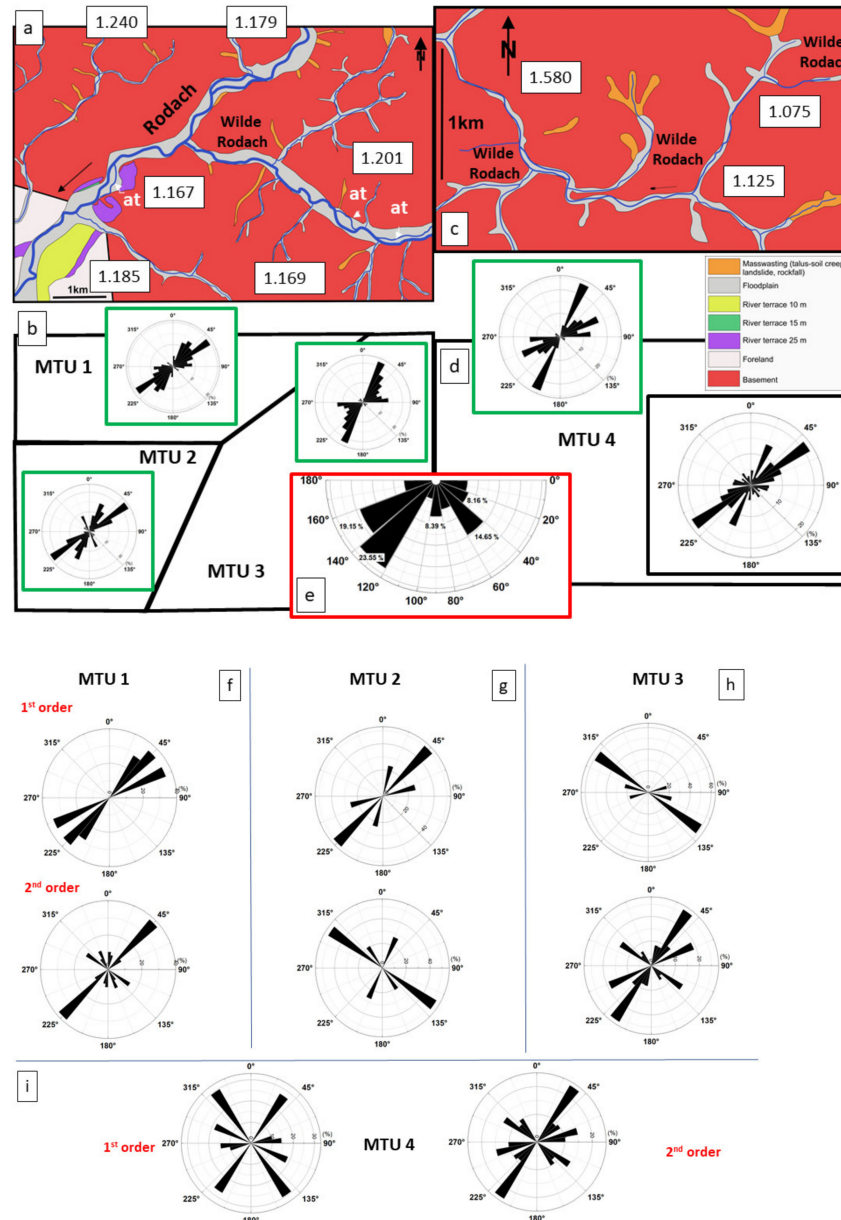
Figure 8. Litho- and morphotectonic units (MTU) characterized by the sinuosity of drainage systems (rectangular boxes) and the structural geology of the bedrock in VLG-type (see Figure 3). Fold structures (**a**–**e**) in full-circle rose diagram framed in green shows the cleavage and full-circle rose diagram framed in black shows the main fault zones (520 data). (**a**) DA and TA of the VLG-type drainage systems; (**b**) Tectonic datasets for (**a**) (MTU 1, MTU 2 and MTU 3); (**c**) TA and CA of the VLG-type drainage systems; (**d**) Tectonic dataset for (**c**) (MTU 4); (**e**) Composite semicircle rose diagram showing the orientation and frequency of faults in the Frankenwald within the Teuschnitz Syncline and the Berga Anticline (Figure 1b); (**f**) Orientation of 1st and 2nd order fluvial channels of MTU 1 (percentage of total length of the drainage system); (**g**) Orientation of 1st and 2nd order fluvial channels of MTU 2 (percentage of total length of the drainage system); (**h**) Orientation of 1st and 2nd order fluvial channels of MTU 3 (percentage of total length of the drainage system); (**i**) Orientation of 1st and 2nd order fluvial channels of MTU 4 (percentage of total length of the drainage system).
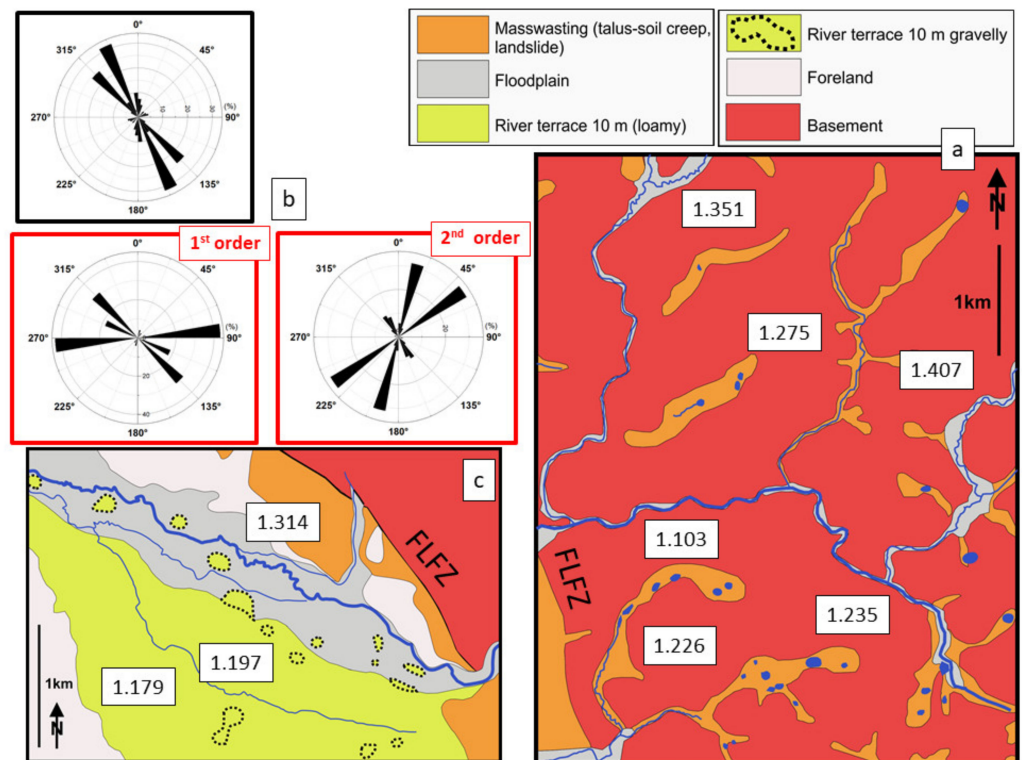
Figure 9. The litho- and morphotectonic unit (MTU) of the Schorgast drainage system characterized by the sinuosity (rectangular boxes) and the structural geology of the bedrock in LHG-type (see Figure 4). For legend see Figure 8 (160 data). (**a**) TA and CA of the Schorgast; (**b**) Fault zones (framed in black) in the MTU in comparison with the 1st (Schorgast River) and 2nd order streams systems the orientation of which are displayed in rose diagrams (percentage of total length of the drainage system); (**c**) DA of the Schorgast drainage system.

Hydrographic analyses: The hydrographic analysis makes use of x-y plots (1-D), drainage and contour maps (2-D) and in one case also of DTM (3-D). The longitudinal profiles of the SSS reference drainage systems are plotted as function of the bedrock lithology in x-y graphs displaying the elevation vs. distance from the watershed in meters (Figure 11). The data have been collected from the topographic map and in the field and the lithology is determined by mapping and petrological analyses (Figure 2a). The slope angle diagram is identical as far as the x-axis is concerned with the host graph (Figure 11a–c). The y-axis, however, is different and yields the maximum slope angle measured with a tilt sensor in the field from the divide to the footslope and calculated from the numerical data which were also used for the construction of the 3-D diagrams (Figures 3–5). The slope angle can be deduced from this sub-diagram and correlated with the three facies zones CA (zone of headwaters), TA (transport area), and DA (deposition area).
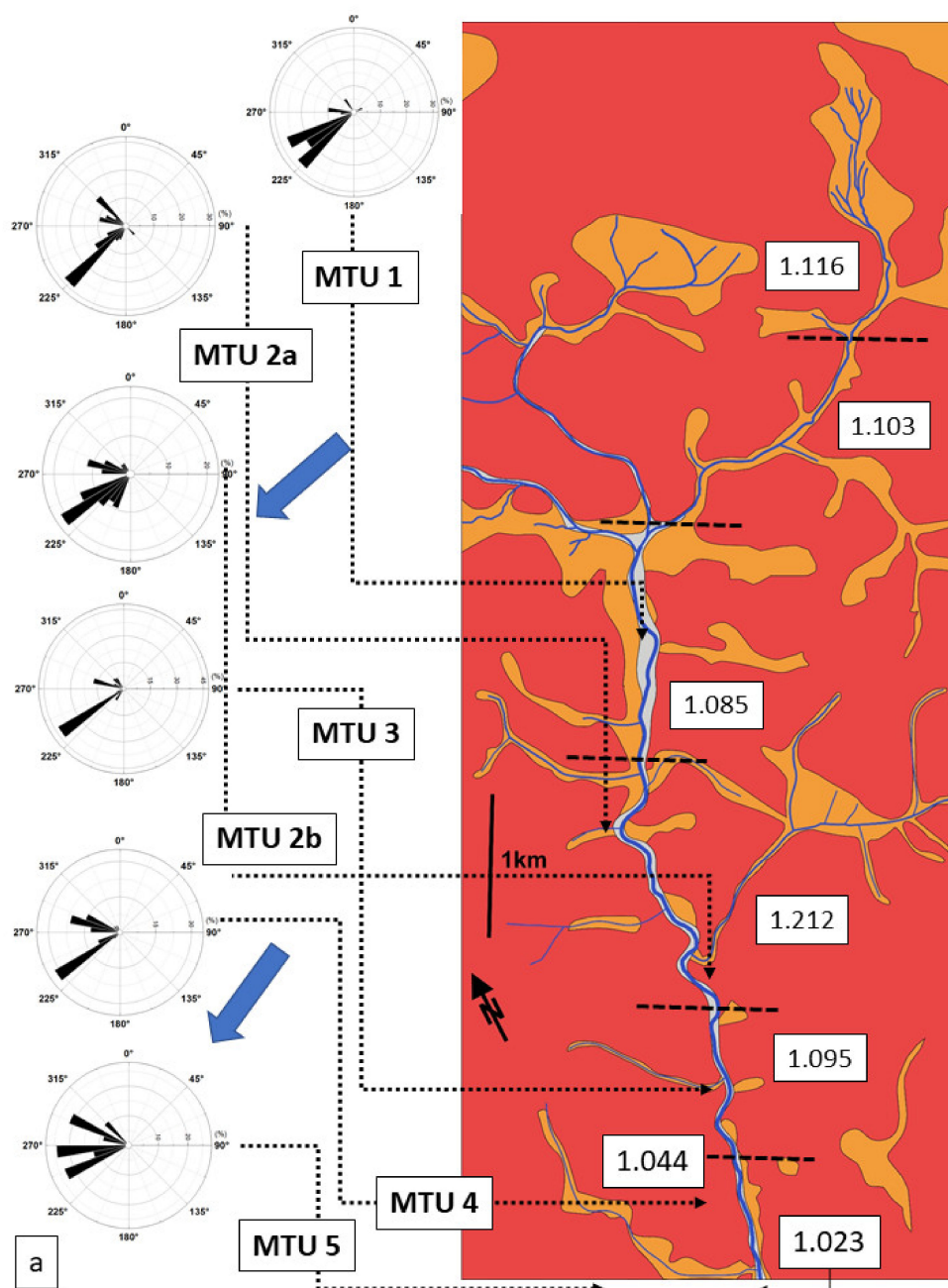
Figure 10. *Cont.*
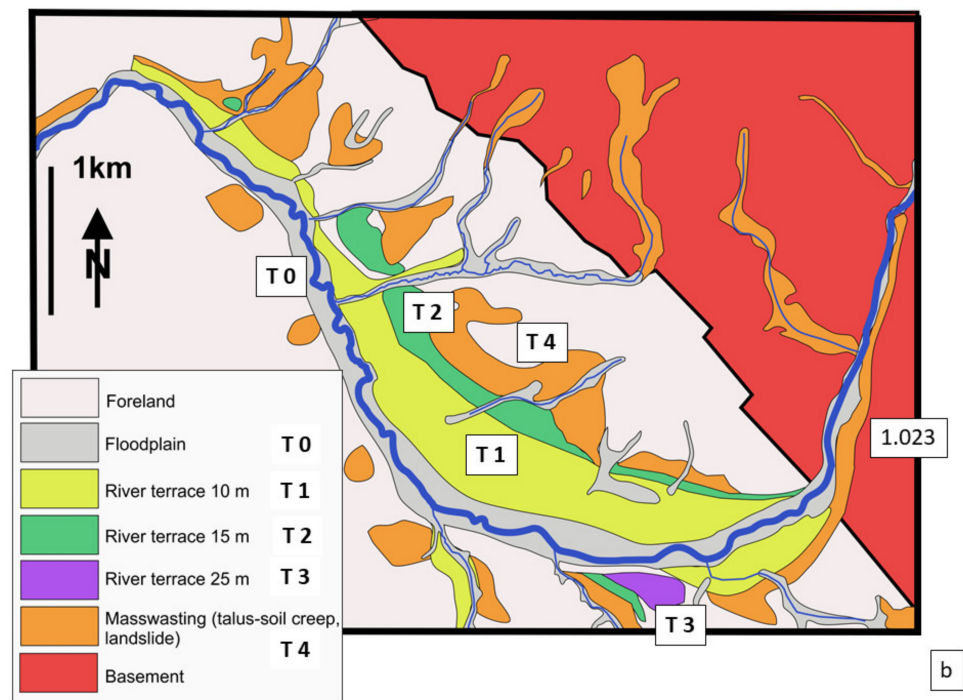
Figure 10. Litho- and morphotectonic units (MTU) characterized by the sinuosity of the Steinach drainage system and the structural geology of the bedrock in LGG-type. (**a**) The MTU of the basement CA and TA are demarcated by the dashed horizontal lines. Sinuosity is given in rectangular boxes (river sections are separated by stippled horizontal lines), full-circle rose diagram show the direction of plunge of the 2nd and 3rd order fold axes of the Fichtelgebirge Anticline (260 data). The direction of the 1st order fold axis is given as blue arrowheads. (**b**) The DA of the Steinach drainage system surrounded by a stacked pattern of depositional terraces (T1 to T4) which gradually pass into mass wasting products which were supplied by the rising basement of the Fichtelgebirge basement.
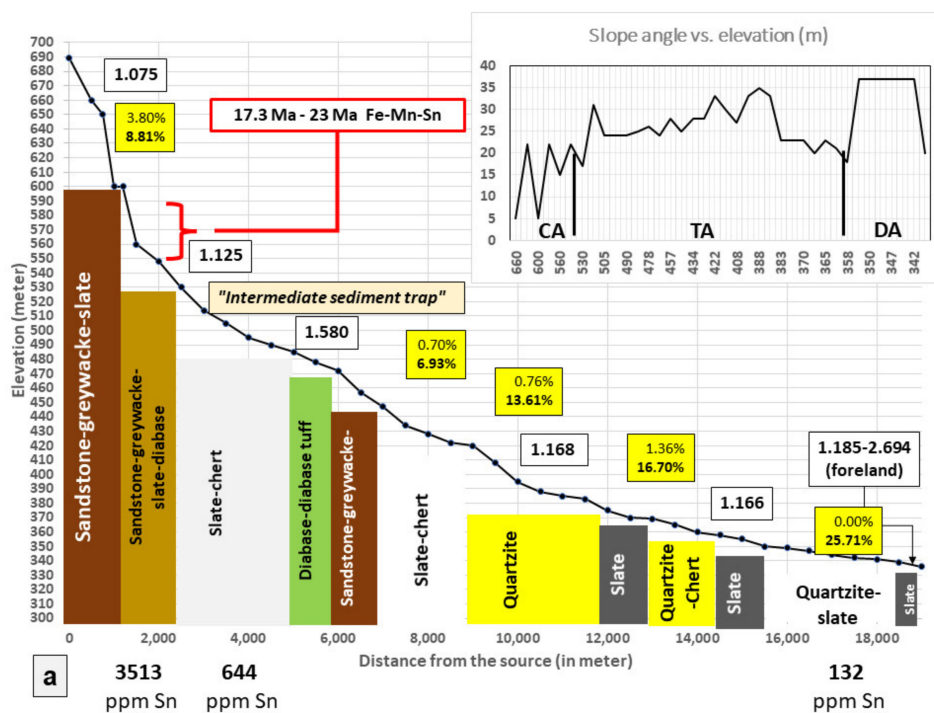
Figure 11. *Cont.*
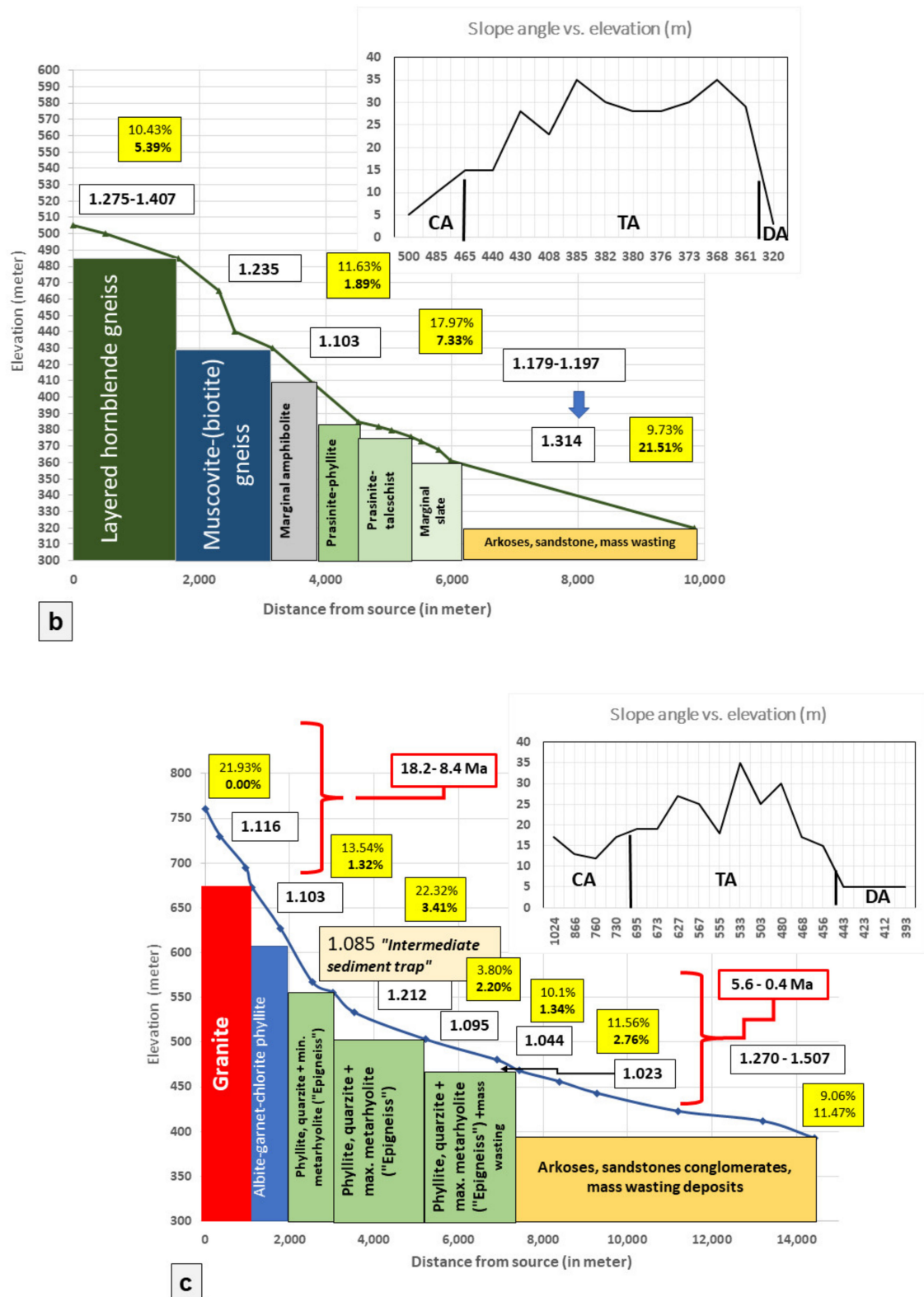
Figure 11. *Cont*.
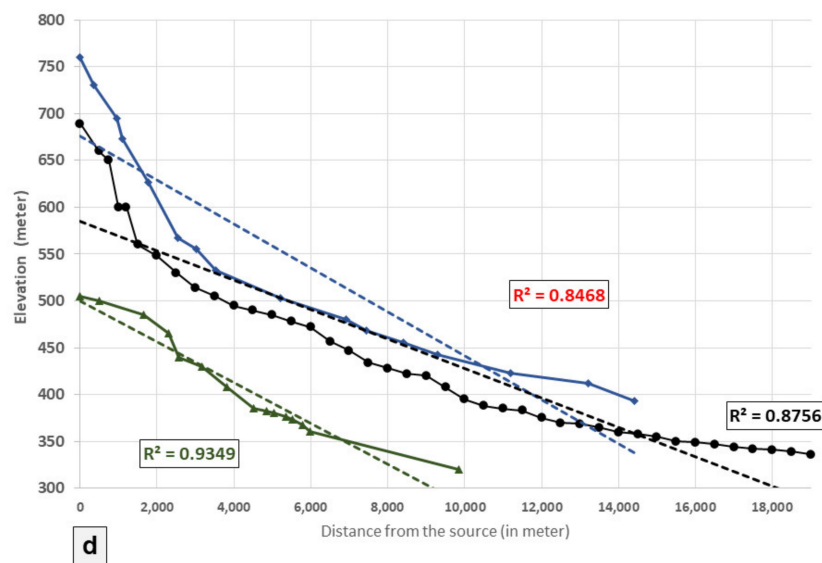
Figure 11. Longitudinal profiles of the SSS reference drainage systems as function of bedrock lithology shown in an x-y plot (elevation vs. distance from the source/watershed in meter). The sinuosity is given in rectangular white boxes. The yellow boxes denote the aerial distribution of mass wasting (normal types) and fluvial deposits (bold types). The inset displays the slope angle as a function of elevation and the subdivision into, CA, TA and DA. The data have been collected during mapping and measurements in the field: (**a**) Rodach River System (VLG-type). The red box gives radiometric age data of the Proto-Rodach, the Sn contents in ppm denote Sn concentration placers along the talweg (90 data); (**b**) Schorgast-Coserbach Drainage System (LHG-type) (42 data); (**c**) Steinach Drainage System (LGG-type). The red boxes give radiometric age data of the Proto-Steinach and the transitional period from the Proto-Steinach into the Pleistocene Steinach. (52 data); (**d**) Fluvial gradients of the VLG-(black line/full dots), LHG-(green line/triangles), and LGG-types (blue line/diamonds) between the top of the upper (peneplain) where the source of the drainage system is situated and the lower (floodplain) planar architectural elements where the river debouches in the foreland. The gradients of the previous longitudinal profiles are determined only for the 1st order drainage systems and numerically expressed as trendlines each of which shown with the correlation coefficients R^2.

The drainage maps (2-D) are simplified geological maps only revealing the geological and hydrographic relevant items such as the bedrock which is subdivided into basement and foreland (Figures 8–10). The hydrographic system is split up into the recent channel system/ floodplains and ancient floodplains/depositional terraces. To allow for a direct comparison between the direction of the talwegs of the 1st and 2nd order channels and the tectonic features, rose diagrams are added up to these maps (see previous paragraph). The degree of the sinuosity is also integrated into these composite maps. Numerical parameters to describe the sinuosity of fluvial channel systems were proposed by Horacio (2014) and Turowski (2018) [52,53]. In the current study a modified approach has been taken based upon the ArcGis software 10.2.2 and the sinuosity is calculated as follows: ratio S = channel length/valley length (Table 2). An ideal straight channel yields a sinuosity degree of S = 1.

The density of drainage systems has been calculated according to the equation recommended by Ahnert (2015) [54]: density (D) = total length of drainage systems in kilometers divided by the size of the area measured in square kilometers. The data have been obtained from hydrographic maps which were subdivided into a grid of squares measuring 1 km × 1 km and 0.5 km × 0.5 km. For each square the density of aquatic systems was calculated (software: Adobe Photoshop CS3). The interpolation maps were created using the IDW interpolation method (Inverse distance weighting) and contour lines were generated after the resultant interpolation raster map was handled by means of ArcGIS 10.2.2. The density is shown by a color key together with the sinuosity and the cross-sectional shape of the valley in Figure 12. In addition to this river density the ratio of between the size of

the floodplain and the size of the stream has been calculated and plotted side-by-side with each other.
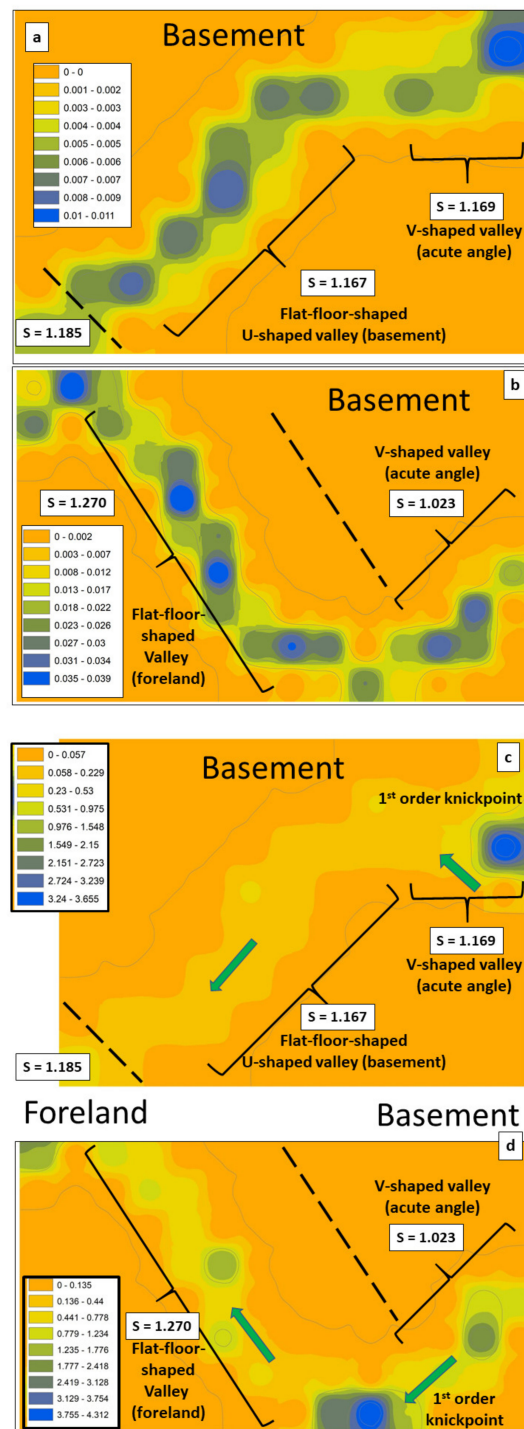
Figure 12. Density of hydrological systems per km^2 and the ratio of channel to floodplain. The sinuosity is given in white rectangular boxes, the cross-sectional shape of the valley is referred to alongside the talweg and the basement—foreland boundary is marked by the ruled boldface line striking NW-SE. The intensity is given by a color key with blue colors expressing the maximum. (**a**) Color composite map of the density of channels of the lower reaches of the VLG-Type. (**b**) Color composite map of the density of channels of the lower reaches of the LGG-Type. (**c**) Ratio of channel/floodplain of the lower reaches of the VLG-Type. (**d**) Ratio of channel/floodplain of the lower reaches of the LGG-Type.

The database of the slope angle measurements consists of field measurements measuring the inclination in some places and a topographic map on a scale of 1:25,000 with a resolution of a 5-m spacing in height of the contour lines. It enables us to achieve a high precision in x-y plots such as Figure 11 and in plan view (Figure 13). The determination of the slope angles was calculated for the same XYZ data by using Surfer's Terrain Slope Calculus gridding function and presented in two different ways. A contour map was designed for each drainage system as exemplified in Figure 13 yielding an inclination from 0 to 40°. The contour map generated by this slope data was then overlaid on the 3 DTM to show areas of relevant slope angle intervals, in this case for the sake of readability, only for the maximum slope angle greater than 25° (Figure 3c,d).
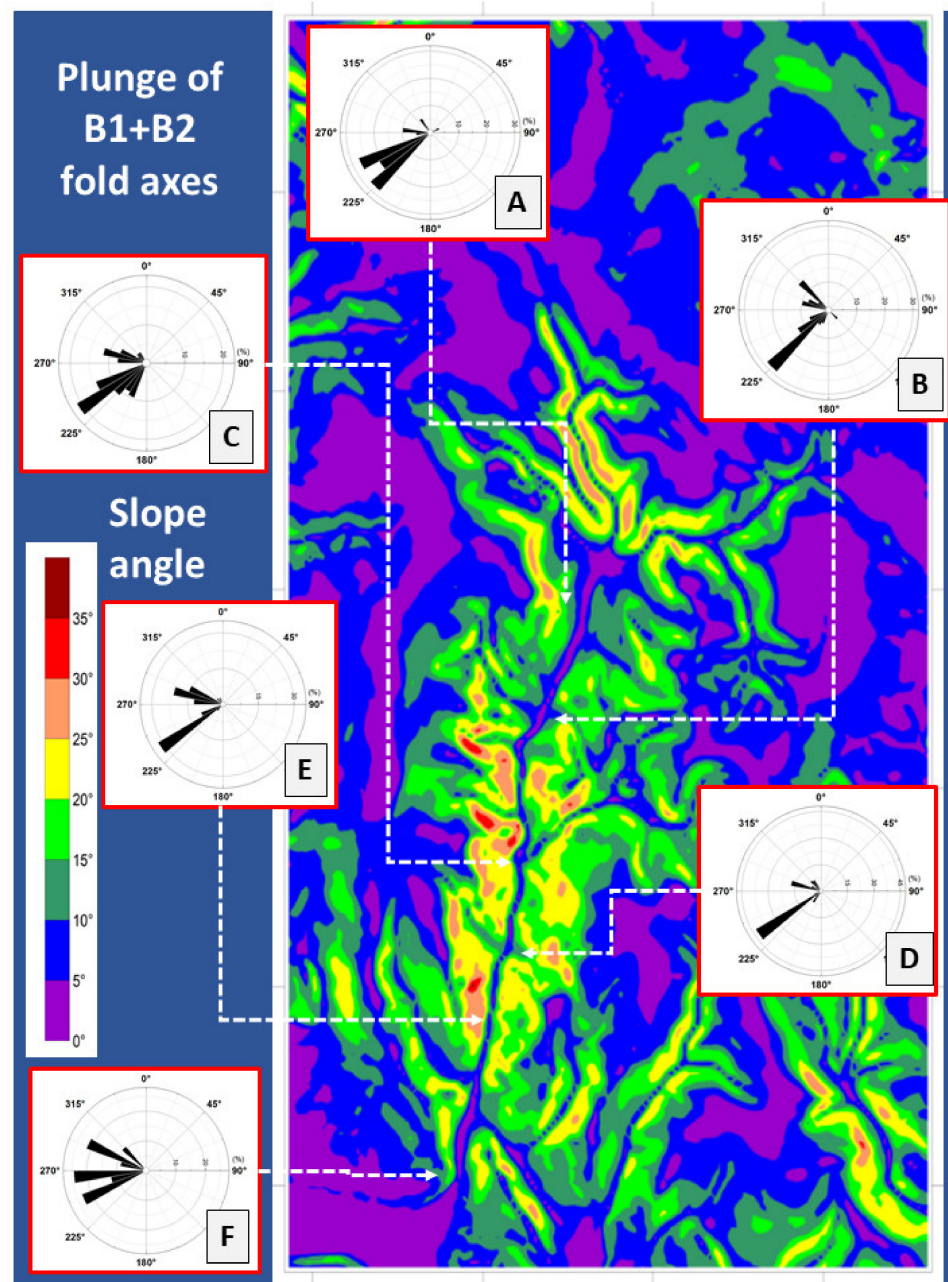
Figure 13. Slope angles (between 0 and 40°) in the Steinach Drainage System as a function of the plunge of fold axes of minor folding phases on the NW limb of the Fichtelgebirge Anticline (see also Figure 10). (**A**) to (**F**) refer to the sections mentioned in the text.

Hydrodynamic analyses: The hydrodynamic analyses focus on the unconsolidated gravel-sized lithoclasts of the three landform types (fluvial, colluvial, cryogenic) identified in the three reference areas (VGL-, LGG- and LHG types) and counts on the GMS tool (**G**ranulometry-**M**orphology-**S**itumetry), listed for the VGL- and LGG types (Table 3). The preparatory work in the field is applicable to each of the three methods. A horizontal square measuring 1 m × 1 m was delineated in the transverse and longitudinal bars of the channels and in some places on the delta plain of some micro-delta wedges produced by 2nd order rivulets debouching the lithoclasts into the 1st order river. These sampling and measuring squares can also be form an overlay for mass wasting and cryogenic products. In outcrops of cryogenic material, the same grid was used in vertical position with sectors measuring 10° to distinguish cryoturbated from fluvial deposits overriding these pockets filled up with lithoclasts (Figure 7g). The number of gravel clasts totals approx. 100 to 150 samples, with the same specimen used for the each of the three methods. The hydrodynamic analysis always begins with the in situ measurements of the clast orientation with a hand-held Brunton compass using as reference the longest axis of the clasts. Its orientation is plotted relative to the width of the fluvial channel. In the case of mass wasting processes, the strike of the ridge of the hill is taken as a baseline for the gravity-driven motion along the slope. There are a few studies mainly devoted to colluvial deposits and to a lesser extent to fluvial or glacial processes [55–58]. The cited researchers plotted the obtained fabric data on stereonets, e.g., on Schmidt nets (Lambert equal-area projection). According to the senior author´s practical experience gathered in the field of structural geology and sedimentology as an economic geologist, the stereonet projection is a valuable tool for a wide range of applications to interpret the distortion of beds by faulting and folding particularly where rather complex polycyclic processes have to be disentangled [59]. In the current situation the rose diagram, however, is the method of choice, since vertical inclination, e.g., imbrication, is negligible. To investigate the mode of transport and deposition of clasts, the use of the stereonet method is time consuming and not economic. The resultant measurements of length and angle are treated with the software ImageJ to plot semicircles with sectors in the intervals of 20°. In case of tectonic structures mirror rose diagrams are used for distinction. For each interval, the segments length was summed up and the values were normalized to 100% (Software: OriginPro 2016). It is sufficient to determine the clast orientation in plain view and if necessary, in vertical cross sections and illustrate the orientation in a rose diagram (Figure 14). The base line of the diagrams is positioned at right angle to the gradient of the fluvial channel or dip direction of the slope measured in the field.

The grain size of gravel is determined by measuring the maximum length of the clast while the individual lengths are plotted into classes of histograms revealing the frequency distribution of each size interval. Most of the samples show a lognormal distribution the graph of which is represented based on a Smooth-Kernel-type distribution function using the software OriginPro 2016.

The grain morphology of gravel cannot be done by automated procedures such as CAMSIZER (only <2000 μm) and therefore, visual inspection using morphology charts subdivided into six classes by Illenberger (1991) [60] is the most suitable method.

Some sites have been surveyed by means of geoelectrical methods using DC (low-frequency AC) geoelectric resistivity measurements according to the "Schlumberger—Array " [61]. This special four-point method enables the operator to determine the thickness and predict the lithological built-up of the overburden by the aid of the resistivities of the clay, sand and encrustations and helps to assess the mass wasting and fluvial deposits.
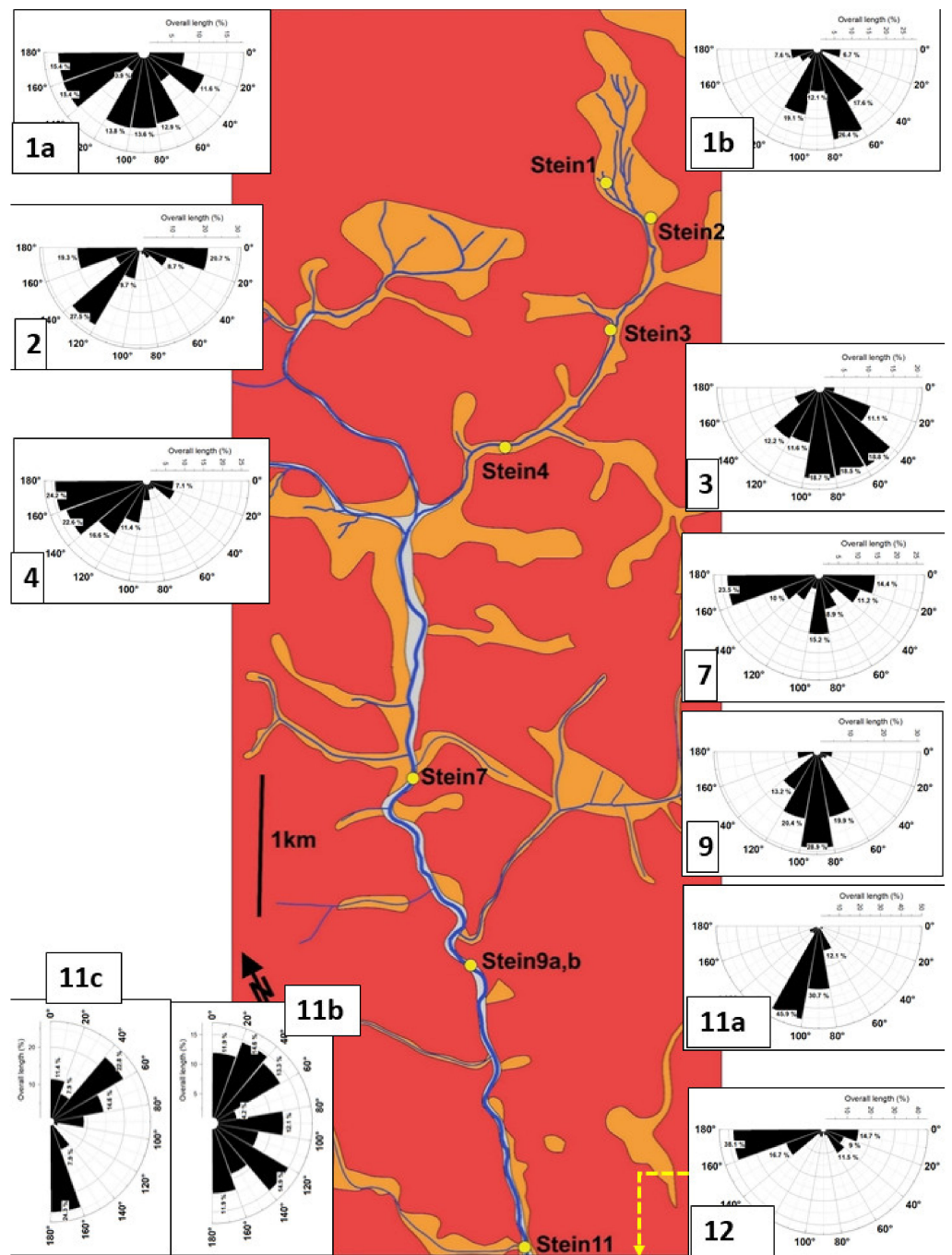
Figure 14. Situmetric measurements (orientation of the longest axis of gravel) along the Steinach River from the source to the point of entrance into the foreland of the Weidenberg Sediment Bowl. All rose diagrams are oriented perpendicular to the fluvial gradient. See also (Table 3a) for more detail. The subfigures (diagrams) and their numbers are referred to in the text.

Table 2. A classification scheme of fluvial drainage systems based on the degree of sinuosity for environment analysis. The numerical data of the fluvial reference types developing within the foreland are taken from Dill et al. (2020a) [62]. Column 1: Classification of the channel system based on visual examination in the field and using maps and satellite images; Column 2: Geological setting in the basement and the adjacent foreland; Column 3: Degree of sinuosity maximum; Column 4: Degree of sinuosity minimum; Column 5: Bedrock lithology in the basement and in the foreland.

Chanel System	Geological-Geotectonic Setting	Sinuosity Max	Sinuosity Min	Type of Drainage System vs. Structural Setting	Bedrock Lithology
Very strongly meandering	Foreland basin, basin-and-swell geomorphology ("washboard landscape") with local volcanic structures	>5 (in the test area mean 8.2916)	5	Dip-, anti-dip and strike-stream, in places, with sedimentary trap sites	Sandstone, arkose, limestone, marl, claystone, evaporite (bedded), volcaniclastic and volcanic rocks (non-metamorphosed rocks) See very-low and low-grade metamorphic rocks and felsic intrusive rocks
Strongly meandering		5 (in the test area mean 4.6159)	2	Mainly dip, anti-dip stream	
Moderately meandering	Foreland basin, basin-and-swell geomorphology ("washboard landscape") with local volcanic structures Also, in front of the basement and the basement, proper, (rarely intermediate sediment trap, deposition and catchment areas)	2 (in the test area mean 1.7209)	1.5	Mainly strike-stream	
Sinuous (high-sinuosity)	Basement, folded-and faulted ridge- and-reef geomorphology with domal structures	1.5 (in the test area mean 1.3789)	1.3	Dip-, anti-dip and strike-stream in the catchment area (CA) of rivers	(Two)-mica gneiss, mafic gneiss, orthogneiss, metaultrabasic and -basic igneous rocks (medium to high grade metamorphic)
Sinuous (low-sinuosity)		1.3 (in the test area mean 1.2357; Ca: 25%, TA: 55%, DA: 20%)	1.1	Dip-, anti-dip and strike-stream in the catchment (CA), transport (TA) and deposition (DA) areas of rivers	(Two)-mica gneiss, mafic gneiss, orthogneiss, metaultrabasic and -basic igneous rocks, calcsilicates, marble, felsic mobilizates, felsic intrusive rocks (medium to high grade metamorphic) Meta-quartzites, phyllites, Meta-felsic rocks (epigneiss), metaultrabasic and -basic igneous rocks felsic intrusive rocks (low-grade metamorphic rocks) Meta-arenites, (meta)-quartzites, slates, greywackes, chert, basic and felsic igneous rocks (very low-grade metamorphic rocks)
Straight	Basement, folded-and faulted ridge- and-reef geomorphology with domal structures	1.1 (in the test area mean 1.0859; Ca: 28%, TA: 72%,)	<1.1	Dip-, anti-dip and strike-stream in the catchment (CA) and transport (TA) areas of rivers	Meta-quartzites, phyllites, Meta-felsic rocks (epigneiss), felsic intrusive rocks (low-grade metamorphic rocks) Meta-arenites, slates, greywackes (very low-grade metamorphic rocks)

Table 3. The GMS (**G**ranulometry-**M**orphology-**S**itumetry) tool applied to the fluvial drainage systems under study in the basement as a function of bedrock lithology aimed at environment and landform analysis. ø = size of gravel specimen. In the situmetric columns the 1st and the 2nd maximum are given in degrees. The values denote the angle between the longest axis of the gravel relative to the reference line 0–180° which is equal the orientation of the width of the channels at the station of measurement. See also semi-circle rose diagrams in Figure 14. (**a**) LGG-Type of the Steinach River in the Fichtelgebirge; (**b**) VLG-Type of the Wilde Rodach River in the Frankenwald.

(a)					
				Situmetry	
Site	**Lithology of Bedrock and Debris**	**Environment Analysis and Landforms**	**Roundness and Grain Size**	**1st Max**	**2nd Max**
Stein 1a Stein 1b	Granite, vein quartz with hematite, dolerite dykes	Re-shaped nivation cirque with alluvial channels Colluvium, soil and talus creep with several small alluvial to non-alluvial rivulets and creeks (<0.5 m in width), peat bog	Very angular-angular gravel, ø 2 cm (max) Angular—subangular gravel, ø 10 cm (max)	180–140 **60** 80–60 **40**	120–60 120–100

Table 3. *Cont.*

(a)

Site	Lithology of Bedrock and Debris	Environment Analysis and Landforms	Roundness and Grain Size	Situmetry	
				1st Max	2nd Max
Stein 2	Granite	Block stream with non-alluvial fluvial channel (wide-angle V-shaped valley). Colluvium talus creep and slide cut by a small a rivulet with cascades, steps and pools filled with granitic grus	Subrounded to rounded ø 55 cm (max)	140–120 **120**	20–0
Stein 3	Albite-garnet phyllite, chlorite phyllite, platy quartzite blanketed with solifluction lobes	Non-alluvial to alluvial channel (V-shaped valley) with steps and pools Colluvium talus creep and slides	Subangular to rounded, gravel ø 12 cm (max)	<u>100–40</u> **40**	140–120
Stein 4	Phyllite-alternating with quartzite (contact- met- amorphic overprinting)	Alluvial channel (V-shaped valley) transitional into an intermediate sediment trap. Colluvium talus creep and slides	Subrounded to rounded, gravel ø 7 cm (max)	<u>180–140</u> **40**	140–120
Stein 7		Alluvial channel (V-shaped valley) Steps	Subangular to subrounded, gravel ø 22 cm (max)	180–160 **80**	100–80
Stein 9	Phyllite alternating with quartz and foliated epigneiss (meta-rhyolite)	Non-alluvial channel	Subrounded, gravel ø 24 cm (max)	100–80 **20**	120–100
Stein 11a		Non-alluvial master channel incised into basement rocks	Subrounded, gravel ø 28 cm (max)	120–100 **20**	100–80
Stein 11b		Tributary, non-alluvial, V-shaped valley delta front + channel	Angular to subangular, gravel ø 13 cm (max)	140–120 **100**	40–20
Stein 11c		Tributary, non-alluvial, V-shaped valley delta plain + channel	Subangular to subrounded, gravel ø 16 cm (max)	180–160 **120**	60–40
Stein12	Phyllite alternating with quartz and foliated epigneiss (meta-rhyolite)	Alluvial channel with steps, pools, and cascades turning into a fluvial floodplain composed of gravel-enriched loam	Subangular to subrounded, gravel ø 43 cm (max)	180–160 **20**	160–140

(b)

Site	Lithology of Bedrock and Debris	Environment Analysis—Landforms	Roundness and Grain Size	1st max	2nd max
CA	Ordovician slates, sandstone, residual clay	Relic large-and-shallow valleys/peneplain, incision of straight stream single channels, non-alluvial to alluvial, colluvium soil and talus creep	Subrounded gravel, ⌀ 15 cm (max)	180–160° **120**	40–20°
TA	Devonian chert	Straight to low-sinuosity streams, flood plains, pools, riffles, steps	Subangular bar to rounded gravel ⌀ 30-40 cm (max)	120–100° **20**	140–120°
DA	Lower Carboniferous slates	Low-sinuosity to meandering streams with wide floodplain and stacked pattern of terraces within the basement and foreland	Subangular (channel) to sub rounded (bar right bank) gravel ⌀ 15-50 cm (max)	120–100° **40**	<u>160–120°</u>

CA, Catchment Area; TA, Transport Area; DA, Deposition Area (Transitional). <u>140–100</u> = wide-angle sector (the frequency between the partial maxima is <2%), **20** = difference between maxima.

3. Geological and Geomorphological Setting

3.1. Geological Setting

The Saxothuringian Zone is a geodynamic unit of the Central European Variscides which subsided during the Cambro-Ordovician as a rift basin NW of the Moldanubian Zone [38]. It is located at the NW edge of the Bohemian Massif, a basement block which has been shared in by Austria, the Czech Republic, Poland, and Germany where it is uplifted

along the FLFZ by as much as 1000 m relative to the Permo-Mesozoic foreland (Figure 1b,c). From the Precambrian through the Lower Carboniferous, a great variety of sedimentary and volcanic rocks formed in this basin until the Visean when tectonic disturbances put an end to the basin subsidence during the main phase of the Variscan Orogeny. This scenario is true for the autochthonous Frankenwald (FW) and Fichtelgebirge (FG) (Figure 1b,c). The Münchberg Gneiss Complex (MGC) is, however, an allochthonous unit that was shifted towards the NW over the FG and emplaced by thrustal nappe movements into its present position. In the MGC, we are faced with an allochthonous synform with a dual litho-stratigraphic subdivision into the "Liegend-Serie" (footwall series) and the "Hangend-Serie" (hanging-wall series) (Figure 1). The Early Paleozoic country rocks of the Fichtelgebirge (FG) are intruded during the Late Carboniferous and the Early Permian by granites. The Mesozoic foreland is made up of Permian to Late Cretaceous sediments. Sediments mainly of Triassic age form the basis of the depositional area of the SSS and the bedrock of the meandering drainage systems discussed in a precursor study of Dill et al. (2020a) [62].

3.2. Geomorphological Setting

The NE Bavarian Basement forms part of the morphostratigraphic and morphotectonic crustal units in Central Europe described by Zöller et al. (2017) [63]. The geomorphological evolution of this basement at the western edge of the Bohemian Massif covers a timespan from the Neogene to the Recent. The basic post-war geomorphological study in the course of which a large area of the basement was mapped on a small-scale topographic map and various levels of relief generations were singled out was published by Thauer (1954) [64]. This purely descriptive study was backed then by paleopedological studies conducted by Strebel (1955) [65]. The timing of the paleosurfaces and terraces encountered in the field at various heights, however, has only been approximated by morphostratigraphic correlation and lacks any radiometric dating still today. There have no chronological data published during the last 70 years relevant for geomorphological processes in the basement others than those used in the current paper. By and large, the basement was taken as a provenance area for marker lithoclasts to create models describing the evolution of the foreland river systems Main and Donau during the Late Cenozoic [66–69]. For the pertinent fluvial landforms no radiometric age data have been provided either, excluding the post-glacial period [68].

4. Results
4.1. Landforms—Identification, Mapping, and Interpretation
4.1.1. Definition and Classification of the Drainage Basin

The 1st order classification scheme of the drainage systems is based upon the metamorphic grade of the bedrocks according to Bucher and Grapes (2011) [70] and the presence of granitic rocks (Table 1). The regional metamorphism of the Variscan Orogeny during the Paleozoic created a great variety of lithologies that can be held accountable for the marked differences in the built-up of landforms during the Neogene and Quaternary. The higher the metamorphic overprinting of the bedrocks, the higher the amount of high-T silicate minerals which are highly vulnerable to chemical weathering. Thereby, the impact of the bedrock on shaping the Cenozoic landscape diminishes because it signifies a loss of structural guidelines for the drainage systems due to the reduced rock strength of the crystalline rocks flanking the valleys—see also Section 5.2.1.

On a 2nd order level, each of the three compartments is subdivided with regard to the two principal groups of methods described in the flow chart of Figure 2a (geoscientific anamnesis and visual examination, geoscientific measurements, analysis, and computations).

The 3rd order classification in the hierarchy is focused on the prevailing channel processes responsible for the tripartite zonation along the talweg. It starts off with the headwaters (=CA) in the hinterland and the provenance area of the fluvial sediments. The three drainage systems are bounded upstream by a watershed forming the natural

boundary. Erosion is operative in the upper reaches of the drainage system causing a retreat of the slopes and the incision into the subhorizontal paleosurfaces. It is denoted by a sudden change in the gradient and the valley slope (Figure 11). The CA passes downstream into the area where transportation (transportation area = TA) of the sediment load prevails over erosion, albeit intermediate sediment traps can still be delineated along the talweg. The final section is called the depositional area (DA) where as a consequence of a sudden reduction in the transport capacity of a flood flow gives rise to flood plains (Table 1) (Figures 9c, 10b, 11a–c and 12). Prior to the quantitative treatment of the hydrographic issues, the basic landforms need to be identified, interpreted, and mapped relative to their topographic position in the DTM (Figures 3–5).

4.1.2. Fluvial Processes and Their Landforms

Objects and purpose (CA): Unless the fluvial landforms in the study area are identified, mapped relative to its topographic position and documented in 2D or 3D plots, a sound platform to build upon does not exist for further quantitative treatment of the hydrographic and hydrological issues (Figures 3–5).

The headwaters and relic landforms: The SSS have their beginning in the CA, where a stacked pattern of paleosurfaces truncated a great variety of basement lithologies at different altitudes, the maximum height of which is reached at 940 m a.m.s.l. in the Fichtelgebirge study area [71] (Figures 3–5). The term peneplain is used here for a subhorizontal planar landform which is still sparking a lot of genetic investigations [72–75]. There is common consensus that these paleosurfaces are irregularly shaped, uneven plains, with low relief. In places, they may show a considerable relief similar to what has been named etch surfaces in the Sudetes Mts. at the eastern edge of the uplifted Variscan basement block by Migón (1997) [76], updating "Büdel´s Doppelte Einebnungsfläche" [77]. The paleosurface with the largest extension of approx. 2500 km^2 has largely been preserved in the study area at an altitude between 580 to 620 m and cuts across different lithologies exposed in the FW, MGC and the FG (Figures 3–5). The fluvial dynamics during the prestage of the SSS has not been precisely proven by sedimentological features or dated [64]. Along the boundary between the FW and MGM a relic wide-and-shallow drainage system has been preserved [50] (Figure 6a). The NE–SW trending alluvial-fluvial channel system has been filled up with silcretes and pebbles and cobbles of quartz (Figure 6a). These shallow depressions passing into the CA of the SSS gave birth to their embryonic rivulets of the fluvial system under study. The channel pattern across these SSS varies from straight non-alluvial to alluvial single channels in the CA of the VLG-type into alluvial multiple channels of the LGG-type. It is called dentritic to parallel with cascades and step-pools according to Easterbrook (1999) [37]. It grades into a wide-angle V-shaped valley (Figure 6c).

The transport area (TA): The transition downstream into the TA is marked by change in the valley profile as V-shaped gorge-like valleys incise into the relic channels of their predecessor fluvial systems (Figures 3–5 and 6d,e). Albeit denominated TA, there are also river sectors with conspicuous sedimentation. In the LGG-type an intermediate sediment trap named herein "Warmensteinach Bowl" can be recognized by its wide flood plain and drastic lowering of the slope angle prior to the Steinach River's incision into the rigid parametamorphic country rocks (Figure 5). The upstream trap of sediments, results in an intensification of the channel erosion and greater downstream sediment supply and transport [78] (Figure 5).

The depositional area (DA): In a cross-sectional view of the VLG-type the V-shaped valley converts downstream into a U-shaped valley. It maintains its steep hill slopes constituted by quartzite and chert while the floodplain is considerably increasing its width (Figure 6f,g). In the VLG- and LGG types, the depositional behavior of the rivers only differs from each other by the absence of terraces within the basement, e.g., the LGG. Its acute-angle V-shaped valleys abruptly turn into a vast floodplain bordered by a tripartite set of terraces along the low scarp of the valley. The most elevated one is located as many as 40 to 50 m above the present-day talweg [79–81]. The sediment load is in both

cases dominated by gravel and abrupt changes in the valley morphology as well as flow direction as the rivers during their incision made contact with faults and lithologies which put up sufficient resistance to change the course of the fluvial system. The LHG-type channel systems lack these landforms owing to the missing bedrock characteristics and a considerably high river gradient (Figures 9c and 11d). In essence, these paired and unpaired terraces formed as a result of two different modes, a fact which is especially well-documented in the LGG-type, where cut-and-fill structures exist with each other in space but different in time (see discussion).

The grain size in the DA of the LHG-type, however, is in stark contrast to the equivalent deposits mentioned previously. The MGC´s gravelly and argillaceous bimodal sediments eventually are spread across a fan-shaped large plain (Table 1, Figure 4). Emmert and Weinelt (1962) [82] reported quartz, black chert, diabase, prasinite, amphibolite, gneiss and late Triassic sandstone to contribute to the gravel assemblage. The sediments gain a thickness of as much as 6 m and an outward appearance of a fining-upward grain size gradation typical of point bar units in the lower part. This sedimentary feature fades out towards the top. Similar sediments have been described from the badland sediments where confined drainage systems (fluvial deposits) give way to unconfined ramifying drainage systems with sediments called hill wash sediments spread between buttes [83,84].

4.1.3. Mass Wasting and Cryogenic Processes and Their Landforms

Objects and purpose: In combination with the processes mentioned under 4.1.2 mass wasting is a decisive modifier of the valley slope leveling it to different intensities, under different degrees of wetness and at different speed of motion by slide, flow, fall or creep, while static cryogenic features are markers of the glacial to periglacial climate regime related in time and space with the evolution of the SSS.

Mass wasting processes: Mass wasting processes are operative in all study areas and they are responsible for the poorly sorted sediments mantling the gently inclined foot slopes of the SSS valleys as well as forming patchy blankets on the subhorizontal paleosurfaces below and above the steeply dipping midslope (Figures 3–5—see steeply dipping mid-slope marked in red). In some valleys, additional granulometric, morphological and situmetric analyses, however, are necessary to distinguish the various gravelly deposits during mapping (Section 4.2.5). Numerical representation has been achieved and given in Table 1 for the CA, TA and DA of each drainage type.

The strength of the mass wasting processes can be deduced from the residual land-forms exhumed on top of the most elevated hills as the debris have been washed out downstream into the TA and DA (Figures 3–5 and 7a–f). From the VLG to the LGG types the number and size of monadnocks erecting from the various paleosurfaces increases accompanied by an enhancement of the roundness of the bare bedrock at outcrop as well as their fragments scattered in the apron around (block field). Pinnacles of very angular Ordovician quartzites and siliceous slates are the most common remnants of confined soil and talus creep of the VGL-type (Figure 7a). In the study area of the LHG-type even moderate variations in the chemical and mineralogical composition of ortho-metamorphic bedrocks provoke different mass wasting-induced landforms and grain morphologies (Figure 7b–d). Metabasic rocks (eclogite, amphibolite) are found surrounded by small blockfields resembling those recorded from many periglacial study sites proximal to the outcrop of metamorphic rocks [85,86]. By contrast, outcrops of metaultrabasic (serpentinite) rocks are depleted in gravel-sized clasts but surrounded by an apron of fine-grained colluvial material instead. When undergoing chemical weathering features of a silicate karst with karren and rillen appear. These fine-grained mass wasting products clog the fluvial drainage systems of the SSS downstream in the TA with a muddy "slurry" and contribute eventually to the hillwash planes in the DA. Mass wasting in the LGG-Type area results in the well-known tors derived from syeno- and monzo-granites in a way similar to many granitic terrains elsewhere when deprived of their regolith (Figure 7e) [87,88]. These landforms and their dislodged blocks present in the upper reaches of the Steinach River

attained the highest degree of roundness ever (woolsack) while being embedded into a thick layer of grus *sensu* [89]. Judging from the landform series observed in the CA and upper reaches of the TA the mass wasting processes is mainly due to talus and soil creep, block sliding, topple and rockfall. Earth flows are subordinate in size and intensity in the study area relative to the afore-mentioned types and only play a significant part where metaultrabasic rocks such as bronzite serpentinites are exposed in the CA (Figure 7c,d). These silica-deficient magmatic rocks are surrounded by an apron of fine-grained weathering loam which increases the rivers' suspended load when washed downslope.

Cryogenic processes: The impact of cryogenic processes on the evolution of the fluvial drainage system can be verified in the CA and DA of the LGG-type where pockets in the Lower Triassic bedrock of the Steinach River are glutted with matrix-supported gravel that has undergone intense cryoturbation (Figure 7g). In the CA of the Steinach River between 720 and 940 cirques are arranged in a staircase-like way (Figure 5) [90,91]. They are filled today with granitic grus and dislodged boulders, separated by lips. They contribute to the bed load of the Steinach River. The concave surface expressions are interpreted in the current setting as nivation cirques rather than relic cirque glacier [92–97]. In conclusions, relic periglacial landforms exist at the beginning (CA) and end of SSS (DA).

4.2. Hydrography of Drainage Systems vs. Compositional and Structural Variations of the Bedrock

4.2.1. Tectonics and Bedrock Lithology in the Study Areas

Objects and purpose: A tectonic analysis is a pre-requisite for the geomorphological follow-up study of the drainage system. It involves statistical spatial treatments of cleavage, joint and fault planes as well as fold axes and handled in the same way as it is performed for the drainage system itself to assure equivalent datasets. The tectonic part is conducted according to the basics published by Fossen (2010) and Lisle et al. (2011) [98,99].

The structural geology at the western edge of the Bohemian Massif is subdivided into two different phases both of which have strong implications on the drainage network under study (Section 4.2.2). The younger Saxonian tectonic deformation or post-Variscan tectonic, a fracture-and-fold tectonic, comprises a protracted history of extension and graben evolution beginning during the Triassic with phases to be observed still during the Neogene and Pleistocene [100–102]. This fault tectonic is syngenetic with the SSS at least during its latest phases. The older structural deformation in the Variscan Basement ended during the Late Carboniferous. The tectonic and lithology of the bedrock constitute the endogenous framework within which the SSS develop. There is one prominent linear fold element common to each of the three study areas striking NE-SW and plunging towards the SW homoclinal with the course of the SSS. From the VGL-type through the LGG-type to the LHG-type the fold axes, however, become more and more overprinted as a morphotectonic element (Figure 1) [71,80–82,103–107].

4.2.2. Channel Network and Structural Geology

Objects and purpose: The morphotectonic analysis involves a direct comparison between the basement tectonic and spatial elements of the drainage system to figure out the marker guidelines for drainage patterns across the SSS.

Similar morphotectonic studies on the most recent tectonic movements provoking changes in the drainage network have been made at the NE edge of the Bohemian Massif, Czech Republic, along the deep-seated lineamentary Sudetic Marginal Fault [20,108]. This fault is a pendant to the FLFZ at the NW edge of the Bohemian Massif. Unlike many papers devoted to the neotectonics sensu stricto, we applied in the current investigation this structural term on a much wider scale, covering the entire Neogene and Quaternary [24,109].

The numbers of structural elements considered throughout each study have been mentioned in the captions of Figures 8–10. The length and orientation of the trunk rivers—1st order—Rodach, Schorgast and Steinach can be deduced from the length and orientation in the pertinent maps (Figures 8–10). The same holds true for the 2nd order tributary rivers considered in the current study. River course and structural elements are compared

with each other using the same type of mirror rose diagram, excluding the synoptical semicircle (Figure 8e).

Based upon the tectonic planar elements the FW study area was compartmental-ized into four morphotectonic units (MTU 1 to 4), all of which reveal a marked NE-SW trend striking parallel to the fold axis of the anti- and synclines, e.g., Berga Anticline and Teuschnitz Syncline (Figures 1 and 8a–e). The channel patterns which are subdivided into 1st (Rodach, Wilde Rodach) and 2nd order streams differ, in places, markedly from the afore-mentioned structural patterns, being endowed with a second maximum displaying a NW-SE trend (Figure 8f–i). While in the Teuschnitz Syncline (MTU 1) the channel pattern accords well with the structural one, in the MTU 2 and MTU 3 the second NW-SE trend stands out irrespective of stream order. The situation becomes more complex upstream where both maxima are present. The closer to the NW-SE striking FLFZ and more down-stream the NW trend prevails in the rose diagrams of the drainage pattern. At a more distal position of this highland boundary fault, the Variscan NE-SW arrangement becomes more pronounced. The latter structural pattern gives rise to a special drainage pattern called "antler-type" (Section 5.4). (Figures 1 and 8e). Artificial channels indicated in Figure 8a trenched to feed saw mills and facilitate the work of raftsmen are mentioned here but they are left unaddressed during any talweg measurements. By and large the SSS reflects a pristine channel system.

In the study area of the MGC, the NW-SE trend of the FLFZ and its parallel parasite faults can also be identified in the pattern of the 1st order stream represented by the Schor-gast River (Figure 9a,b). The 2nd maximum straddling around ENE-WSW recorded from the 1st order rivers can be traced back to the Variscan fold axis which rotated anticlockwise from the NE-SW towards ENE-WSW. The "antler pattern" visualized by two equivalent maxima running NNE and NE find only representation in the drainage pattern of the 2nd order streams associated with a minor NW-SE maximum.

The south-eastern-most study area in the FG provides a different picture far more conspicuous than its NW counterparts. Its major anticline still stands out as a NE-SW striking domal structure, reaching an elevation of as much as 1052 m with the Schneeberg summit. The "antler pattern" of the river drainage system got almost obliterated (Figure 10). The Steinach River no longer runs parallel to the 1st order fold axis or hinge line draining down towards SW but runs along its WNW limb as a straight strike stream parallel to the outcrop of the low-grade metamorphic rock series (Figure 9). The 2nd and 3rd order fold axes run perpendicularly to the tributaries on the right side of the valley.

4.2.3. Degree of Sinuosity and Drainage Classification

Objects and purpose The hydrographic parameter channel sinuosity (=S value) is the principal tool to categorize the fluvial drainage systems, in general, and to draw a more detailed picture of the current SSS, in particular.

After Schumm´s (1963) [110] classical studies of the sinuosity of alluvial channels, an progress report of investigations has been given by Church (2002) and Beechie et al. (2006) [111,112]. The S values obtained by the method put forward in Section 2 directly translate into the classification scheme proposed by Charlton (2014) [10]: Straight < 1.1, sinuous 1.1 to 1.5, meandering > 1.5. An amendment has been made based upon the datasets obtained from our previous studies of the proximal foreland rivers enabling us to subject the different streams to a more subtle subdivision and genetic interpretation. This newly introduced classification scheme can be applied to the basin-and-range topography in a sedimentary foreland and the upstream basement, alike (Figures 8–10, Table 2): Straight: <1.1, low-sinuosity: 1.1 to 1.3, high-sinuosity: 1.3 to 1.5, moderately meandering: 1.5 to 2.0, strongly meandering: 2 to 5, very strongly meandering with sedimentary trap sites > 5 [62]. According to this classification scheme the majority of channel systems under examination plot into the pigeonhole low-sinuosity, a channel type mostly found in the TA of the study areas (Table 2). True straight rivers are restricted to the CA and TA of low-grade and very-low-grade metamorphic rocks (Table 2, Figure 11a–c).

4.2.4. Channel Density and Channel Floodplain Ratio

Objects and purpose: The analyses of the channel density and channel-floodplain ratio are markers for the paleo-gradient, the flow rate and can be used as flow confinement indices. They should always be handled side-by-side with each other to find out which scope can be achieved most successfully by this approach (Figure 12).

The contour maps of the channel density of the VLG and LGG-types are rather homogeneous with a distribution of blue anomalies aligned like pearls on a string in a characteristic zig-tag pattern (Figure 12a,b). This regular patterns mirror a downstream trend of increasing sinuosity. The contour map illustrating the channel/flood plain ratio shows two eye-catching anomalies in each contour map (Figure 12c,d). They are remarkable in two different ways. It is the river section where older floodplains in the TA manifested by a tripartite set of intra–basement-paired and unpaired depositional terraces of the 440–500 m-level came into existence and they mark the transition from the TA into the DA (Figures 3b and 8a). Similar features in the LGG-type witness a stacked pattern of depositional terraces in the Fichtelgebirge Foreland of the "Weidenberg Bowl" (Figure 5).

4.2.5. Slope Morphology vs. Bedrock-Lithology and Tectonic

Objects and purpose: The x-y plot of elevation vs. distance illustrates the direct response of the talweg to the bedrock lithology from source to the point of confluence. It is not the first attempt of highlighting this fluvial relationship as shown by Hack (1973) [113] who put forward a stream gradient index. Substituting the slope angle in the x-y plot for the elevation gives an additional insight into the variation of valley morphology as a function of the fluvial facies (CA, TA, DA): wide-and-shallow valley ⇒ wide-angle ⇒ acute-angle V-shaped ⇒ U-shaped valleys (Figure 11a–c). Combining it with the sinuosity allows for a direct comparison of 1-D and 2-D patterns.

Longitudinal profiles of the rivers have been studied by Gomez et al. (1996), Zuchiewicz (1995) and Demoulin (1998) [114–116]. The latter study refers to a basement resembling, as far as the lithology and metamorphic regime are concerned, the VLG-type (Table 1). The VLG and LGG types are described as concave with some knickpoints highlighting 2nd order concave riverbed sectors. The gradient of the LHG is made up of convex subsections within the basement and warrant an overall classification as convex. In the x-y plot illustrating the steepness of the three gradients the LHG type stands out by the steepest inclination ever in the area under study (Figure 11d). All longitudinal profiles start at the watershed and end on the floodplains in front of the basement edge so as enable a direct comparison of the SSS.

There is a third parameter related to the slope angle; it is the linear fold tectonic elements and the dip of slope in the Steinach drainage system (Figure 13—see also section A to F). The Steinach River runs at an acute angle along the WNW limb of the Fichtelgebirge Anticline. The most steeply dipping slopes in the Steinach drainage system are within the 2nd order channels debouching into the 1st order river from the right-hand side (Figure 13). The 2nd order channels are governed by NW-SE trending tectonic structures perpendicular to the 1st order fold axis of the Fichtelgebirge Anticline. The maximum of slope steepness is attained where the SW plunging fold axes of the B 1 and B 2 folding stage on the NW limb are perpendicular to the slope of the 2nd order channels.

4.3. Hydrodynamics and Grain Parameters (GMS Tool)

Objects and purpose: Reliable data on the most recent hydrodynamic regime can only be obtained by the GMS analysis of particles eroded, transported and deposited within these three SSS which mostly consist of gravel-sized siliciclasts (Table 1). It is an aid to the precise differentiate the landforms (Section 4.1) and determine its proportion to mixed-type depositional environments from land to sea. This is common in the SSS where fluvial, colluvial and cryogenic processes contribute to shaping the valleys.

A tripartite methodological approach has successfully been taken in previous projects investigating coarse-grained glacial, fluvial, marine sediments and different sorts of

mass wasting products and named as GMS gravel analysis: Granulometry-morphology-situmetry (orientation of gravelly clasts) [62,84,117]. The gravel is subjected to a visual morphological examination while subdivided into six classes of roundness from very angular to well-rounded according to Illenberger (1991) [60] and discriminated granulometrically using the suggestions put forward by Pettijohn et al. (1987) [118]. The 3rd method is called situmetry which sedimentologists and geomorphologists have been losing sight of during the recent past, excluding applied geoscientists who use clast orientation in glacial till for mineral exploration [56,57,119]. To exemplify the tripartite approach of the GMS tool, an in-depth treatment of the LGG-Type has been conducted (Table 3, Figure 14).

The clast orientations suggest both colluvial and alluvial/fluvial deposits exist in the CA as indicated by the orientation of the 1st and 2nd order maxima and the angle between them (Table 3). As noted in Table 3 and illustrated in Figure 14, the four major parameters are (1) the orientation parallel (Figure 14 diagram 11a), or (2) perpendicular to the paleocurrent/slope direction (Figure 14 diagram 12), (3) the angle between the maxima, and (4) the merging of maxima producing a fan-shape wide-angle sector. A trend to alluvial/fluvial processes is indicated by acute-angle maxima conspicuously well separated from each other, whereas colluvial and deltaic processes tend to form obtuse-angle maxima and an amalgamation to fans. The method ought to be run in combination with grain size and morphology of clasts (Table 3).

In the TA, the channel system evolves from an intermediate sediment trap into a channel system which at its end converts into the foreland DA. The minor straight creeks of 2nd order debouch into the trunk river via coarse-grained deltas. The small channels in the CA of the VLG-type resemble its counterparts in the LGG-type and based upon that enable a morpho-stratigraphic correlation of the tributaries (Table 3—Stein 2, 11b, 11c). The LHG-type is a mixture of the two end-member types LGG and VLG.

4.4. The Composition of Autochthonous and Allochthonous Mineralization of the SSS

Objects and purpose: There are two types of mineralization. The autochthonous overburden contains the minerals useful for thermodynamical computations of the physical-chemical regime of the chemical weathering. The parameters are the redox conditions (Eh), the acidity/alkalinity of the meteoric fluids (Eh) and the near-ambient temperature regime. Radioactive age dating, e.g., U/Pb, and organic methods such as palynology allow a determination of the paleoclimate (Table 5). The gravel-size debris are representative of the allochthonous mineral aggregates. Thermodynamic computations and age dating encompass a wider field of geosciences and therefore, the results are discussed in Section 5. This is also true for the composition of the debris (Table 4).

4.4.1. Composition and Age of Formation of the Mineral Association of the Supergene Alteration

The supergene alteration zone is subdivided into two alteration zones, one called zone of argillitization, due to the abundance in phyllosilicates and the other zone of duricrusts/orecretes rife with chemical residues made up mainly of Fe, Mn, Ti and Al [120] (Figure 15, Table 1). A comparison of the mineral associations reveals great similarities between the VLG- and LHG types (Figure 15). Both types only differ from each other by the absence of orecretes in the LHG-type (Mn orecretes, uraniferous orecretes and aluminum-phosphate-sulfate minerals (APS)). The LGG-type is underlain by crystalline bedrocks abundant in alkaline feldspar and primary U-bearing host minerals rendering its bedrocks highly susceptible to chemical weathering. It is abundant in newly formed smectite, mainly nontronite, kaolinite and a varied spectrum of uranyl phosphates (torbernite, saléeite) and hydrosilicates (uranophane), all of which are amenable to radiometric age dating as it is the case with the Fe-Mn counterparts from the VLG-type (Figure 15). Both sorts of duricrusts reflect paleo-aquifers that had direct implications as redox indicators and geo-acidometer on the chemical weathering of the bedrock in the CA and the incision of the drainage systems in the TA (Figures 11a,c and 15). Uraniferous phoscretes and silcretes and manganiferous ferricretes are two sides of the same coin, representatives of the continental

aquatic regime. In one deposit of cryptomelane, a direct comparison has been conducted and yielded an age of formation of 4.20 ± 0.33 Ma for cryptomelane while torbernite gave an age of 4.55 ± 0.02 Ma. Thereby they furnish convincing evidence to belong to the same Pliocene groundwater system and cast in to the role of environment markers [48,49].
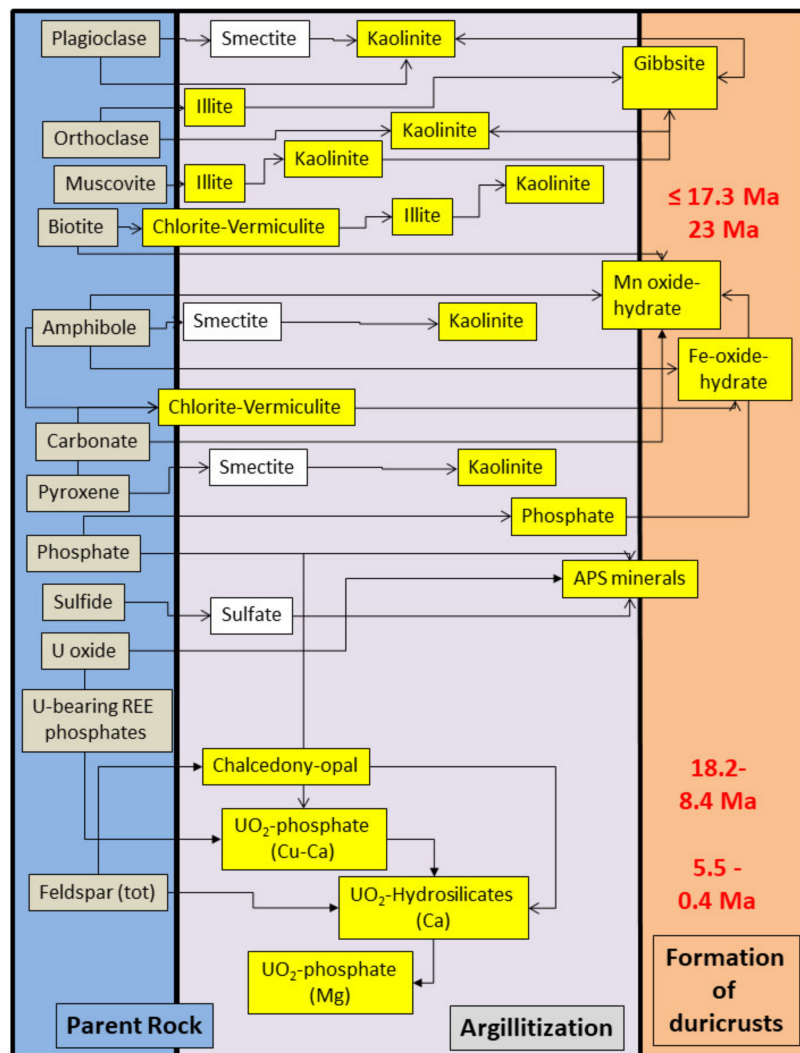

Figure 15. Parent rock and the binary subdivision of the supergene alteration zone.

4.4.2. Thickness and Variation of Autochthonous Mineralization

In the LHG-type, reworked regolith is second to none compared to the adjacent study areas in terms of aerial distribution and thickness (Figures 8a,c, 9a,c and 10a,b, Table 1). Its loamy weathering mantle attains as much as 27 m on gneissic bedrock, with mean thicknesses around 11 m and minimum thicknesses of around 1.5 m on steeper slopes while it goes down to zero on bluffs [104,121]. Along the talweg of the TA the thickness diminishes to almost zero in the non-alluvial sectors of the SSS. By contrast in the DA the thickness increases again to values to more than 6 m [82]. Despite of this considerable thickness no regolith profiles have been well preserved due to its cryogenic reworking. Irrespective of the age of formation and its redeposition, the fine-grained weathering mantle is crucial as to the degree of sinuosity in the CA (Section 5.3.2). Over time as a channel incises through the regolith the sinuosity increases until the channel hits the rigid basement rocks underneath. There the channels had to succumb again to the guidance of the straight tectonic elements and the rigid lithology of the basement (Figures 8–10).

The size of deposits produced by mass wasting in the various sites well accord with the size of monadnocks and block fields and testifies the genetic relation between the two

landform types (Table 1). The quantification of fluvial and colluvial deposits is given by area percentage in Table 1 and displayed in the maps of Figures 8–10. Measuring the thickness of the overburden on top of the entire basement cannot be achieved without geophysical surveys across the entire study area supported by shallow drill holes used for reference and calibration. Geoelectrical methods have been applied selectively to get an insight into the thickness and the composition of the colluvial and fluvial deposits throughout the assessment of mass wasting [61]. The apparent resistivity values are as follows and arranged in order of increasing depth for comparison: Fluvial bedload deposits: 120–150 Ωm, solifluction creep: approx. 95 Ωm, mud and debris flow: 50–60 Ωm, regolith: 90–130 Ωm, basement: 340–750 Ωm. Fluvial deposits, mass wasting products, regolith and bedrocks can precisely be defined and the thickness determined. Therefore, based on the mapping results in Figures 8–10 and some thickness data from outcrops, geophysical logs and shallow drill holes the following zonation can be reported: CA very high thickness (max. 27 m), TA: considerably reduced thickness (max. 1.5 m), DA thickness increases (max. > 6 m).

5. Discussion

5.1. The Physical-Chemical Conditions and the Paleo-Climatic Regime

The origin of the variable landforms is the result of endogenous (structural landforms) as well as the exogenous forces (sculptural landforms). The landforms developed at the interface between lithosphere, atmosphere, and hydrosphere leading to a special landscape, in the current study to these three SSS in a basement landscape (Table 1, Figure 16).

Weathering/supergene alteration mediating at the interface of the different spheres where the SSS formed [122–128]. It is a series of physical-chemical processes that is governed by the climate during the Neogene and Quaternary established on a Paleozoic and Mesozoic-Paleogene platform (Table 5, Figures 2b and 16a,b). The thermo-dynamic calculations to constrain this physical-chemical regime have been extensively discussed in Dill et al. (2010a, b) and in Dill and Wemmer (2012) [48–50] and the results of which are portrayed for the region in Figure 16c–f. The translation of these physico-chemical data into the Cenozoic paleoclimate is discussed in context with the age data obtained from uranyl silicates and phosphates as well as K-Mn-Fe oxide hydroxides, unless stated otherwise (Figure 2b). The latter chemical systems U-Si-Mg-Ca-Cu-P and K-Mn-Fe are the only ones which can successfully be applied to the Cenozoic land-forming processes because both parameters, the "temporal" and "environmental" ones are inherent to each of the afore-mentioned mineral series.

Prestage of the SSS: The prestage of these SSS covers the Early to Middle Miocene (23 to 14 Ma) where lignite seams came into existence immediately SE of the study area of the LGG-Type in the Eger Rift Graben [51]. Forest peat swamps developed under oscillating water levels in a fluvial—lacustrine environment on the Neogene regolith. More basin-ward black shales yielded a palaeoflora of early Miocene age [129]. The Middle- to Late Miocene age (8.4–5.6 Ma) has been obtained from torbernite-bearing uranyl-phoscretes $[Cu[UO_2 \mid PO_4]_2 \cdot 12H_2O]$ reflecting a paleo aquifer under subtropical wet and dry conditions [49]. Moser et al. (2009) [130] described this climatic and ecological situation based on a continental mollusk fauna as an open scrubland with temporary waters and damp forests. In the VLG-type, wide-and-shallow valleys were filled with gravel cemented by Fe-Mn encrustations between 17.3 and 23.0 Ma abundant in cryptomelane $[K(Mn^{4+}_7Mn^{3+})O_{16}]$ and goethite $[\alpha\text{-}Fe^{3+}O(OH)]$ (Figure 16a,c,d). The Middle to Late Miocene age (8.4–5.6 Ma) has been obtained from uranyl-bearing orecretes reflecting a paleo aquifer under subtropical conditions enriched autunite $[Ca[(UO_2)(PO_4)]_2 \cdot 11\,H_2O]$ together with torbernite [48,49].
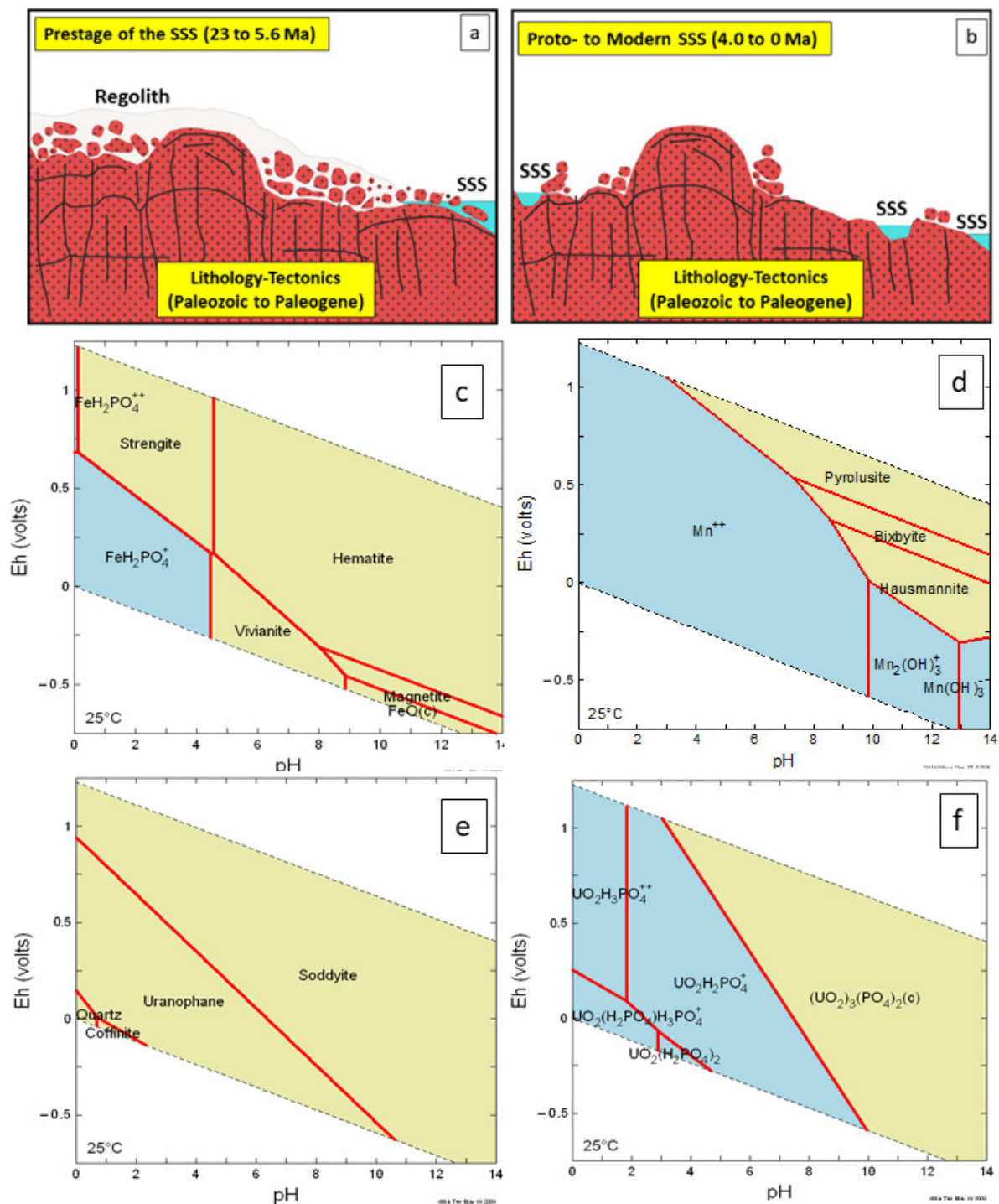
Figure 16. Cartoons to illustrate the stage-wise geomorphological evolution of the SSS during the Neogene and Quaternary which has been derived from a lithological and structural frame supplemented (**a,b**) with thermo-chemical calculations to bolster the chronological and climatic constraints of the succession of the SSS (**c–f**). Assumed concentrations of dissolved species are given below in mol/L. (**a**) Formation of supergene alteration surfaces (etch planation/surface, regolith) and encrustations (silcrete, phoscretes, ferricretes) defined by U-P-Si-Fe-Mn mineralizations as to the age of formation and the physical chemical regime. Onset of the formation of domal landforms, e.g., inselbergs, wide-and-shallow valleys formed by braided and meandering drainage systems. For calculations see (**c,d**); (**b**) Denudation of regolith and tor formation and fluvial incision of the SSS into exposed crystalline basement rocks. For calculations see (**d–f**).; (**c**) Eh-pH diagram to show the Fe-P mineralization at 25 °C using the dissolved species as $\log_{aFe} = -3$, $\log_{aHPO4} = -5$; (**d**) Eh-pH diagram to show the Mn mineralization at 25 °C using the dissolved species as $\log_{aMn} = -6$; (**e**) Eh-pH diagram to show the U-Si mineralization at 25 °C using the dissolved species as $\log_{aU4+} = -7$, $\log_{aSiO2(aq)} = -3$, $\log_{a\,ca2+} = -3$; (**f**) Eh-pH diagram to show the U-P mineralization at 25 °C using the dissolved species as $\log_{aU} = -7$, $\log_{aHPO4} = -5$.

Proto-SSS: The Pliocene to Early Pleistocene (4.0–1.8 Ma) evolution of the fluvial drainage systems is based on uranyl phosphates and –hydrosilicates/uranophane [Ca[UO$_2$ | SiO$_3$OH]$_2$·5H$_2$O] which evolved under a subtropical climate but slightly drier conditions as far as the Pliocene part of the fluvial landscape is concerned when silica-cemented gravelly deposits developed (Figure 16b,e,f) [131,132].

Modern SSS: The Early to Middle Pleistocene age (Early Pleistocene < 1.8 Ma) has been constrained based on the Mg uranyl phosphate saléeite [Mg[UO$_2$ | PO$_4$]$_2$·10–12H$_2$O] referring to a period of time which is synonymous in Central Europe with the early phases of the glacial period. In the study area it is only represented by periglacial landforms within the CA and DA of the SSS such as nivation cirques and pockets undergoing cryoturbation (Tables 4 and 5) [92,93,97] (Figure 7g).

The youngest floodplains in the DA of the SSS are Holocene in age, the humid mid-latitude temperate climate of which has been investigated by (Zöller et al., 2007; Dill et al., 2020a) [62,68].

Table 4. Composition of gravel assemblages on different terraces laid down in the foreland (DA) of the Fichtelgebirge (LGG-Type). For locality see Figure 10b.

Site	Gravel (%)	Height (m)	Age Dating	Interpretation (Current Study)
Steinach "Terrace T4"	Epigneiss 20, phyllite 60, quartz, quartz 10, quartzite 10	>480	Middle Pleistocene	Alluvial and colluvial sediments on the low scarp mixed with relic fluvial deposits (unconfined flow and creep)
Steinach "Terrace T3"	Epigneiss 6, phyllite, 18, quartz 70, quartzite 6	480	Middle Pleistocene	Fluvial terrace
Steinach "Terrace T2"	Epigneiss 10, phyllite 80, quartzite 9 Quartz + granite 1	460	Middle to Late Pleistocene	Fluvial terrace
Steinach "Terrace T1"	Epigneiss 6, phyllite 75, quartzite 12, quartz 5, granite 1	440	Late Pleistocene to Early Holocene	Fluvial terrace
Recent floodplains "T0"	Epigneiss 12, phyllite 70, quartzite 12, quartz 6	400–420	Holocene	Floodplain

Table 5. The Quadripartite approach to the evolution of the straight to low-sinuosity drainage system (SSS) in a mature basement and its immediate foreland as a function of lithology and tectonic (see VLG-, LGG- and LHG types) and climate change during the Late Cenozoic. (1) The geological framework of SSS: Forming the lithological and structural features in the bedrock as a result of different temperature, pressure and dynamic processes. (2) Prestage of SSS: Forming the paleo-landscape with a stable fluvial regime. (3) Proto-SSS: Transition into a metastable fluvial regime. Modern SSS: Operation of the metastable fluvial regime with the tendency to achieve a stable regime at the boundary basement-foreland. Each compartment shows the geological and geomorphological processes and landforms essential for the evolution of the SSS together with the degree of sinuosity and the slope angle. The tectonic event denotes the onset of the SSS formation *sensu lato*.

Stages	VLG-Type	LGG-Type	LHG-Type	Climate	Age
Forming the lithological and structural (folding + faulting) framework for the SSS	Very-Low Grade metamorphic basement	Low-Grade metamorphic basement intruded by Granites	Low/medium-to High-Grade metamorphic basement	Variable climate regimes	Late Paleozoic Variscan Orogeny
Forming the structural framework (faulting) for the SSS	Strong faulting, uplift and erosion of topstrata	Strong faulting, updoming, uplift and erosion of topstrata	Strong faulting, uplift and erosion of topstrata	Variable climate regimes	Mesozoic to Paleogene
Tectonic Event (Driver I)	Fracturing, uplift, tilting of the paleosurface as a consequence of the NE-SW striking Eger- Graben Rift. Tectonically- related formation of the prestage drainage systems *Forming the blue print" of the SSS*				Late Oligocene to Middle Miocene 29–19 Ma

Table 5. *Cont.*

Stages	VLG-Type	LGG-Type	LHG-Type	Climate	Age
Prestage-Fluvial-alluvial-(lacustrine) Paleo-landscape	Wide and shallow valleys braided to meandering rivers/ coarse-gr. deposits *Sinuosity > 2.5*	Wide and shallow valleys braided to meandering rivers/ coarse-gr. deposits *Sinuosity > 2.5*	Wide and shallow valleys braided to meandering rivers/ coarse-gr. deposits *Sinuosity > 2.5*	Humid tropical to subtropical wet and dry climate	Early- to Middle Miocene 23–14 Ma
Prestage Fluvial paleo-landscape	Regolitisation, etch planation, formation of inselbergs in the basement, trunk rivers in the foreland (e.g., Main, Rhein.)	Regolitisation, etch planation, formation of inselbergs in the basement, trunk rivers in the foreland (e.g., Main, Rhein	Regolitisation, etch planation, formation of inselbergs in the basement, trunk rivers in the foreland (e.g., Main, Rhein.)	subtropical wet and dry climate	Middle to Late Miocene 8.4–5.6 Ma
Tectonic Event (Driver II)	Fracturing, uplift in the South German Block and reactivation of the NW-SE striking FLFZ accompanied by a rising gradient *Starting drainage and accelerating incision of the SSS*				Middle Miocene to Plio-Pleistocene 15.3–2.3 Ma
Proto-Straight to low sinuosity drainage system (SSS) (CA)⇒ Modern SSS	Onset of the zone of headwaters of the SSS *Sinuosity 1.075 Slope angle 5 to 22° F/M ratio: 2.323*	Formation of tors, palisades Onset of the zone of headwaters of the SSS *Sinuosity 1.116 Slope angle 2 to 18° F/M ratio: 0.062*	Formation of tors, palisades Onset of the zone of headwaters of the SSS *Sinuosity 1.275–1.407 Slope angle 5 to 15° F/M ratio: 0.517*	subtropical climate drier regime	Pliocene to Early Pleistocene 4.0–1.8 Ma
Modern SSS (TA)	Incision of V-shaped wide-angle valleys *Sinuosity 1.125 Slope angle 18 to 31°*	Block stream Incision of V-shaped wide-angle valleys *Sinuosity 1.103 Slope angle 15 to 27°*	Block stream	Glacial period with cold and warmer stages	Early Pleistocene < 1.8 Ma
Modern SSS (TA)	Intermediate sediment traps	Intermediate sediment traps	Not developed **Erosional unconformity**	Glacial period with cold and longer warmer stages	
Modern SSS (TA)	Mass wasting landforms Incision of V-shaped acute valleys *Sinuosity 1.580–1.169 Slope angle 31 to 35° KP F/M ratio: 17.908 KP*	Mass wasting landforms Incision of V-shaped acute *Sinuosity 1.212–1.023 Slope angle 27 to 35° F/M ratio: 0.153*	Mass wasting landforms Incision of V-shaped acute *Sinuosity 1.235–1.103 Slope angle 24 to 35° F/M ratio: 0.163*	Glacial period with cold and warmer stages	0.4 Ma Middle Pleistocene
Modern SSS (TA)	Mass wasting landforms Flat-floor-shaped/ U-shaped valley *Sinuosity 1.167 Slope angle 19 to 35°*	Not developed		Glacial period to postglacial warm temperate	Holocene
Modern SSS (DA)	Mass wasting landforms Fluvial depositional terrace (T4) *Slope angle < 20°*	Mass wasting landforms Fluvial depositional terrace (T4) *Slope angle < 5°*	Not developed *KP*	Glacial period with cold and warmer stages	0.4 Ma Middle Pleistocene
Modern SSS (DA)	Fluvial depositional terrace (T3)	Fluvial depositional terrace (T3)			
Modern SSS (DA)	Fluvial depositional terrace (T2)	Fluvial depositional terrace (T2)			Middle to Late Pleistocene
Modern SSS (DA)	Cryogenic landforms Fluvial depositional terrace (T1) *Sinuosity 1.185 F/M ratio: 18.904*	Cryogenic landforms Fluvial depositional terrace (T1) *Sinuosity 1.270 KP F/M ratio: 0.987 KP*	Hillwash plain (T1) *Sinuosity 1.197 Slope angle < 5° F/M ratio: 1.197*	Glacial period with cold and warmer stages	Late Pleistocene to Early Holocene
Modern SSS (DA)	Floodplain (T0) Sinuosity 2.694	Floodplain (T0) Sinuosity 1.507	Floodplain (T0) *1.314*	Postglacial moderate humid temperate	Holocene

5.2. Maintenance of a Metastable Hydrodynamic State Needs the Constraints of a Structural-Lithological Framework and Effective Drivers

The implementation of a SSS in nature needs a framework-driver couple. Both are linked with each other like "hardware" and "software".

The framework: Due to the metastable character of the SSS, its channels always tend to convert into a drainage system of higher sinuosity and try to achieve a higher level of hydrodynamic stability [11,111,133] (Table 2, Figure 6e). To maintain a SSS over a longer period of time and distance the course of the channels must be coerced into a rigid framework. For the case of the three SSS under study, such a setting is well established in basement terrains composed of sturdy bedrock lithologies and subjected to a tectonic overprinting that led to a perfectly well-structured fold and fault pattern with a pronounced morphotectonic outward appearance (Tables 1 and 5, Figures 3–5). A Paleozoic through Paleogene framework is mandatory to create a SSS (Figure 16a,b).

The drivers: Additionally, an SSS terrain needs a driver to assure a constant high gradient and to ensure continual erosion, transport, and deposition by fluvial and mass wasting processes (Figure 11). In the present study areas, this driver is guaranteed by syngenetic tectonic pulses during the Cenozoic and fostered by contrasting climate regimes controlling the state of the agent water and impacting on the supergene alteration (Figures 2b and 15, Tables 4 and 5). The current study of the sinuosity over the full length of the drainage system illustrates that its development is not unidirectional in nature.

Stable drainage systems with a fairly high sinuosity degree of S > 2.5 occurred at the beginning but they developed into a metastable type with sinuosity degrees approximating S = 1; farther downstream they end up in the foreland in an ultrastable drainage systems as the S values reach values of as much as 11 at very low gradient (Tables 2 and 5) [62]. Such abnormally high values are indicative of the marginal facies of a fluvial—lacustrine environment. In the fluvial regime upstream of the entrance into this sediment trap sinuosity S values in the range 2 to 5 are common (Table 2). They may episodically turn into more stable drainage systems within intermediate sediment traps of the SSS. This bimodal sinuosity distribution has been elaborated for the three facies zones CA, TA, and DA of the SSS—see Section 4.4.2. It is a consequence of climate change and caliber of sediment load delivered by fluvial and mass wasting processes.

5.2.1. The Paleozoic Tectonic Framework

Each of the three study areas has a south-westerly plunging 1st order anticline, the backbone of the framework (Figure 1). Their outward expression when exposed to surface; however, strongly differs as a function of the metamorphic-dynamic evolution during the Variscan orogeny and so does their impact several hundred million years later on the morphotectonic expression. The reference sites are arranged in order of increasing grade of dynamo-metamorphism, the lithological-structural features of which provoke a different morphotectonic expression in the landscape of the basement and thereby endow every type of SSS with peculiar features (Tables 1 and 5).

The deformation in the study area of the VLG-type took place between 360 Ma and 320 Ma. The orientation of the SSS can still be traced back to this folding because of the very low grade of metamorphic overprinting which left the structural features relevant for the SSS almost unaffected (Figure 8). The planar tectonic elements governed the river course of the Rodach drainage system, guided the progradation of the terraces into the VLG basement and the subsidence of the U-shaped valleys in the lower reaches of the Rodach drainage system (Figures 1, 3b, 6f,g and 8a). Upstream of the Wilde Rodach the stepwise piedmont staircase system evolved in accordance with the axial-plane parallel fault zones, and the litho-variance of the Paleozoic basement rocks (Figures 3a and 8b–e).

These NE-SW striking Variscan structural elements also contribute to the several riffles, cascades and rough bedforms particularly when chert forms the bedrock in low-sinuosity channels (Figures 6a and 8c). They are the sites where straight channels deviate into sinuous ones as the pebbles and boulders tend to increase in the sediment load (Figure 8c). Slight changes, be it an increase or decrease in the input of gravelly sediments, give rise to moderately meandering streams via wandering channels (Figures 6e and 8c—sinuosity: 1.125 ⇒ 1.580).

The NE-SW-, draining rivers display a ramification towards NE into two, rarely three, rivulets like the paired or triple-pointed ends of the antler of a roebuck ("antler drainage pattern"). This newly introduced channel pattern is intermediate between the dentritic and parallel ones [10]. The 1st order rivers, such as the Rodach River mark the 1st order fold axis of the large anticlines such as the Berga Anticline which plunges towards the SW. The 2nd and 3rd order axial plane parallel folds homoclinal with the major one are represented by the ramification of the channel network observed in the NE-SW and SW-NE draining 2nd order streams. Being homoclinal with the 1st order anticline provokes the "antler" open towards the NE. If the plunge of the 2nd and 3rd order folds reverses, the "antler" will be open towards the SW (Figure 8).

The "antler" pattern is vaguely expressed in the 2nd order streams of the MGC (Figure 8), because the Central Anticline in the MGC is rather poorly represented and only recognized in the lower reaches of the 1st order pattern. The middle- to high-temperature regional metamorphism between 430 and 360 Ma largely eradicated the fold structures [134].

The asymmetric development of the Steinach River, occurring as a consequence of an anti-clockwise rotation from the hinge-line parallel Proto-Steinach to the current position, did not allow for such antler patterns to survive undistorted. The rotation point is situated where the modern Steinach leaves the basement to debouch its bed load into the "Weidenberg Bowl" where it triggered a set of at least three depositional terraces arranged in a staircase-like manner- see examples from the South Swedish Dome [135] (Figures 5, 10 and 13).

The low-pressure regional metamorphism in the FG began around 330 Ma and was immediately succeeded by the intrusion of granitic magmas which ceased around 290 Ma. Approximately 270 million years later, the Steinach fluvial system came into existing when doming along the FG Anticline forced the river to incise along the NE-SW hinge line from its culmination towards SW (1st order fold axis) and ended up on the WNW limp. As a result of this asymmetry the fluvial undercutting gradually shifted from the trunk river to the right-hand tributaries (2nd order stream) the steepest slopes at an almost right angle to the 2nd and 3rd order Variscan fold axes (Figure 13).

During the Mesozoic uplift processes have been recognized in the area and proved by apatite-fission track studies [136]. They are, however, without any relevance for the evolution of the SSS. No proven chronologically tested evidence of landforms has been preserved.

5.2.2. The Cenozoic Tectonic Driver

The effect of these tectonic drivers impacting on the SSS need to be split up into three classes. They are destructive or non-destructive with regard to the bedrock of the SSS, they follow a tectonic "blue print" newly established during the Cenozoic or rejuvenate ancient structures of the framework, and can be named as 1st order or 2nd order knickpoint makers. It has to be noted that some methodological restrictions are imposed on the timing of the neotectonic processes. The interval between 0. 4 Ma (lower limit of U/Pb dating) and the time covered by radiocarbon data provided by Zöller et al. (2007) and Dill et al. (2020a) [62,68] is not covered by absolute age data but based only on lithostratigraphic correlation of terraces and a more precise chronological assignment cannot be given here.

Framework- vs. *bedrock-related tectonic processes*: The NE-SW striking structural elements are prevalently caused by rejuvenation of the pre-existing Variscan-type near and planar tectonic elements (see Section 5.2.1). The NW-SE striking structural elements are provoked by neotectonic processes. Its most conspicuous representative is the FLFZ (Figure 1).

Non-destructive vs. *destructive processes*: Non-destructive processes reactivated the Variscan structures following the same NE-SW trend as their Paleozoic predecessors and normally resulting elongated domelike structures. The role model is the "Fichtelgebirge Anticline", the host structure of the LGG-type drainage pattern the onset of which can be traced back into the Mid- to Late Mesozoic (see Section 5.2.1). Similar to the SSS under study in Germany, domelike uplifts in a passive-margin domain strongly impacted in Sweden on the development of Neogene drainage systems such as the Eridano River of the Baltic Basin during Late Jurassic or Early Cretaceous also [135,137]. A newly formed non-destructive element, a swell running NW-SE terminates the study area towards the NE and is herein referred to as "Franconian Traverse Swell" (=FTS) (Figure 1). Its hinge line act as the watershed between the Rivers Rhein and Elbe/Labe and two subhorizontal paleosurfaces tilted away from it. The western paleosurface is under study in this project and homoclinal with the SSS. The destructive counterpart to it is the FLFZ bounding the basement towards the SW against the foreland (Figure 1). These planar architectural elements constitute the Cenozoic or neotectonic structural framework for the study area

and come into effect in the SSS on a regional scale as 1st order knickpoints and on fluvial scale as 2nd order knickpoints (Figures 11 and 12).

1st and 2nd order knickpoints: When it comes to decipher the evolution of the Cenozoic tectonic processes within the lower reaches of the SSS, three parameters are important; the absolute height of vertical displacement, the type of displacement (e.g., non-destructive), and the positioning of the fault plane relative to the basement-foreland topography and the 1st order knickpoint of the SSS. The NW-SE trending FLFZ measures different heights of vertical displacement from NW towards the SE. The actual difference between the lowest erosional terrace on the fault´s basement shoulder and the fault´s lowest foreland floodplain measures in the VLG 140 m, in the LHG 200 m and the LGG types 150 m (Figures 3–5). The lowest erosional terraces are genetically different from the Quaternary depositional terraces situated at a height of 10 to 25 m above the present floodplain.

Faults, which are the leverage to rise the gradient of the SSS, reach its maximum in gradient and vertical displacement in the LHG-type (Figures 4, 9, 11d and 17). The basement-foreland topography coincides in this site with the FLFZ (Figure 9). In the LHG-type a sharp contact exists between the TA and DA, accentuated by the steepest escarpment ever observed in the region. The original river course started to follow the Variscan plan of construction being oriented NE-SW, while ongoing deepening during the Cenozoic redirect its course into the NW-SE direction of the FLFZ (Figure 9a,b). In the LHG-type, the NW-SE trend of the FLFZ can be identified in the pattern of the 1st order streams where it is represented by the upper reaches of the Schorgast River (Figures 9a,b and 11d). The geomorphological evolution of these SSS coincides with the tectonic evolution and the SSS development is held to be synkinematic—destructive (Figure 17b).
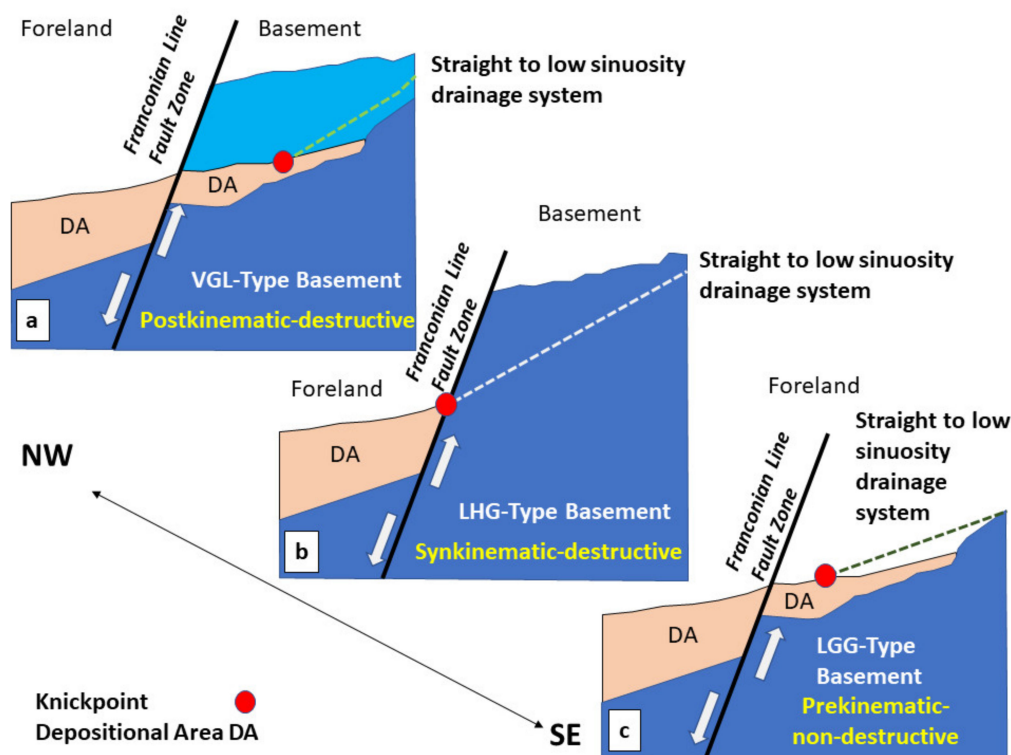
Figure 17. Cartoon to illustrate the relation between Cenozoic fault kinematic along the Franconian Line Fault Zone (FLFZ) and the evolution of the straight to low sinuosity drainage systems of the basement in the various reference sites from NW to SE. The 1st order knickpoint is indicated by the red dot. (**a**) VGL-Type; (**b**) LHG-Type; (**c**) LGG-Type.

Vertical movements along the FLFZ are also responsible for the development and preservation of paired and unpaired depositional terraces (Figures 8a, 10b and 12c,d). In

the VLG-type area, the knickpoint of the gradient as well as the boundary between the DA-TA provoking the widening of the V-shaped valley to convert into a U-shaped one is located inside the basement (Figures 8a and 12c). In the VLG-type the DA invades along U-shaped valleys the basement while the FLFZ is located approx. 3 km to the W of the knickpoint which is denoted by a hydrographic anomaly (Figure 12c). The U-shaped valley is the outward expression of a tectonically abandoned part of the SSS and the system, consequently categorized as postkinematic—destructive (Figure 17a).

In the LGG-type this relation is reversed, the foreland sediments unconformably rest upon the basement forming a non-destructive flexure bulge. The FLFZ cuts through the Mesozoic foreland sediments in the "Weidenberg Bowl" which is largely occupied by fluvial terraces of Pleistocene to Holocene age located outside the basement, as it is with the 1st knickpoint (Figures 10b and 12d, Table 4).

The staircase-like bedsets of terraces known from the "Weidenberg Bowl" can be taken as reference for the fluvial incision and deposition adjacent to the FLFZ along the basement. These terraces evolved from ancient fluvial terraces and fluvial to colluvial pediment-glacis deposits of Neogene age laid down in the foreland of the basement by torrential rivers debouching into the Mesozoic Foreland Basin. They were subsequently almost completely "eaten away" during the Quaternary by the ongoing fluvial incision. The earlier terraces developed following a cycle of deposition and entrenchment in the formerly deposited sediments or as a secondary "inner" valley by entrenchment into older deposits provoked by morpho-tectonic processes under climatic regime strongly contrasting with the more recent ones (see climatic evolution this study). During the Pleistocene and Holocene a constant but stepwise adaptation to the changing climate shifted more and more to a forward carving out of the valley prior to the fluvial deposition. The geomorphological system is categorized as prekinematic-non-destructive (Figure 17c).

The knickpoint zones in the VLG- and LGG reference types are not only marked by a striking hydrographic anomaly but also accentuated by an "elbow" in the channel system (Figure 12c,d). These anomalies furnish evidence for a "bottleneck" attesting to a rising flow rate in the river course (highly confined flow) before relaxation into the flat-floor-shaped valley (unconfined flow) inside the basement or in the adjacent foreland according to the hydrodynamic Bernoulli Law. The 1st order tectonic knickpoints separate the DA from the TA of the SSS and help to constrain the relation between shaping the landscape by the SSS and the tectonic events. In connection with the terraces, each of which are assigned a post Middle Pleistocene age, these morpho-tectonic processes in the SSS are of younger than 0.4 Ma.

Parasite faults running parallel to the FLFZ within the basement created knickpoints in the talweg sparking different fluvial-colluvial environments to develop in the upper reaches of the SSS (Figures 9, 10 and 12c,d). They control the internal structuring of the TA and are denominated as 2nd order knickpoints. The latter are accountable for intermediate sediment traps within the LGG- and VLG types but not in the multiple-convex profile of the LHG-type which misses a tectonic pulse during this period of time. As a consequence of uplift in the VLG- and LGG-type the incision of both reference rivers could not keep pace and their upper reaches were dammed giving rise to the intermediate sediment traps while downstream a knickpoint developed in the river run (Figure 11a,c). In the LHG type, a series of staircase-like convex increments evolved instead (Figures 9b and 11b). In the LHG-type a convex knickpoint exists between 465 and 500 m a.m.s.l. marking the transition from a poorly developed CA into the TA accompanied by an erosional unconformity that "has eaten away" the wide-angle V-shaped valleys present in the neighboring reference study area (Table 5, Figure 11a–c).

5.3. The Lithological Impact on the SSS

The interaction of the bedrock lithology with the hydrographic (Figures 3–7, 11 and 15) and hydrodynamic processes operative in these SSS (Figures 1 and 14, Tables 1, 3a,b and 4)

are a consequence of the mediating climatic regime leading to different cross-sectional morphologies of the valley and longitudinal profiles of the talweg (Figure 16).

5.3.1. Bedrock Geology—Strongly Altered by the Climate

The uplifted bedrock is truncated by a subhorizontal paleosurface tilted away from the watershed, with a relic landscape carved out of it—see Section 5.2. The paleosurface is interpreted as a peneplain or etch surfaces, the formation of which is still subject to controversial debate on a regional scale [76,77] and international level [138] (1) peneplanation (Davis' theory), (2) pediplanation (Penck's theory), (3) etchplanation (Wayland's theory). What is beyond any debate is the strike of the paleochannels and the ensuing modern fluvial equivalents of the prestage and proto channels of the SSS all of which show a NE-SW trend and a drainage, homoclinal with the dip of relic landscape/peneplain (Figure 16, Table 5). A great deal of the drainage channels is oriented along the Variscan anti- and synclines as to strike and dip which experienced a Neogene reactivation as the Eger Graben (Oherský příkop) subsided [139,140]. The latter tectonic process has already been heralded during the Late Cretaceous to Paleocene (68 to 59 Ma) (Table 5) [141]. This period of time was constrained geochronologically at the interval from 29 to 19 Ma by Huckenholz and Kunzmann (1993) [142] and marks the period when the wide-and-shallow drainage system with a sinuosity > 2.5 and coarse-grained channel fill came into existence (Table 5). The widespread occurrence of kaolinite-group clay minerals supports the idea of a humid tropical climate during this period which is also attested to by the presence of Fe phosphates. The variable contents of bivalent and trivalent Fe accommodated into the lattice of phosphates point to oscillating redox conditions and acidic meteoric fluids (Figure 16c). The wide-and-shallow valley of the VLG-type are filled with siliceous gravel and cemented by Fe-Mn orecretes under an oxidizing redox regime (Figures 6a, 11a and 16a,d). Gravel beds with encrustations of Fe-Mn oxides occur also in the Eger Rift Graben similar to those found in the wide valleys at Stegenwaldhaus. The lateral facies change in a fluvial-lacustrine regime reveals a trend to more allitic-sialitic weathering conditions [143]. This is also corroborated by the silicate karst observed in ultrabasic igneous rocks of the LHG-Type [144] (Figure 7c).

The ancient wide-and-shallow valleys are also the protore-collectors [subeconomic mineralized matter which was concentrated at a lower tenor than the subsequent ore that has been derived from this prestage mineral assemblage] for the V-shaped valleys which host the true ore deposits [145,146]. The genetic link between the Miocene predecessor drainage system and the VLG-type river is proved by the accumulation of cassiterite and the formation of Sn placers along the river run of the Wilde Rodach (Figure 11a).

During the waning prestage another tectonic phase took effect along the SW boundary of the basement under consideration in the South German Block [102] (Figure 1, Table 5). Uplift along the NW-SE running FLFZ are crucial for the height difference and the different fluvial gradients (Figures 1, 3–5 and 11). Tilting, uplift and disintegration of the South German Block that is geomorphologically synonymous with the foreland of the South German Basin, kickstarted the development of the Proto-SSS during the Plio-Pleistocene with the creation of the headwaters of the SSS [102] (Table 5, Figure 16b).

5.3.2. Bedrock Geology—Unaltered to Slightly Altered by the Climate

The headwaters (CA): The onset of the CA is marked by a steepening of the slope angle along with a diminishing degree of sinuosity (Figure 11a–d, Table 5). The drainage sector resembles the Modern SSS as far as the sinuosity is concerned but still possesses all hallmarks of the relic Neogene fluvial system as to the slope angle and the valley fill (Figure 11a–c) (Section 5.3.1). In the CA of the LGG- and LHG-types the slope angles are far below 20°. Palisades and tors arise from hilltops the subhorizontal surface of which has an inclination of between 5° to 10°. Due to the joint action of fluvial and mass wasting (slide, creep) erosion at slope angles greater than 10° these landforms with almost subvertical walls tend to disintegrate into felsenmeers, blockmeers, blockfields

and block streams (Figures 7b,c,e and 16b, Table 5). The final result is a skeletal highly permeable landform series surrounded by deposits completely depleted as to their argillaceous matter and undergoing reworking and sorting during cold climates and periglacial conditions [86,147–155].

Landforms and slope angles correlate with the F/M ratios (ratio of fluvial to mass wasting products) which are below 1 in contrast to the VLG-type where the ratio exceeds 2 (Table 5). The less permeable lithologies of the slate mountains of the VLG exceed the LHG and LGG types with regard to the aerial extension of floodplain deposits; they are characterized by the highest drainage density, the highest degree of sinuosity and a high rate of slate pebbles and gravel in the sediment load. Their smooth hilltops are blanketed all across with topsoil and densely forested with softwood trees. This is also corroborated by the mass wasting products which rank lowest among the reference types (Table 1). The slates that were subjected to very-low-grade regional metamorphism still feature the low permeability of their argillaceous parent material yet do no longer show the weathering behavior of their predecessors, grey and black shales [95,156–158].

The LHG- and LGG-types preserved most conspicuously the Neogene supergene alteration with a thick regolith that was reworked under colder climatic condition into the CA by mass wasting processes, leaving as residues the different monadnocks which became instable on gentle inclined slopes. It has to be noted, that etch planation is held to be the initial process accountable for the built-up of the afore-mentioned landforms on hilltops but subsequent cryoplanation cannot be sidelined to have contributed to the formation and preservation of these rocky hilltops. On the other hand, the sinuosity increases relative to that of the VLG, where the fluvial deposits are more widespread around the hilltop devoid of monadnocks. This triple of numerical parameters sinuosity, slope angle and the F/M ratio is a diagnostic dataset to assess the supergene alteration or prestage impact on the development of the CA of the SSS.

The transport area (TA): The Steinach River is running subparallel to the strike of the metamorphic host rocks (Figures 10a and 13). Sectors of the drainage system framed by epigneisses of high rock strength tend to form fluvial deposits in a narrow gorge with a steepening of the slope angle accompanied by outcrops of the bare rocks and a decrease in the sinuosity between 1.023 and 1.095. In those sectors where phyllitic-quartzitic metasediments constitute the country rocks colluvial sediments prevail over fluvial deposits and the sinuosity increases to 1.085 to 1.116 while the valley widens, and the slope angle diminishes (Figures 10 and 13). Where the fresh bedrocks are largely exposed in the valley, irrespective of the varied lithology the slope angles are quite similar (Table 1): VGL:18°–26.2°–35°, LGG: 15°–23.4°–35°, LHG: 15°–26.9°–35° (min-mean-max). However, there are also marked differences in the lack of the V-shaped wide-angle valleys in the LHG-Type. The VLG-Type shows the steepest slopes, exceptionally high F/M ratios and the greatest variety in the cross-sectional valley morphology from wide-angle V-shaped valleys to flat-floor-shaped/U-shaped valleys. This fact closely correlated with elevated rock strength and low vulnerability of the bedrock against chemical weathering. The TA was shaped under oscillating cold and warmer phases of the glacial period (Table 5).

The depositional area (DA): Only in the DA of the VLG-Type, with its intra-basement terraces and floodplains, occur exceptionally steep slopes in a fluvial landform denominated as flat-floor-shaped U-shaped valley (basement) (15°–32.1°–37°) (Figures 8a and 12a). Its rectangular cross-sectional shape originated from quartzitic bedrocks and chert of the high rock strength ever reported from this study area. (Figures 8a and 9c). The sinuosity of the SSS conspicuously rises when leaving the basement whereas the slope angles decrease (Tables 1 and 5). The size of the large plains of the DA in front of the basement is a function of the gradient attaining a maximum around the fan delta of the Schorgast-Coserbach Drainage System (LHG-Type) (Figure 11b,d). It is the only site where terraces were completely eradicated leaving behind some butte-like gravel piles (Figure 9c). On the hillwash plain boulders and gravel do not form part of the alluvial-fluvial flow processes. They are either supplied to the channels and rills (confined drainage system) by talus

creep or respond only passively in the apron at the foot of triangular slopes as they got deprived of their fine-grained matrix by hillwash [84]. The stacked pattern of terraces within the DA formed during the glacial period between the Middle Pleistocene and the Holocene [81,108,159]. Štěpančíková et al. (2008) [160] recorded a similar set of terraces with the oldest one forming during the Elsterian 2 (0.40–0.46 Ma) from the East Sudeten Mountains. Younger terraces aged Saalian 1 (240–280 ka), Saalian 2 (130–180 ka) and Weichselian (10–80 ka), respectively, might be correlated with the three younger floodplains in front of the FLFZ.

5.4. The Sediment Load and Its Implication on the Drainage System of the SSS

5.4.1. Hydrodynamic Regime and the GMS Tool

Fresh to slightly altered (limonitic rims) rock fragments are selected during gravel analysis using the GMS tool (Table 3). This sedimentological approach taken in different depositional environments from Antarctica to the Arctic is an additional means to decipher the mode of slope and valley formation in the *statu nascendi* at the beaches, in fluvial channels, mass wasting lobes and wedges and the periglacial (para)autochthonous landforms [62,84,117,161]. Situmetric measurements of the angle between the 1st and 2nd maximum in bimodal distributions of the clast orientation widen as the mass wasting on the valley fill increases relative to the fluvial deposition in the river sector (Table 3).

Cryogenic influence can be figured out using the situmetric reference plain in vertical position as exemplified by the sedimentology and sedimentary petrography of fluvial and cryogenic gravel deposits of the terrace T 1 of the LGG-Type in the "Weidenberg Bowl" (Figures 5a,b and 10b). Fluvial gravel deposits override randomly distributed lithoclasts in a cryoturbated cavity which has been dragged downstream. The vertical situgram displays fluvial gravel beds mixed with colluvial sediments underneath. Both maxima are aligned at acute angle to the floodplain. The vertical situgram of the cryoturbated sediments trapped in a pocket and fluvially reworked still shows a subvertical maximum between 40 to 80°. The subvertical positioning of gravel underneath terraces and in fluvial sediments is indicative of periglacial landforms such as ice wedges. There are fluvial-(peri)glacial gravelly deposits in the DA of VLG and of the LGG types SSS in which based upon the situmetric measurements the relative influence of fluvial, cryogenic and mass wasting processes can be assessed (see Figure 8a, Table 1).

One can assess and describe the impact of cryogenic processes in a model as follows. Narrow V-shaped valleys carved out of the crystalline bedrock by ideal straight channels as at LGG-type are depleted in bed load deposits (Bernoulli Effect). There exists an intermittent but unimpeded flow regime at rather high speed in the straight channels so that gravel plains can easily be piled up and triggered by outburst and flash floods upstream in the nival zone. Conclusively, a low degree of sinuosity and a high gradient (see LHG-type) are both instrumental for the emplacement of such vast plains at the downstream end of the river run. Albeit no glaciers are covering the mountain tops, periglacially-related landslide triggered outburst floods, attested to by the 1st and 2nd order valleys clogged with mass wasting deposits work in the same way as even better due to the higher frequency [162,163]. Such indirect catastrophic lake outburst floods need no true glacier on the retreat but are typical proglacial lakes and especially destructive as the straight channel system does not slow down movement of the water mass but speed the process up [164].

The passage from the CA into the TA and from the TA into the DA is marked by an abrupt grain size increase caused by changes in the gradient and the presence of knick-points. It is accompanied by a change of grain morphology as a function of facies with the roundness $max_{fluvial}$ is significantly greater than the roundness $max_{colluvial}$. Considering the gravel size interval as a single entity, the gravel analyses of the SSS shows a rather homogeneous picture making up around 70% of the total grain size of the fluvial sediments (Table 1). A more subtle analysis discriminating the particle size into boulder, cobble, pebble and sand yields a characteristic split of the grain size range in the VLG-type, with the finer-grained lithoclasts to prevail over the coarser-grained ones:

lithoclasts$_{pebble}$ > lithoclasts$_{cobble+boulder}$ (Table 1). This behavior of the clast community correlates with the metamorphic grade of the bedrock. Even though having been derived from the same pelitic parent material (mudstone, shales) they show up as different metapelites and with different ways of disintegration on erosion and transport in the SSS: VLG: slate (and flagstone), LGG: phyllite, LHG: paragneiss (Table 1). The paragneisses of the LHG are most susceptible to chemical weathering during the Neogene and therefore the bedload got reduced at the expense of clay and silt (Section 5.4.2).

5.4.2. Lithology and Suspended Load

The mineralization in the regolith is controlled by the basement lithology and by the climate as exemplified in Figure 2b. The climate has a strong influence on the physical-chemical regime of aquatic system provoking a drop of the pH far below pH 7 and led to oscillating redox conditions around 0 (Section 5.1). It affected the Paleozoic bedrock (Section 5.3) to a different degree resultant in an argillaceous regolith of particular widespread occurrence in LHG (Section 5.3.1) (Tables 1 and 5, Figure 2b). The clay mineral assemblages in the reference types closely resemble each other. Some striking difference occur in ultrabasic rocks which create serpentine and talc when undergoing chemical weathering in the LHG-type bedrocks as a result of the high Mg content in the parent material. Smectite and nontronite are neither accounted for by a different climate nor by any pyroclastic input but caused by the preponderance of feldspar in the source rock such as the granites of the LGG type. Even at a high uplift rate a constant supply with feldspar is guaranteed in the LGG-type so as to maintain a considerable high pH in the saprock. Expandable clay minerals are very common within the proximal alteration zone of feldspar-enriched basic magmatic rocks [165,166]. The end product of this supergene argillitization/regolith is kaolinite, a marker mineral for acidic meteoric fluids in the LHG- and the LGG-types (Figure 15).

In the VLG-type kaolinite co-exists with illite-muscovite, chlorite and vermiculite as a primary phyllosilicate in the slates. The primary metamorphic mineral assemblage is in equilibrium with the secondary supergene neomorphic mineral assemblage. Flakes of unaltered slate only need to get chipped off mechanically and transported by the SSS in the pebble grain-size fraction of the bedload (Table 1). The same holds true also for the metapelites as far as the chloritic and micaceous phyllosilicates are concerned which are reworked as chlorite-mica-quartz phyllite gravel (Table 1). The situation completely differs from that of the LHG-type where the high-grade metamorphic rocks are strongly susceptible to the pervasive chemical weathering and the adjustment of the clay mineral association by supergene alteration brought about loamy substrate and a complete eradication of the primary structures (Table 1, Figure 11b). In the CA, large areas are covered by sediments derived from argillaceous fluvial and mass wasting processes attaining in places a regolith as much as 23 m thick and unaltered gneissic gravel are the exception than the rule. Therefore, fluvial gravel in the TA are rare and a turbid slurry comes into existence which at the very end spreads across the hillwash plain in the DA (Figures 2b, 4, 9 and 11b,d). Unlike in many regolith blankets elsewhere, the results of supergene alteration in these basement regions are no longer in situ but have to be denominated as parautochthonous due to the reworking by periglacial land-forming processes [167–171].

5.4.3. Lithology and Bedload

Besides clay and silt, gravel-sized clasts form the second maximum within the bimodal grain-size distribution of the fluvial and colluvial sediments (Tables 1 and 4). This bimodal grain-size distribution is conspicuously expressed numerically by the three reference types all of which are undernourished with regard to sand relative to clay+silt and gravel (Table 1). The coarse-grained fraction is especially widespread in the clast community of the VLG- and LGG types (Table 4). This is especially true for the FG Anticline which forms one of the most significant watersheds between the drainage systems of the Rhein and Donau Rivers (Figure 11c). Considering the DA of the Steinach River, a conspicuous impoverishment of the gravel assemblage in granite clasts is evident. They are very rare

constituents in terrace No 2 and No1- Marginal Granite G2 and Core Granite G 3 (Table 4). At the transition CA-TA, the fresh granite exposed in the non-alluvial channels, abruptly converts via large blocks into grus at the edge of the granite. It disappears from the clast size amenable for differentiation with the unarmed eye in the field into a phyllosilicate spectrum sampled at the same site of observation made up of Illite/muscovite < 70%, vermiculite < 30%, kaolinite < 10% (Figure 11c). These mineralogical/ lithological observations agree with those made by Migoń and Lidmar-Bergström (2002) [172] who recorded increased amounts of 7-Å phyllosilicates from the Mesozoic and Paleogene saprolite but not from the Neogene-Quaternary interval. The phyllosilicate assemblage recorded above from the SSS does not only corroborate the attribution in time to the Quaternary but also delineates the metamorphic host rocks of the granite as the major provenance for the bedload. Creeks flowing into the Steinach originate from rills upstream, through confined debris flows grade into fan delta deposits that do not differ from the Pleistocene fluvial deposits of the master river with regard to the gravel assemblage (Figure 14, Stein 11b, 11c) [173–177]. The bedload and suspended load representative of a bimodal distribution is in terms of size and composition typical of the SSS are another combination mirroring the bimodality during evolution of the drainage system (Table 5, Figure 2b).

5.5. The SSS in View of Geodynamics and Crustal Maturity

The SSS reflects a metastable hydrodynamic system which whenever it is possible tries to approximate the stable meandering final state. To force the channel to maintain its straight to low-sinuosity pattern needs a stringent control by the geology and petrography of the country rocks over a significant period of time which measures millions rather than thousands of years. The link between the endogenous processes litho-genesis and tectonics and the hydrodynamic evolution of the drainage systems is provided by the supergene alteration/ weathering [122,124–128,178,179]. The joint action of the aforementioned processes related to the maturity of the geodynamic units, in the Central European Variscides, which can be subdivided on a global basis into three categories: (1) supermature, (2) mature, (3) pre-mature [120] (Table 6, Figure 1c). Due to the outstanding geodynamic position of the Central European Variscides (Figure 18), in general, and the Bohemian Massif, forming the core zone of Mesoeurope, in particular, the current study area can be taken as the reference type of the mature state of an orogenic crustal section. The supermature stage is today well exposed in the lowlands and peneplains of the deeply eroded Precambrian cratons. It is likewise different as to the landforms and earth surface processes from the mature state as it is the immature state represented, by modern fold belts, both of which need a separate treatment with regard to these drainage regimes and it would go far beyond the present topic to discuss the interlocking of them in more detail (Table 6). This maturity concept applicable to drainage systems has been tested by Dill et al. (2019) [180] for the marginal zones of the Variscan Orogen of Mesoeuropean landscape in Morocco as well as by Dill et al. (2020c) [84] for the Mesoeuropean landscape of the Gondwana Continent in the South Atlantic Ocean (Figure 1c).

Table 6. Classification scheme of crustal maturity. The mature state is equivalent to the Variscan-type referred to in the current study.

The Geomorphological-Geodynamic Maturity Stages	Maturity		
	Pre-Mature	**Mature**	**Super-Mature**
Geodynamic setting	Moderately eroded and active mountain belts of Late Mesozoic to Cenozoic age (e.g., Andes) + island arcs	Highly eroded mountain belts of Paleozoic and Early Mesozoic age (e.g., Hercynian/Variscan Mountain Ridges) + continental grabens	Deeply eroded cratons of Precambrian age (e.g., Guyana Shield) + continental grabens + island arcs
Occurrence of weathering (see Figure 15)	Absent (only slightly altered parent material) moderate argillitization	Argillitization >> duricrusts	Duricrusts—argillitization
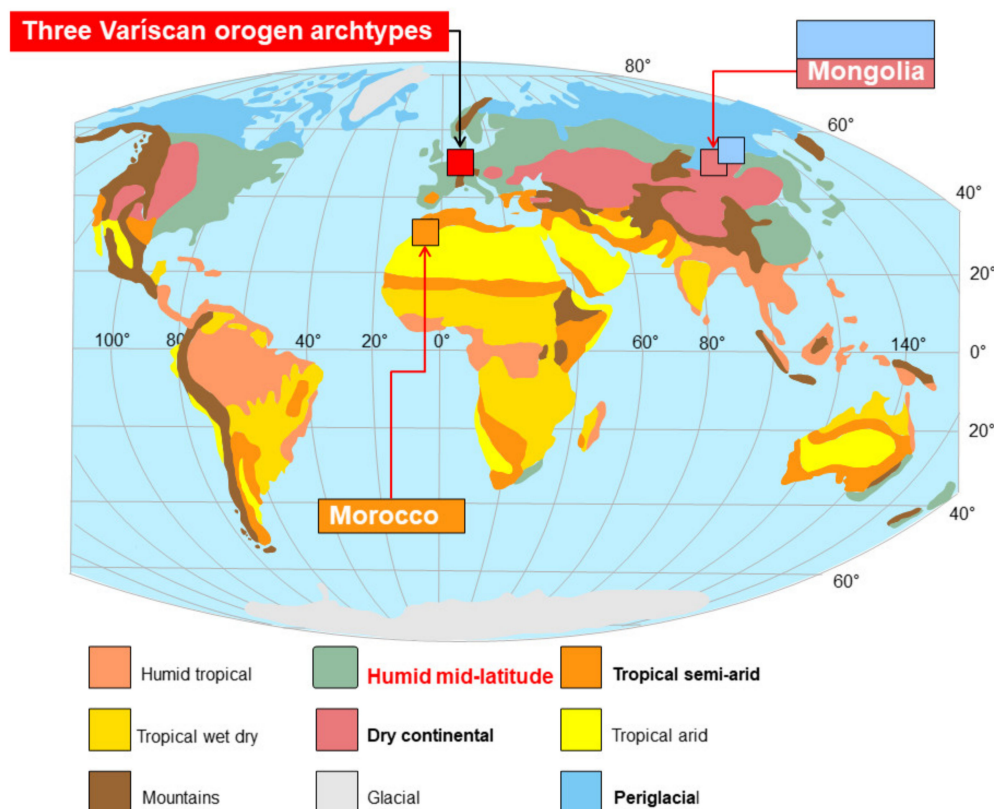
Figure 18. The position of the study areas referred to in the text in relation to morphoclimatic zonation of the globe during the period of time < 2 Ma/Quaternary (modified from Tricart and Cailleux, 1972; Scotese, 2002 [181,182] http://www.scotese.com/legend.htm) (accessed on 10 February 2013).

5.6. The SSS in View of Higher and Lower Latitude Climate Zones

The modern SSS which in a Variscan-type orogen today is active in a humid mid-latitude climate zone in Central Europe (Figure 18). What is the drainage system like in a Variscan-type orogen located higher and lower latitudes than the archetypes (Figures 1c and 18)? For reference, the SSS equivalent drainage systems at higher latitude under dry continental to periglacial climatic conditions an area near Lake Hovsgul, Mongolia, has been considered. The landscape formed part of geomorphological transect from the taiga to the desert [42,183]. The drainage pattern of the very coarse-grained streams develops in a transition from the mountain forest steppe into a grass steppe. The channel systems is trellis-like with coarse grained -meandering streams, wide flood plains and terraces on both valley sides but of ephemeral type. Low-sinuosity to straight channel systems are consequent dip-stream systems. The higher sinuosity values are encountered in subsequent strike stream systems. In the Moroccan Meseta reference sites at lower latitude which evolved under tropical semiarid climatic conditions strike streams and anti-dip streams that break through the steeply dipping carbonate ridges evolved in some kind of a badland landscape [180,184,185]. Similar to the archetype in Germany and irrespective of the climate and latitude the typical SSS evolved where the tectonic drivers be it folding or faulting create the highest gradient and where a marked contrast in rock strength occurs. The sediment load, however, is controlled by the country rocks and the (paleo)climate which impacts on the lithosphere via the pedosphere and supergene alteration.

6. Conclusions

- The "key message" to the evolution of the SSS is as follows (Table 5, Figure 2b): The SSS analyzed in this study are metastable drainage systems which are maintained over a longer period of time (approx. 25 Ma) and distance from source to confluence

(approx. 30 km) by a rigid framework provided by the tectonics and bedrock lithology. The SSS is kept operating by a climate change from humid tropical through periglacial into humid temperate. In terms of chronology, it is most suitably described by a four-stage succession.

1. The geological framework of the SSS: Forming the lithological and structural features in the bedrock as a result of different temperature, pressure and dynamic metamorphic processes.
2. Prestage of SSS: Forming the paleo-landscape with a stable fluvial regime as starting point for the SSS
3. Proto-SSS: Transition into the metastable fluvial regime of the SSS
4. Modern SSS: Operation of the metastable fluvial regime with the tendency to regain a stable hydrodynamic state in the adjacent foreland

- Tectonics plays a dual role. Late Paleozoic fold tectonic affects the Paleozoic bedrock and creates the basis for the drainage pattern of these SSS. Its influence diminishes from the very-low-grade to the high-grade stage of metamorphism (VLG⇒LGG⇒LHG). So does its guiding effect on the emplacement of the drainage systems during the Neogene and Quaternary. Late Cenozoic fault tectonic triggered the onset of the SSS to incise into the basement. The impact of fault tectonic on the SSS depends on the vertical displacement that correlates with the fluvial gradient of the SSS, the development of knickpoints, the occurrence of intermediate sediment traps and the cross-sectional shape of valleys.
- The change in the bedrock lithology has an impact on the fluvial and colluvial sediments and their pertinent landforms. From slate to mica-gneiss (VLG⇒LGG⇒LHG) the vulnerability to chemical weathering increases and as a consequence of this a change among the process-related sediments takes place: gravel ⇒ clay + silt. The change of landforms follows suit: drainage system of straight ⇒ higher sinuosity and paired terraces ⇒ hillwash plains.
- The climate change has a mediating effect via the bedrock controlling the intensity of mechanical and chemical weathering. The first type of supergene alteration increases towards younger intervals, whereas the second one shows a decreasing trend. Together with the Cenozoic tectonic, climate governs the intensity of fluvial, colluvial and cryogenic land-forming processes.
- The elaborated genetic model of the SSS is restricted to the basement of the Variscan -Type orogens which are representative of an intermediate maturity state between the pre-mature Cenozoic fold belts and the super-mature Precambrian cratons.
- Geomorphological-geological mapping of the fluvial, colluvial and cryogenic landform types is the descriptive part of the study while capturing numerical data relevant for the hydrographic studies of the SSS each reference area forms the geomorphometric one: (1) Quantification of fluvial and colluvial deposits along the drainage system, (2) slope angles, (3) degree of sinuosity as a function of river facies, (4) grain size distribution, (5) grain morphological categorization, (6) grain orientation ("situmetry"), (7) channel density, (8) channel/floodplain ratios.
- The compositional approach involves new mineralogical for the regolith which has been subdivided into a zone of argillitization and duricrusts. Their mineral assemblages are the basis for the thermodynamic computations (Eh, pH, concentration of solubles) to constrain the paleoclimatic regime during formation of the SSS.
- Comparing Variscan-type drainage systems from higher and lower-latitude climate zones relative to the archetypes reveals, the physical part (landform) of the SSS is controlled by tectonic and bedrock, whereas its chemical part (sediment composition) by the climate/weathering interacting with the country rocks.

References

1. Williams, G.P. River meanders and channel size. *J. Hydrol.* **1986**, *88*, 147–164. [CrossRef]
2. Miall, A.D. *The Geology of Fluvial Deposits*; Springer: New York, NY, USA, 1996; 582p.
3. Knighton, D.A. *Fluvial Forms and Processes: A New Perspective*; Arnold: London, UK, 1998; 400p.
4. Nanson, G.C.; Knighton, A.D. Anabranching rivers: Their cause, character and classification. *Earth Surf. Process. Landf.* **1996**, *21*, 217–239. [CrossRef]
5. Selley, R.C. *Applied Sedimentology*, 2nd ed.; Academic Press: New York, NY, USA, 2000; 523p.
6. Chin, A. The periodic nature of step-pool mountain streams. *Am. J. Sci.* **2002**, *302*, 144–167. [CrossRef]
7. Moody, J.A.; Troutman, B.M. Characterization of the spatial variability of channel morphology. *Earth Surf. Process. Landf.* **2002**, *27*, 1251–1266. [CrossRef]
8. Bridge, J.S. *Rivers and Floodplains*; Whiley-Blackwell: Oxford, UK, 2003; 504p.
9. Robert, A. *River Processes: An Introduction to Fluvial Dynamics*; Routledge: Abingdon, UK, 2003; 238p.
10. Charlton, R. *Fundamentals of Fluvial Geomorphology*; Routledge: Abingdon, UK, 2014; 214p.
11. Wang, S.; Ni, J. Straight river: Its formation and speciality. *J. Geogr. Sci.* **2002**, *12*, 72–80.
12. Audemard, F.A. Morpho-structural expression of active thrust fault systems in the humid tropical foothills of Colombia and Venezuela. *Zeitschrift für Geomorphologie Supplementband* **1999**, *118*, 227–244.
13. Whipple, K. Bedrock rivers and the geomorphology of active orogens. *Annu. Rev. Earth Planet. Sci.* **2004**, *32*, 151–185. [CrossRef]
14. Castillo, M.; Munoz-Salinas, E.; Ferrari, L. Response of a landscape to tectonics using channel steepness indices (ksn) and OSL: A case of study from the Jalisco Block, Western Mexico. *Geomorphology* **2014**, *221*, 204–214. [CrossRef]
15. Gong, Z.; Li, S.; Li, B. The evolution of a terrace sequence along the Manas River in the northern foreland basin of Tian Shan, China, as inferred from optical dating. *Geomorphology* **2014**, *213*, 201–212. [CrossRef]
16. Papanikolaou, I.D.; Van Balen, R.; Silva, P.G.; Reicherter, K. Geomorphology of active faulting and seismic hazard assessment: New tools and future challenges. *Geomorphology* **2015**, *237*, 1–13. [CrossRef]
17. Zondervan, J.R.; Stokes, M.; Boulton, S.J.; Telfer, M.W.; Mather, A.E. Rock strength and structural controls on fluvial erodibility: Implications for drainage divide mobility in a collisional mountain belt. *Earth Planet. Sci. Lett.* **2020**, *538*, 116221. [CrossRef]
18. Sancho, C.; Pena, J.L.; Rivelli, F.; Rhodes, E.; Munoz, A. Geomorphological evolution of the Tilcara alluvial fan (Jujuy Province, NW Argentina): Tectonic implications and palaeoenvironmental considerations. *J. S. Am. Earth Sci.* **2008**, *26*, 68–77. [CrossRef]
19. Stokes, M.; Mather, A.E.; Belfoul, A.; Farik, F. Active and passive tectonic controls for transverse drainage and river gorge development in a collisional mountain belt (Dades Gorges, High Atlas Mountains, Morocco). *Geomorphology* **2008**, *102*, 2–20. [CrossRef]
20. Perez-Pena, J.V.; Azor, A.; Azanon, J.M.; Keller, E.A. Active tectonics in the Sierra Nevada (Betic Cordillera, SE Spain): Insights from geomorphic indexes and drainage pattern analysis. *Geomorphology* **2010**, *119*, 74–87. [CrossRef]
21. Burbank, D.; Anderson, R. *Tectonic Geomorphology*; John Wiley & Sons: New York, NY, USA, 2011; 274p.
22. Molin, P.; Fubelli, G.; Nocentini, M.; Sperini, S.; Ignat, P.; Grecu, F.; Dramis, F. Interaction of mantle dynamics, crustal tectonics and surface processes in the topography of the Romanian Carpathians: A geomorphological approach. *Glob. Planet. Chang.* **2012**, *90*, 58–72. [CrossRef]
23. García, V.; Hongn, F.; Cristallini, E. Late Miocene to recent morphotectonic evolution and potential seismic hazard of the northern Lerma valley: Clues from Lomas de Medeiros, Cordillera Oriental, NW Argentina. *Tectonophysics* **2013**, *608*, 1238–1253. [CrossRef]
24. Jelínek, J.; Staněk, F.; Thomas, J.; Daněk, T.; Mališ, J. The application of morphostructural analysis and its validation by comparison with documented faults within the Zlaté Hory ore district (the Northeastern part of the Bohemian Massif). *Acta Geodyn. Geomater.* **2013**, *10*, 5–17. [CrossRef]
25. Melosh, B.L.; Keller, E.A. Effects of active folding and reverse faulting on stream channel evolution, Santa Barbara Fold Belt, California. *Geomorphology* **2013**, *186*, 119–135. [CrossRef]
26. Milliman, J.D.; Syvitski, J.P.M. Geomorphic/tectonic control of sediment discharge to the ocean: The importance of small mountainous rivers. *J. Geol.* **1992**, *100*, 525–544. [CrossRef]
27. Harbor, D.J.; Schumm, S.A.; Harvey, M.D. Tectonic control of the Indus River in Sindh, Pakistan. In *The Variability of Large Alluvial Rivers*; Schumm, S.S., Winkley, B.R., Eds.; American Association of Civil Engineers Press: New York, NY, USA, 1994; pp. 161–176.
28. Ruddiman, W.F. *Tectonic Uplift and Climate Change*; Springer: New York, NY, USA, 1997; 556p.

29. Tinkler, K.J.; Wohl, E.E. *Rivers over Rock: Fluvial Processes in Bedrock Channels*; Geophysical Monograph; John Wiley & Sons: New York, NY, USA, 1998; Volume 107, 323p.

30. Wohl, E.E. Bedrock channel morphology in relation to erosional processes. In *Rivers Over Rock: Fluvial Processes in Bedrock Channels*; Geophysical Monograph Series; Tinkler, K.J., Wohl, E.E., Eds.; American Geophysical Union: Washington, DC, USA, 1998; pp. 133–151.

31. Schumm, S.A. *Active Tectonics and Alluvial Rivers*; Cambridge University Press: Cambridge, UK, 2000; 290p.

32. Leeder, M. *Sedimentology and Sedimentary Basins: From Turbulence to Tectonics*; John Wiley & Sons: New York, NY, USA, 2011; 794p.

33. Gutiérrez, F.; Gutiérrez, M. *Landforms of the Earth*; Springer: New York, NY, USA, 2016; 284p.

34. Kasanin-Grubin, M.; Yair, A.; Romero, E.N.; Vergari, F.; Troiani, F.; Desloges, J.; Yan, L.; Moreno de las Heras, M.; Della Seta, M.; Hardenbicker, U.M.; et al. 2018 The role of lithological properties on badland development. In *Geophysical Research Abstracts 21*; EGU 2019-1021; EGU General Assembly: Vienna, Austria, 2019; Volume 21, p. 1.

35. Emmert, U.; Horstig, G.V.; Stettner, G. *Geologische Übersichtkarte 1:200000 CC 6334 Bayreuth*; BGR: Hannover, Germany, 1981.

36. Summerfield, M.A. *Global Geomorphology*; John Wiley and Sons Inc.: New York, NY, USA, 1991; 537p.

37. Easterbrook, D.J. *Surface Processes and Landforms*, 2nd ed.; Prentice Hall: New York, NY, USA, 1999; 546p.

38. McCann, T. *The Geology of Central Europe: Precambrian and Paleozoic: 1*; Special Volume; The Geological Society of London: London, UK, 2008; 748p.

39. McCann, T. *The Geology of Central Europe: Mesozoic and Cenozoic: 2*; Special Volume; The Geological Society of London: London, UK, 2008; 700p.

40. Bates, R.L.; Jackson, J.A. *Glossary of Geology*; American Geological Institute: Alexandria, VA, USA, 2005; 779p.

41. Evans, I.S.; Minár, J. A classification of geometric variables. *Geomorphometry* **2011**, *2011*, 105–107.

42. Dill, H.G.; Ludwig, R.-R.; Kathewera, A.; Mwenelupembe, J. A lithofacies terrain model for the Blantyre Region: Implications for the interpretation of palaeo savanna depositional systems and for environmental geology and economic geology in southern Malawi. *J. Afr. Earth Sci.* **2005**, *41*, 341–393. [CrossRef]

43. Callahan, J. A nontoxic heavy liquid and inexpensive filters for separation of minerals grains. *J. Sediment. Petrol.* **1987**, *57*, 765–766. [CrossRef]

44. Brookins, D.G. *Eh-pH Diagrams for Geochemistry*; Springer: Heidelberg, Germany, 1987; 176p.

45. Geyh, M.A.; Schleicher, H. *Absolute Age Dating Determination Physical and Chemical Dating Methods and Their Application*; Springer: Berlin, Germany, 1990; 63p.

46. Wallinga, J. Optically luminescence dating of fluvial deposits: A review. *Boreas* **2002**, *31*, 303–322. [CrossRef]

47. Onac, B.P. Mineralogical studies and Uranium-series dating of speleothems from Scǎricoara Glacier Cave (Bihor Mountains, Romania). *Theor. Appl. Karstology* **2001**, *13*, 33–38.

48. Dill, H.G.; Hansen, B.; Keck, E.; Weber, B. Cryptomelane a tool to determine the age and the physical-chemical regime of a Plio-Pleistocene weathering zone in a granitic terrain (Hagendorf, SE Germany). *Geomorphology* **2010**, *121*, 370–377. [CrossRef]

49. Dill, H.G.; Gerdes, A.; Weber, B. Age and mineralogy of supergene uranium minerals—Tools to unravel geomorphological and palaeohydrological processes in granitic terrains (Bohemian Massif, SE Germany). *Geomorphology* **2010**, *117*, 44–65. [CrossRef]

50. Dill, H.G.; Wemmer, K. Origin and K/Ar age of cryptomelane-bearing Sn placers on silcretes, SE Germany. *Sediment. Geol.* **2012**, *275*, 70–78. [CrossRef]

51. Dill, H.G.; Wehner, H. The depositional environment and mineralogical and chemical compositions of high ash brown coal resting on early Tertiary saprock (Schirnding Coal Basin, SE Germany). *Int. J. Coal Geol.* **1999**, *39*, 301–328. [CrossRef]

52. Horacio, J. River sinuosity index: Geomorphological characterization. In *Technical Note 2 CIREF and Wetlands International*; Physical Geography, Santiago de Compostela University: Santiago de Compostela, Spain, 2014; 6p.

53. Turowski, J.M. Alluvial cover controlling the width, slope and sinuosity of bedrock channels. *Earth Surf. Dyn.* **2018**, *6*, 29–48. [CrossRef]

54. Ahnert, F.O. *Einführung in Die Geomorphologie*; UTB GmbH: Stuttgart, Germany, 2015; 458p.

55. Nelson, F.E. A preliminary investigation of solifluction macrofabrics. *Catena* **1985**, *12*, 23–33. [CrossRef]

56. Nieuwenhuijzen, M.E.; Van Steijn, H. Alpine debris flows and their sedimentary properties. A case study from the French Alps. *Permafr. Periglac. Process.* **1990**, *1*, 111–128. [CrossRef]

57. Millar, S.W.; Nelson, F.E. Sampling-surface orientation and clast macrofabric in periglacial colluviums. Earth surface pro-cesses and landforms. *Earth Surf. Process. Landf.* **2001**, *26*, 523–529. [CrossRef]

58. Lindsey, D.A.; Langer, W.H.; Van Gosen, B.S. Using pebble lithology and roundness to interpret gravel provenance in pied-mont fluvial systems of the Rocky Mountains, USA. *Sediment. Geol.* **2007**, *199*, 223–232. [CrossRef]

59. Dill, H.G. Geology and chemistry of Variscan-type pegmatite systems (SE Germany)—With special reference to structural and chemical pattern recognition of felsic mobile components in the crust. *Ore Geol. Rev.* **2018**, *92*, 205–239. [CrossRef]

60. Illenberger, W.K. Pebble shape (and size?). *J. Sediment. Res.* **1991**, *61*, 756–767.

61. Dill, H.G.; Ulrich, H.-J. Geoelectric deep sounding—A contribution to constrain the genesis of siliceous ferromanganese duri-crusts on deeply weathered Palaeozoic basement rocks (N. Bavaria, F.R. Germany). *Z. Geomorphol.* **1987**, *31*, 361–370. [CrossRef]

62. Dill, H.G.; Buzatu, A.; Balaban, S.-I.; Ufer, K.; Techmer, A.; Schedlinsky, W.; Füssl, M. The transition of very coarse-grained meandering to straight fluvial drainage systems in a tectonized foreland-basement landscape during the Holocene (SE Germany)—A joint geomorphological-geological study. *Geomorphology* **2020**, *370*, 107364. [CrossRef]

63. Zöller, L.; Beierkuhnlein, C.; Samimi, C.; Faust, D. *Die Physische Geographie Deutschlands*; WBG—Wissenschaftliche Buchgesellschaft: Darmstadt, Germany, 2017; 208p.

64. Thauer, W. Morphologische Studien im Frankenwald und im Frankenwaldvorland. *Mitt. Fränkischen Geogr. Ges.* **1954**, *1*, 168–169.

65. Strebel, O. Tertiäre Reliktböden, Tertiäre Verwitterungsreste und Eiszeitliche Bodenumlagerungen im Frankenwald. Ph.D. Thesis, Universität Würzburg, Würzburg, Germany, 1955; 53p.

66. Drexler, O. Das Espich-Sediment bei Kulmbach. *Bayreuther Geowiss. Arb.* **1980**, *1*, 9–38.

67. Kleber, A.; Stingl, H. Zur Flußgeschichte des Trebgasttals nördlich von Bayreuth. Eine zweiphasige Talverlegung im Rotmainsystem. In *Beiträge zur Landeskunde Oberfrankens. Festschrift zum 65. Geburtstag von Bezirkstagspräsidenten Edgar Sitzmann*; Becker, H., Ed.; University Bamberg: Bamberg, Germany, 2000; pp. 191–208.

68. Zöller, L.; Stingl, H.; Kleber, A. Das Trebgasttal—Tal- und Landschaftsentwicklung nahe der Europäischen Hauptwasserscheide im Raum Bayreuth. *Bayreuther Geogr. Arb.* **2007**, *28*, 70–101.

69. Schirmer, W. Die Geschichte von Moenodanuvius und Main in Oberfranken. In *Streifzüge Durch Franken Band*; Dippold, G., Ed.; Lichtenfels: Lichtenfels, Germany, 2010; Volume 1, pp. 9–24.

70. Bucher, K.; Grapes, R. *Petrogenesis of Metamorphic Rocks*; Springer Science & Business Media: New York, NY, USA, 2011; 428p.

71. Stettner, G. *Geologische Karte von Bayern 1:25,000 Erläuterung Blatt 5936 Bad Berneck München*; Geologisches Landesamt: München, Germany, 1977; 225p.

72. Kennan, L.; Lamb, S.H.; Hoke, L. High-altitude palaeosurfaces in the Bolivian Andes: Evidence for late Cenozoic surface uplift. *Spec. Publ. Geol. Soc. Lond.* **1997**, *120*, 307–323. [CrossRef]

73. Babault, J.; Bonnet, S.; Driessche, J.V.D.; Crave, A. High elevation of low-relief surfaces in mountain belts: Does it equate to post-orogenic surface uplift? *Terra Nova* **2007**, *19*, 272–277. [CrossRef]

74. Landis, C.A.; Campbell, H.J.; Begg, J.G.; Mildenhall, D.C.; Paterson, A.M.; Trewick, S.A. The Waipounamu erosion surface: Questioning the antiquity of the New Zealand land surface and terrestrial fauna and flora. *Geol. Mag.* **2008**, *145*, 173–197. [CrossRef]

75. Hall, A.M.; Ebert, K.; Kleman, J.; Nesje, A.; Ottesen, D. Selective glacial erosion on the Norwegian passive margin. *Geology* **2013**, *41*, 1203–1206. [CrossRef]

76. Migoń, P. Tertiary etch surfaces in the Sudetes Mountains, SW Poland: A contribution to the preQuaternary morphology of Central Europe". In *Palaeosurfaces: Recognition, Reconstruction and Palaeoenvironmental Interpretation*; Special Publications; Widdowson, M., Ed.; Geological Society: London, UK, 1997; Volume 120, pp. 187–202.

77. Büdel, J. Die "Doppelten Einebnungsflächen" in den feuchten Tropen. *Z. Geomorphol. NF* **1957**, *1*, 201–228.

78. Jacobson, R.B.; Blevins, B.W.; Bitner, C.J. Sediment regime constraints on river restoration—An example from the Lower Missouri River. In *Management and Restoration of Fluvial Systems with Broad Historical Changes and Human Impacts*; James, L.A., Rathburn, S.L., Whittecar, G.R., Eds.; Geological Society of America Special Paper: Boulder, CO, USA, 2009; Volume 451, pp. 1–22.

79. Emmert, U. Ein Beitrag zur Flußgeschichte des Frankenwaldes und seines Vorlandes im Bereich des Kartenblattes Stadtsteinach (1:25,000). *Geol. Bl. NO-Bayern* **1953**, *3*, 36–42.

80. Emmert, U.; von Horstig, G. *Geologische Karte von Bayern 1:25,000 Erläuterung Blatt 5734 Wallenfels München*; Geologisches Landesamt: München, Germany, 1972; 240p.

81. Emmert, U.; Stettner, G. *Geologische Karte von Bayern 1:25,000 Erläuterung Blatt 6036 Weidenberg München*; Geologisches Landesamt: München, Germany, 1995; 239p.

82. Emmert, U.; Weinelt, W. *Geologische Karte von Bayern 1:25,000 Erläuterung Blatt 5935 Marktschorgast München*; Geologisches Landesamt: München, Germany, 1962; 286p.

83. Bryan, R.; Yair, A. Perspectives on studies of badland geomorphology. In *Badland Geomorphology and Piping*; Bryan, R., Yair, A., Eds.; Geobooks: Norwick, UK, 1982; pp. 1–12.

84. Dill, H.G.; Buzatu, A.; Goldmann, S.; Kaufhold, S.; Bîrgăoanu, D. Coastal landforms of "Meso-Afro-American" and "Neo-American" landscapes in the periglacial South Atlantic Ocean: With special reference to the clast orientation, morphology, and granulometry of continental and marine sediments. *J. S. Am. Earth Sci.* **2020**, *98*, 102385. [CrossRef]

85. Rea, B.R.; Whalley, W.B.; Rainey, M.M.; Gordon, J.E. Blockfields, old or new? Evidence and implications from some plateaus in northern Norway. *Geomorphology* **1996**, *15*, 109–121. [CrossRef]

86. Fjellanger, J.; Sørbel, L.; Linge, H.; Brook, E.J.; Raisbeck, G.M.; Yiou, F. Glacial survival of blockfields on the Varanger Peninsula, northern Norway. *Geomorphology* **2006**, *82*, 255–272. [CrossRef]

87. Twidale, C.R.; Vidal Romani, J.R. *Landforms and Geology of Granite Terrains*; Taylor & Francis Ltd.: London, UK, 2005; 354p.

88. Migoń, P. Granite Landscapes of the World. In *Geomorphological Landscapes of the World 22*; Oxford University Press: Oxford, UK, 2006; 416p.

89. Migoń, P.; Thomas, M.F. Grus weathering mantles—Problems of interpretation. *Catena* **2002**, *49*, 5–24. [CrossRef]

90. Shakesby, R.A. Pronival (protalus) ramparts: A review of forms, processes, diagnostic criteria and palaeoenvironmental implications. *Prog. Phys. Geogr.* **1997**, *21*, 394–418. [CrossRef]

91. Matthews, J.A.; Wilson, P.; Mourne, R.W. Landform transitions from pronival ramparts to moraines and rock glaciers: A case study from the Smørbotn cirque, Romsdalsalpane, southern Norway. *Geogr. Ann. Ser. A Phys. Geogr.* **2017**, *99*, 15–37. [CrossRef]

92. Watson, E. Two nivation cirques near Aberystwyth, Wales. *Biul. Peryglac.* **1966**, *15*, 79–101.

93. Christiansen, H.H. Nivation forms and processes in unconsolidated sediments, NE Greenland. *Earth Surf. Process Landforms* **1998**, *23*, 751–760. [CrossRef]

94. Raab, T.; Völkel, J. Late Pleistocene glaciation of the Kleiner Arbersee area in the Bavarian Forest, South Germany. *Quat. Sci. Rev.* **2003**, *22*, 581–593. [CrossRef]

95. Ehlers, J.; Eissmann, L.; Lippstreu, L.; Stephan, H.-J.; Wansa, S. Pleistocene Glaciations of North Germany. *Dev. Quat. Sci. 2* **2004**, *2*, 135–145.

96. Rinterknecht, V.; Matoshko, A.; Gorokhovich, Y.; Fabel, D.; Xu, S. Expression of the Younger Dryas cold event in the Carpa-thian Mountains, Ukraine. *Quat. Sci. Rev.* **2012**, *39*, 106–114. [CrossRef]

97. Fiebig, M.; Buiter, S.J.H.; Ellwanger, D. Pleistocene glaciations of South Germany. *Dev. Quat. Sci. 2* **2004**, 147–154.

98. Fossen, H. *Structural Geology*; Cambridge University Press: Cambridge, UK, 2010; p. 480.

99. Lisle, R.J.; Brabham, P.; Barnes, J.W. *Basic Geological Mapping (Geological Field Guide)*, 5th ed.; John Wiley & Sons: New York, NY, USA, 2011; 230p.

100. Seidel, G. *Geologie von Thüringen*; Schweitzerbartsche Verlagsbuchhandlung: Stuttgart, Germany, 1995; 556p.

101. Kley, J. "Saxonian tectonics" in the 21st century. *Z. Dtsch. Ges. Geowiss.* **2013**, *164*, 295–311. [CrossRef]

102. Ring, U.; Bolhar, R. Tilting, uplift, volcanism, and disintegration of the South German Block. *Tectonophysics* **2020**, *795*, 228611. [CrossRef]

103. Emmert, U.; von Horstig, G.; Weinelt, W.i. *Geologische Karte von Bayern 1:25,000 Erläuterung Blatt 5835 Stadtsteinach*; München, Geologisches Landesamt: München, Germany, 1960; 279p.

104. Von Horstig, G. *Geologische Karte von Bayern 1:25,000 Erläuterung Blatt 5635 Nordhalben München*; Geologisches Landesamt: München, Germany, 1966; 167p.

105. Von Horstig, G.; Stettner, G. *Geologische Karte von Bayern 1:25,000 Erläuterung Blatt 5636 Naila München*; Geologisches Landesamt: München, Germany, 1962; 192p.

106. Von Horstig, G.; Stettner, G. *Geologische Karte von Bayern 1:25,000 Erläuterung Blatt 5736 Helmbrechts München*; Geologisches Landesamt: München, Germany, 1970; 176p.

107. Von Horstig, G.; Stettner, G. *Geologische Karte von Bayern 1:25,000 Erläuterung Blatt 5735 Schwarzenbach a. Wald. München*; Geologisches Landesamt: München, Germany, 1976; 178p.

108. Štěpančíková, P.; Stemberk, J.; Vilímek, V.; Košťák, B. Neotectonic development of drainage networks in the East Sudeten Mountains and monitoring of recent fault displacements (Czech Republic). *Geomorphology* **2008**, *102*, 68–80. [CrossRef]

109. Vita-Finzi, C. *Recent Earth Movements: An Introduction to Neotectonics*; Academic Press: Cambridge, UK, 1986; 226p.

110. Schumm, S.A. Sinuosity of alluvial channels on the Great Plains. *Geol. Soc. Am. Bull.* **1963**, *74*, 1089–1100. [CrossRef]

111. Church, M. Geomorphic thresholds in riverine landscapes. *Freshw. Biol.* **2002**, *47*, 541–557. [CrossRef]

112. Beechie, T.J.; Liermann, M.; Pollock, M.M.; Baker, S.; Davies, J. Channel pattern and river-floodplain dynamics in forested mountain river systems. *Geomorphology* **2006**, *78*, 124–141. [CrossRef]

113. Hack, J.T. Stream-Profile Analysis and Stream-Gradient Index. *J. Res. U. S. Geol. Surv.* **1973**, *1*, 421–429.

114. Gomez, F.; Barazangi, M.; Bensaid, M. Active tectonism in the intracontinental Middle Atlas Mountains of Morocco: Syn-chronous crustal shortening and extension. *J. Geol. Soc. Lond.* **1996**, *153*, 389–402. [CrossRef]

115. Zuchiewicz, W. Time-series analysis of river bed gradients in the Polish Carpathians: A statistical approach to the studies on young tectonic activity. *Z. Geomorphol.* **1995**, *39*, 461–477. [CrossRef]

116. Demoulin, A. Testing the tectonic significance of some parameters of longitudinal river profiles: The case of the Ardenne (Bel-gium, NW Europe). *Geomorphology* **1998**, *24*, 189–208. [CrossRef]

117. Dill, H.G.; Buzatu, A.; Balaban, S.-I.; Ufer, K.; Gómez Tapias, J.; Bîrgăoanu, D.; Cramer, T. The "badland trilogy" of the Desierto de la Tatacoa, Upper Magdalena Valley, Colombia, a result of geodynamics and climate: With a review of badland landscapes. *Catena* **2020**, *194*, 104696. [CrossRef]

118. Pettijohn, F.J.; Potter, P.E.; Siever, R. *Sand and Sandstone*; Springer: Berlin, Germany, 1987; 553p.

119. Bertran, P.; Hétu, B.; Texier, J.-P.; Van Steijn, H. Fabric characteristics of subaerial slope deposits. *Sedimentology* **1997**, *44*, 1–16. [CrossRef]

120. Dill, H.G. Residual clay deposits on basement rocks: The impact of climate and the geological setting on supergene argillitization in the Bohemian Massif (Central Europe) and across the globe. *Earth Sci. Rev.* **2017**, *165*, 1–58. [CrossRef]

121. Emmert, U.; Stettner, G. *Geologische Karte von Bayern 1:25,000 Erläuterung Blatt 5737 Schwarzenbach a. d. Saale München*; Geologisches Landesamt München: München, Germany, 1968; 236p.

122. Dupré, B.; Dessert, C.; Oliva, P.; Goddéris, Y.; Viers, J.; François, L.; Millot, R.; Gaillardet, J. Rivers, chemical weathering and Earth's climate. *Comptes Rendus Geosci.* **2003**, *335*, 1141–1160. [CrossRef]

123. Retallack, G.J. Soils and global change in the carbon cycle over geological time. *Treatise Geochem.* **2003**, *5*, 605.

124. Rosing, M.T.; Bird, D.K.; Sleep, N.H.; Glassley, W.; Albarede, F. The rise of continents—An essay on the geologic consequences of photosynthesis. *Palaeogeogr. Palaeoclimatol. Palaeoecol.* **2006**, *232*, 99–113. [CrossRef]

125. Bishop, P. Long-term landscape evolution: Linking tectonics and surface processes. *Earth Surf. Process. Landf.* **2007**, *32*, 329–365. [CrossRef]

126. Lee, C.-T.A.; Morton, D.M.; Kistler, R.W.; Baird, A.K. Petrology and tectonics of Phanerozoic continent formation: From island arcs to accretion and continental arc magmatism. *Earth Planet. Sci. Lett.* **2007**, *263*, 370–387. [CrossRef]

127. Chadwick, O.A.; Roering, J.J.; Heimsath, A.M.; Levick, S.R.; Asner, G.P.; Khomo, L. Shaping post-orogenic landscapes by climate and chemical weathering. *Geology* **2013**, *41*, 1171–1174. [CrossRef]

128. Khomo, L.; Bern, C.R.; Hartshorn, A.S.; Rogers, K.H.; Chadwick, O.A. Chemical transfers along slowly eroding catenas de-veloped on granitic cratons in southern Africa. *Geoderma* **2013**, *202*, 192–202. [CrossRef]

129. Knobloch, E. Die tertiäre Flora von Seußen und Pilgramsreuth in Nordbayern. *Erlanger Geol. Abh.* **1971**, *87*, 1–20.

130. Moser, M.; Niederhöfer, H.-J.; Falkner, G. Continental mollusks of the fossil site Sandelzhausen (Miocene; Upper Freshwater Molasse from Bavaria) and their value for palaeoecological assessment. *Paläontologische Z.* **2009**, *83*, 25–54. [CrossRef]

131. Summerfield, M.A. Silcretes. In *Chemical Sediments and Their Geomorphology*; Goudie, A.S., Pye, K., Eds.; Academic Press: London, UK, 1983; pp. 59–92.

132. Summerfield, M.A. Silcrete as a palaeoclimatic indicator: Evidence from southern Africa. *Palaeogeogr. Palaeoclimatol. Palaeoecol.* **1983**, *41*, 65–79. [CrossRef]

133. Gibling, M.R. Width and thickness of fluvial channel bodies and valley fills in the geological record: A literature compilation and classification. *J. Sediment. Res.* **2006**, *76*, 731–770. [CrossRef]

134. Dill, H.G. The Hagendorf-Pleystein Pegmatite Province, SE Germany: The center of pegmatites in an ensialic orogen. In *Modern Approaches in Solid Earth Sciences*; Springer: Dortrecht, The Netherlands; Heidelberg, Germany; London, UK; New York, NY, USA, 2015; 343p.

135. Lidmar-Bergström, K.; Olvmo, M.; Bonow, J.M. The South Swedish Dome: A key structure for identification of peneplains and conclusions on Phanerozoic tectonics of an ancient shield. *GFF* **2017**, *139*, 244–259. [CrossRef]

136. Bischoff, R.; Semmel, A.; Wagner, G.A. Fission-track analysis and geomorphology in the surroundings of the drill site of the German Continental Deep Drilling Project (KTB)/Northeast Bavaria. *Z. Geomorphol. Suppl.* **1993**, *92*, 127–143.

137. Redfield, T.F.; Osmundsen, P.T. The long-term topographic response of a continent adjacent to a hyperextended margin: A case study from Scandinavia. *GSA Bull.* **2013**, *125*, 184–200. [CrossRef]

138. Godard, A.; Lagasquie, J.-J. *Basement Regions*; Springer: New York, NY, USA; London, UK, 2012; 324p.

139. Rojík, P. New stratigraphic subdivision of the Tertiary of the Sokolov Basin in the Northwestern Bohemia. *J. Czech Geol. Soc.* **2004**, *49*, 173–185.

140. Rojík, P. Zur Geologie des Tertiärbeckens von Sokolov. In Proceedings of the 21. Jahreshauptversammlung Thüringischer Geologischer Verein, Jena, Germany, 24–27 June 2011.

141. Ulrych, J.; Dostal, J.; Hegner, E.; Balogh, K.; Ackerman, L. Late Cretaceous to Paleocene melilitic rocks of the Ohře/Eger Rift in northern Bohemia, Czech Republic: Insights into the initial stages of continental rifting. *Lithos* **2008**, *101*, 141–161. [CrossRef]

142. Huckenholz, H.G.; Kunzmann, T. Tertiärer Vulkanismus im bayerischen Teil des Egergrabens und des mesozoischen Vorlandes. *Ber. Dtsch. Mineral. Ges.* **1993**, *5*, 1–34.

143. Schwarz, T. Lateritic bauxite in central Germany and implications for Miocene palaeoclimate. *Palaeogeogr. Palaeoclimatol. Pal-aeoecol.* **1997**, *129*, 37–50. [CrossRef]

144. Wray, R.A.L. Silicate Karst: Quartzite dissolution: Karst or pseudokarst? *Cave Karst Sci.* **1997**, *24*, 81–86.

145. Stanaway, K.J. Heavy mineral placers. *Min. Eng.* **1992**, *44*, 352–358.

146. Dill, H.G.; Techmer, A.; Weber, B.; Fuessl, M. Mineralogical and chemical distribution patterns of placers and ferricretes in Quaternary sediments in SE Germany: The impact of nature and man on the unroofing of pegmatites. *J. Geochem. Explor.* **2008**, *96*, 1–24. [CrossRef]

147. Dahl, E. The nunatak theory reconsidered. *Ecol. Bull.* **1987**, *38*, 77–94.

148. Dahl, R. Block fields, weathering pits and tor-like forms in the Narvik Mountains, Nordland, Norway. *Geogr. Ann. A* **1966**, *48*, 55–85. [CrossRef]

149. André, M.-F. The geomorphic impact of glaciers as indicated by tors in North Sweden (Aurivaara, 681N). *Geomorphology* **2004**, *57*, 403–421. [CrossRef]

150. André, M.-F. Do periglacial landscapes evolve under periglacial conditions? *Geomorphology* **2003**, *52*, 149–164. [CrossRef]

151. Marquette, G.C.; Gray, J.T.; Gosse, J.C.; Courschene, F.; Stockli, L.; Macpherson, G.; Finkel, R. Felsenmeer, persistence under non-erosive ice in the Torngat and Kaumajet mountains, Quebec and Labrador, as determined by soil weathering and cosmogenic nuclide exposure dating. *Can. J. Earth Sci.* **2004**, *41*, 19–38. [CrossRef]

152. Paasche, Ø.; Strømsøe, J.R.; Dahl, S.E.; Linge, H. Weathering characteristics of arctic islands in northern Norway. *Geomor-Phology* **2006**, *82*, 430–452. [CrossRef]

153. Ballantyne, C.K. A general model of autochthonous blockfield evolution. *Permafr. Periglac. Process.* **2010**, *21*, 289–300. [CrossRef]

154. Ballantyne, C.K.; McCarroll, D.; Nesje, A.; Dahl, S.O.; Stone, J.O. The last ice sheet in North-West Scotland: Reconstruction and implications. *Quat. Sci. Rev.* **1998**, *17*, 1149–1184. [CrossRef]

155. Strømsøe, J.R.; Paasche, Ø. Weathering patterns in high-latitude regolith. *J. Geophys. Res.* **2011**, *116*, F3. [CrossRef]

156. Kolowith, L.C.; Berner, R.A. Weathering of phosphorus in black shales. *Glob. Biogeochem. Cycles* **2002**, *16*, 87-1–87-8. [CrossRef]

157. Tuttle, M.L.W.; Breit, G.N. Weathering of the New Albany Shale, Kentucky, USA: I. Weathering zones defined by mineralogy and major-element composition. *Appl. Geochem.* **2009**, *24*, 1549–1564. [CrossRef]

158. Jin, L.; Mathur, R.; Rother, G.; Cole, D.; Bazilevskaya, E.; Williams, J.; Carone, A.; Brantley, S. Evolution of porosity and geo-chemistry in Marcellus Formation black shale during weathering. *Chem. Geol.* **2013**, *356*, 50–63. [CrossRef]

159. Körber, H. Die Entwicklung des Maintales. *Würzburger Geogra. Arbeiten* **1962**, *10*, 1–170.

160. Dill, H.G. Der Formenschatz des Quartärs zwischen Untersteinach und Weidenberg. *Geol. Blätter Nord.-Bayern* **1979**, *29*, 61–76.

161. Dill, H.G.; Kus, J.; Buzatu, A.; Balaban, S.-I.; Kaufhold, S.; Borrego, A.G. Organic debris and allochthonous coal in Quaternary landforms within a periglacial setting (Longyearbyen Mining District, Norway)—A multi-disciplinary study (coal geology-geomorphology-sedimentology). *Int. J. Coal Geol.* **2021**, *233*, 103625. [CrossRef]

162. Gupta, V.; Sah, M.P. Impact of the trans-Himalayan landslide lake outburst flood (LLOF) in the Satluj catchment, Himachal Pradesh, India. *Nat. Hazards* **2008**, *45*, 379–390. [CrossRef]

163. Dussaillant, A.; Benito, G.; Buytaert, W.; Carling, P.; Meier, C.; Espinoza, F. Repeated glacial-lake outburst floods in Patagonia: An increasing hazard? *Nat. Hazards* **2010**, *54*, 469–481. [CrossRef]

164. Bennett, M.M.; Glasser, N.F. *Glacial Geology: Ice Sheets and Landforms*; John Wiley & Sons: New York, NY, USA, 2009; 400p.

165. Hausrath, E.M.; Navarre-Sitchler, A.K.; Sak, P.B.; Williams, J.Z.; Brantley, S.L. Soil profiles as indicators of mineral weathering rates and organic interactions for a Pennsylvania diabase. *Chem. Geol.* **2011**, *290*, 89–100. [CrossRef]

166. Kaufhold, S.; Dill, H.G.; Dohrmann, R. Clay mineralogy and rock strength of a Mid-German diabase—Implications for im-proved quality control. *Clay Miner.* **2012**, *47*, 419–428. [CrossRef]

167. Taylor, G.; Eggleton, R.A. *Regolith Geology and Geomorphology*; John Wiley & Sons: New York, NY, USA, 2001; 375p.

168. Allen, C.E.; Darmody, R.G.; Thorn, C.E.; Dixon, J.C.; Schlyter, P. Clay mineralogy, chemical weathering and landscape evo-lution in Arctic-Alpine Sweden. *Geoderma* **2001**, *99*, 277–294. [CrossRef]

169. Bouzari, F.; Clark, A. Anatomy, evolution, and metallogenic significance of the supergene ore body of the Cerro Colorado porphyry copper deposit, I Región, Northern Chile. *Econ. Geol.* **2002**, *97*, 1701–1740. [CrossRef]

170. Arancibia, G.; Matthews, S.J.; Pérez de Arce, C. K–Ar and 40Ar/39Ar geochronology of supergene processes in the Atacama Desert, Northern Chile, tectonic and climatic relations. *J. Geol. Soc.* **2006**, *163*, 107–118. [CrossRef]

171. Warren, I.; Archibald, D.A.; Simmons, S.F. Geochronology of epithermal Au-Ag mineralization, magmatic-hydrothermal alteration, and supergene weathering in the El Peñón District, Northern Chile. *Econ. Geol.* **2008**, *103*, 851–864. [CrossRef]

172. Migoń, P.; Lidmar-Bergström, K. Deep weathering through time in central and northwestern Europe: Problems of dating and interpretation of geological record. *Catena* **2002**, *49*, 25–40. [CrossRef]

173. Beavis, S.G. Structural controls on the orientation of erosion gullies in mid-western New South Wales, Australia. *Geomorphology* **2000**, *33*, 59–72. [CrossRef]

174. Bardou, E.; Jaboyedoff, M. Debris flows as a factor of hillslope evolution controlled by a continuous or a pulse process. In *Landscape Evolution: Denudation, Climate and Tectonic over Different Time and Space Scales*; Gallagher, K., Jones, S.J., Wainwright, J., Eds.; Geological Society: London, UK, 2008; Volume 296, pp. 63–78.

175. Hinchcliffe, S.; Ballantyne, C.K. Talus structure and evolution on sandstone mountains in NW Scotland. *Holocene* **2009**, *19*, 477–486. [CrossRef]

176. Sanders, D. Sedimentary facies and progradational style of a Pleistocene talus-slope succession, Northern Calcareous Alps, Austria. *Sediment. Geol.* **2010**, *228*, 271–283. [CrossRef]

177. Luckman, B.H. Debris flow and snow avalanche landforms in the Lairig Ghru, Cairngorm Mountains, Scotland. *Geogr. Ann. A* **1992**, *74*, 109–121. [CrossRef]

178. Kamber, B.S.; Greig, A.; Collerson, K.D. A new estimate for the composition of weathered young upper continental crust from alluvial sediments, Queensland, Australia. *Geochim. Cosmochim. Acta* **2005**, *69*, 1041–1058. [CrossRef]

179. Arvidson, R.E.; Mackenzie, F.T.; Guidry, M. MAGic: A Phanerozoic model for the geochemical cycling of major rock-forming components. *Am. J. Sci.* **2006**, *306*, 135–190. [CrossRef]

180. Dill, H.G.; Kaufhold, S.; Techmer, A.; Baritz, R.; Moussadek, R. A joint study in geomorphology, pedology and sedimentology of a Mesoeuropean landscape in the Meseta and Atlas Foreland (NW Morocco). A function of parent lithology, geodynamics and climate. *J. Afr. Earth Sci.* **2019**, *158*, 103531. [CrossRef]

181. Tricart, J.; Cailleux, A. *Introduction to Climatic Geomorphology*; Longman: London, UK, 1972; p. 295.

182. Scotese, C.R. *Atlas of the Earth History*; Paleomap Project; University of Arlington: Arlington, TX, USA, 2002; p. 52.

183. Hilbig, W. *The Vegetation of Mongolia*; SPB Academic: Amsterdam, The Netherlands, 1995.

184. Weisrock, A. Géomorphologie et Paléoenvironnements de l'Atlas atlantique. Maroc. Doctor's Thesis, Université de Paris, Paris, France, 1993. Volume 1. 831p. publiée in Notes et Mémoires du Service Géologique du Maroc, 1993, Volume 332, pp. 487.

185. Weisrock, A. Niveaux marins du Maroc atlantique durant le dernier Interglaciaire (SIM 5.5, SIM 5.3 et SIM 5.1). *Geomorphologie* **2016**, *22*, 245–251. [CrossRef]